Ultrafast optical parametric oscillators

Novel systems, techniques, and concepts

Venkata Ramaiah-Badarla

Thesis Advisor

Majid Ebrahim-Zadeh

Thesis Co-Advisor

Adolfo Esteban-Martin

To my Family and Friends

Abstract

In this thesis, we have demonstrated various ultrafast optical parametric oscillators (OPOs) based on different nonlinear media. The thesis consists of OPO systems, novel techniques, designs, and concepts that has facilitated the wavelength accessibility from 1 μm in the *near-infrared* region to as far as 8 μm in the *mid-infrared* region.

We developed a *fs* OPO based on BiB_3O_6 (BIBO) directly pumped the Kerr-lens mode-locked (KLM) Ti:sapphire laser. This system could provide broad and rapid tuning from 1420-1560 nm just by changing the cavity length. Also, by exploiting the unique optical properties of BIBO under *type I (e→oo)* interaction, we have demonstrated the first self-phase-locked degenerate *fs* OPO. Further, we have developed a technique called synchronous retro-reflection for threshold reduction and signal amplification before the onset of the oscillation. This technique is generic and is particularly useful while deploying ultrafast OPOs with birefringent materials that have relatively low nonlinear gain and when we have limited pump power.

In addition, we have developed a dual-wavelength *fs* OPO with arbitrary and independent tuning by making use of anti-resonant-ring (ARR) or Sagnac interferometer. This universal technique of coupling two optical oscillators can be employed in any time regime (cw to ultrafast pico or *fs*) irrespective of the operating wavelengths. This conceptual technique can be used for intracavity terahertz (THz) generation which exploits the high intensity intracavity oscillating pulses. Also, we have developed a dual-crystal, double-pumped OPOs for intracavity signal amplification in *fs* regime as well as in ps regime, for arbitrary and independent wavelength tuning. In both systems two crystals share the same optical cavity but are pumped independently by a single laser source.

Finally, we have devised and experimentally demonstrated a novel concept of pumping an OPO within another OPO using a composite cascaded cavity design. This all solid-state Ti:sapphire-pumped *fs* OPO system is potentially capable of providing access to *mid-infrared* region beyond 4 μm to as far as 18 μm by careful selection of the nonlinear medium.

Resumen

En esta tesis, hemos demostrado varios osciladores ópticos paramétricos ultrarrápidos (OPO) basados en diferentes medios no lineales. La tesis consta de sistemas OPO, técnicas novedosas, diseños y conceptos que han facilitado el acceso a longitudes de onda de 1 μm en la región del infrarrojo cercano, así como hasta 8 μm en la región del infrarrojo medio.

Hemos desarrollado un femtosegundo (fs) OPO basado en BiB_3O_6 (BIBO) directamente bombeado por un láser Kerr-lens mode-locked (KLM) de Ti:zafiro. Este sistema proporciona amplia y rápida sintonización en el rango 1400-1560 nm con sólo cambiar la longitud de la cavidad. También, gracias a las propiedades ópticas únicas de BIBO en la interacción *tipo I (e→oo)*, hemos demostrado el primer fs OPO self-phaselocked degenerado. Además, hemos desarrollado una técnica llamada retro reflexión sincronizada para la reducción del umbral y amplificación de señal, antes de la aparición de la oscilación. Esta técnica es genérica y es particularmente útil para implementar OPOs ultrarrápidos con materiales birrefringentes que tienen relativamente baja ganancia no lineal y cuando existe una limitación de la potencia de bombeo.

Adicionalmente, hemos desarrollado un fs OPO con longitud de onda dual que presenta sintonización arbitraria e independiente mediante el uso de un interferómetro de anillo antirresonante (ARR) o Sagnac. Esta técnica universal de acoplamiento de dos osciladores ópticos puede ser empleada en cualquier régimen temporal (desde *cw* a ultrarrápido de pico o femtosegundo) e independientemente de las longitudes de onda de operación. Esta técnica puede ser utilizada para la generación de THz intracavidad, permitiendo aprovechar la alta intensidad de los pulsos oscilantes.

Además, hemos desarrollado un sistema OPO de doble cristal y doble bombeo para la amplificación de la señal dentro de la cavidad tanto en régimen de fs como de ps, para el ajuste de longitud de onda arbitraria e independiente. En ambos sistemas los dos cristales comparten la misma cavidad óptica, pero son bombeados independientemente por una sola fuente láser.

Por último, hemos diseñado y demostrado experimentalmente un concepto novedoso para bombear un OPO dentro de otro OPO mediante un diseño de

cavidad compuesta en cascada. Este sistema de estado sólido OPO de femtosegundo bombeado por el láser de Ti: zafiro es potencialmente capaz de proporcionar acceso a la región del infrarrojo medio más allá de 4 μm incluso hasta las 18 μm, realizando una cuidadosa selección del medio no lineal.

Acknowledgements

First of all, I would like to express my sincere gratitude to Prof. Majid Ebrahim-Zadeh, for giving me the opportunity to conduct research in his group. Also, I thank Dr. Adolfo Esteban-Martin my co-advisor, for rendering his continuous support in the lab during the last four years. The various discussions among the group have been very fruitful and inculcated in me intellectual skills such as critical thinking, consistency, research design and problem-solving. I acknowledge the kind and helping nature of my colleagues in the group - Gautam, Chaitanya, Kavita, Enrique and Ossi. I really appreciate your help in various aspects that made my working environment enjoyable and happier. I would also like to thank the different units at ICFO such as administration, KTT, mechanical, electronic, IT and logistics for their help and organised coordination.

I am indebted to my parents, sister (Indira) and brother (Manoj) for their unconditional love, affection and encouragement. I would also like to thank Rev. Jacob John and Charles John whose teachings have/had made a profound impact in my life. ICFO has been a marvellous institution not only for research but also a place with various seasonal activities which keeps you always refreshed. Here I got the opportunity to meet many wonderful people from different countries and continents. Thanks to all of my friends at ICFO who made my times in and outside ICFO memorable. I thank Yannick, Anaid, Isabel, Claudia, Valeria, Mariale, Kenny, Camila, Jiri, Luis and Alberto for inviting me to various fiestas. The late night discussions with Alberto Curto and his hard-working nature has always motivated me. I would also like to thank Mathieu Mivelle, Kyra, Gaetan for various suggestions, barbecues and hangouts. I would like to specially thank my best pals at ICFO Roberto (LB), Rafa (Greyiish), and Alex (Zamora) with whom I always felt and will feel cherished. Anshuman, you have been my second mentor, philosopher friend and a dear well wisher, many thanks for listening to me at hard times and for all those prudent suggestions. I also thank the Indian community (Dhriti, Arup, Saurabh, Hari Varma, Amit (Thursday), Venkatesh, Kavita jr.) at ICFO for those food festivals, get together and din-

ners. I would like to thank Ion, James, Lukasz, Isa, Bruno, Juan, Alberto, Pablo, Carmelo, Jonas and Adrian, with your help I learned the futbolin. During the last three years, Friday has always been a special day not only because of the start of the weekend but also for the salsa classes. I thank Telma, Juan Jo, Mari Carmen and Miguel for their patience, perseverance, and exemplary teaching skills.

I would like to thank my previous mentors from University of Hyderabad (UoH) who introduced me to the field of ultrafast optics. I thank Dr. Soma Venugopal Rao and O. E. Jagadeesh for teaching me the alignment and trouble shooting of various ultrafast lasers such as femtosecond oscillator (Micra), regenerative amplifiers (Legend pico and femto) and optical parametric amplifiers (Topas). I gratefully acknowledge the help from Dr. Prem Kiran for his encouragement and support at times of trouble. I thank Dr. Manoj Kumar for the various informal logical discussions which illuminated my curiosity in the process of learning. The technical knowledge and experience which I gained at UoH is invaluable. I am also thankful to Dr. Vaithee for his moral support. I would like to thank my friends at UoH Deepak, Sriram, Rajkumar, GK, Ramesh (Bonda) and Mukund for helping in various occasions. Finally, from Andhra university, along with my Master's degree, I am lucky to get good friends like Ramesh, Anji, Srinu, and Nehru who have been supportive and encouraging me through all these years. I would like to thank my wife for her support and encouragement in the process of writing this thesis. Above all I thank MY LORD GOD ALMIGHTY for blessing me all these years with good Health, Wisdom and Knowledge through his Amazing Grace.

Journal publications

1. **V. Ramaiah-Badarla**, A. Esteban-Martin, S. Chaitanya Kumar, K. T. Zawilski, P. G. Schunemann, and M. Ebrahim-Zadeh, "Ti:sapphire-pumped, deep-mid-infrared optical parametric oscillator based on $CdSiP_2$ tunable across 6-8 μm," (submitted)
2. **V. Ramaiah-Badarla**, A. Esteban-Martin and M. Ebrahim-Zadeh,"Double-crystal, dual-synchronously-pumped femtosecond optical parametric oscillator," (submitted)
3. **V. Ramaiah-Badarla**, S. Chaitanya Kumar, and M. Ebrahim-Zadeh,"Fiber-laser-pumped, dual-wavelength, picosecond optical parametric oscillator," Opt. Lett. **39**, 2739-2742 (2014).
4. **V. Ramaiah-Badarla**, A. Esteban-Martin, and M. Ebrahim-Zadeh, "Self-phase-locked degenerate femtosecond optical parametric oscillator based on BiB_3O_6," Laser Photonics Rev. **7**, L55-L60 (2013).
5. A. Esteban-Martin, **V. Ramaiah-Badarla**, and M. Ebrahim-Zadeh, "Dual-wavelength optical parametric oscillator using antiresonant ring interferometer," Laser Photonics Rev. **6**, L7-L11 (2012).
6. A. Esteban-Martin, **V. Ramaiah-Badarla**, and M. Ebrahim-Zadeh, "Synchronized retro-reflection-pumped femtosecond optical parametric oscillator," Opt. Lett. **37**, 1091-1093 (2012).
7. A. Esteban-Martin, **V. Ramaiah-Badarla**, V. Petrov, and M. Ebrahim-Zadeh, "Broadband, rapidly tunable Ti:sapphire-pumped bismuth triborate femtosecond optical parametric oscillator," Opt. Lett. **36**, 1671-1673 (2011)

Conference papers

1. **V. Ramaiah-Badarla**, A. Esteban-Martin, S. Chaitanya Kumar, K. Devi, K. Zawilski, P. Schunemann, M. Ebrahim-Zadeh,“ Ti:sapphire-pumped, deep-mid-infrared, intracavity-cascaded femtosecond optical parametric oscillator,” Euro Photonics Conference, Nauchatel, Switzerland, August, 2014.
2. **V. Ramaiah-Badarla**, A. Esteban-Martin, S. Chaitanya Kumar, K. Devi, K. Zawilski, P. Schunemann, M. Ebrahim-Zadeh,“ $CdSiP_2$ optical parametric oscillator tunable across 6-8 μm synchronously pumped by a Ti:sapphire laser,” Advanced Photonics Congress, Barcelona, July, 2014.
3. **V. Ramaiah-Badarla**, S. Chaitanya Kumar, and M. Ebrahim-Zadeh,“Yb-Fiber-Laser-Pumped, High-Power, High-repetition-rate Dual-Wavelength Picosecond Optical Parametric Oscillator,” Conf. Lasers and Electro-Optics (CLEO), San Jose, California, USA, May 2014.
4. **V. Ramaiah-Badarla**, A. Esteban-Martin, and M. Ebrahim-Zadeh, “Self-phase-locked sub-harmonic femtosecond optical parametric oscillator based on BiB_3O_6,” Frontiers in optics, Orlando , Florida, USA , October 2013
5. A. Esteban-Martin, **V. Ramaiah-Badarla**, and M. Ebrahim-Zadeh,“ Dual-wavelength synchronously-pumped femtosecond optical parametric oscillator using antiresonant ring interferometer,” CLEO/Europe-EQEC, Munich, Germany, May 2013
6. **V. Ramaiah-Badarla**, K. Devi, S. Chaitanya Kumar, A. Esteban-Martin, M. Ebrahim-Zadeh, “Interferometrically coupled two-color femtosecond optical parametric oscillator,” The International Conference on Fiber Optics and Photonics, Madras, India, December 2012.

7. **V. Ramaiah-Badarla**, A. Esteban-Martin, and M. Ebrahim-Zadeh, "Interferometrically-coupled, dual-wavelength femtosecond optical parametric oscillator," NLO 50 International Symposium, Barcelona, Spain, October 2012 .

8. A. Esteban-Martin, **V. Ramaiah-Badarla**, and M. Ebrahim-Zadeh, "Synchronized retro-reflection-pumped femtosecond optical parametric oscillator," CLEO, San Jose, USA, May 2012.

9. A. Esteban-Martin, **V. Ramaiah-Badarla**, V. Petrov, and M. Ebrahim-Zadeh, "Broadband, rapidly tunable, BiB_3O_6 femtosecond optical parametric oscillator directly pumped by a Ti:sapphire," CLEO/ Europe-EQEC 2011, Munich, Germany, May 2011.

Patents

M. Ebrahim-Zadeh, **V. Ramaiah-Badarla**, A. Esteban-Martin, S. Chaitanya Kumar "Internally cascaded optical parametric oscillators" (International patent).

Contents

Chapter 1

Introduction

1.1 Background

Nonlinear optics is the study of optical manifestations of the dielectric medium when subjected to *intense optical electromagnetic fields*. Though several nonlinear optical phenomena such as *Kerr*, *Pockel*, and *Raman* effects were known till early twentieth century, the true visibility for nonlinear optical frequency conversion processes was enabled only after the invention of the light amplification by stimulated emission of radiation (LASER) [1] in 1960. This was rapidly followed by the milestone experiment of optical harmonics generation by Franken [2] in 1961 popularly known as second harmonic generation (SHG). Soon afterwards, sum frequency generation (SFG) was reported by Bass [3]. Both of these experiments suffered from the effects of dispersion due to different phase velocities of the interacting waves inside the non-centrosymmetric nonlinear media (quartz and tri glycine sulphate crystals), thus resulting in poor conversion efficiency. In 1962, Giordmaine [4] and Maker [5] independently put forward the idea of phase-matching and described how birefringent materials can be used to offset the phase-mismatch (or also known as conservation of *electromagnetic* momentum). The exploitation of birefringence to phase-match the interacting fields in a non-centrosymmetric medium is popularly known as birefringent phase-matching. Another means of phase-matching was suggested by

Armstrong [6] called quasi-phase-matching (QPM) which involves periodic modulation of the sign of the nonlinear coefficient of the medium to compensate for the phase-mismatch. Later the experiments of sum frequency generation (SFG) [7] and optical rectification (OR) [3] were demonstrated in potassium dihydrogen phosphate (KDP), ammonium dihydrogen phosphate (ADP) and potassium di deuturium phosphate (KD*P) respectively. In 1965, the first *near-infrared* tunable nanosecond (ns) optical parametric oscillator (OPO) based on lithium niobate ($LiNbO_3$) was reported by Giordmaine [8], followed by difference frequency generation (DFG) into *far-infrared* in Quartz by Zernike [9]. Later in 1968, Byer [10] reported the first continuous-wave (cw) *visible* OPO based on $LiNbO_3$.

As one can see, in less than eight years after the invention of laser, all the second order nonlinear parametric processes and devices such as SHG, SFG, OR, DFG and OPOs were demonstrated to conquer the various regions of the *electromagnetic* spectra not accessible through lasers. *This proves the strength of all second order nonlinear optical devices - Tunability.*

With the development of laser technology in conjunction with the discoveries of new and novel nonlinear media, unprecedented progress has been achieved in the field of nonlinear optics. During the past fifty years several optical parametric sources have been developed in various spectral and temporal regimes. Among these devices, especially, OPOs have now established themselves as viable and reliable sources for coherent generation of radiation by bridging various gaps in the *electromagnetic* spectrum all the way from *ultraviolet* (UV), *visible*, *near-infrared* to as far as *mid-infrared* regions [11]. The OPOs can be classified into three broad categories depending on the temporal regimes - continuous-wave (cw), nanosecond (ns), ultrafast picosecond (ps) and femtosecond (fs). In the context of this thesis, we focus mainly on ultrafast optical parametric oscillators, also known as synchronously-pumped optical parametric oscillators (SPOPOs). The first report of a *fs* SPOPO was made by Edelstein [12] in 1989, based on potassium titanyl phosphate ($KTiOPO_4$ or KTP) as a nonlinear medium and pumped by a colliding pulse-mode-locked dye laser. To access the high intensities necessary to reach the oscillation threshold, the KTP crystal was

deployed at the intracavity focus of the dye laser and the SPOPO produced milliwatts of average power under singly-resonant operation mode. In a similar SPOPO,with external pumping, Mak [13] reported generation of nearly 30 mW of average power.

However, the progress in *fs* SPOPO technology was triggered with the invention of Kerr-lens-mode-locked (KLM) Ti:sapphire [14] laser by Spence [15] in 1990. In 1992, Fu [16] and Pelouch [17] independently reported two different SPOPOs based on KTP pumped by high repetition rate (76 *MHz*) KLM *fs* Ti:sapphire laser. Since then, the KLM *fs* Ti:sapphire laser has been adopted as the workhorse for pumping SPOPOs in *fs* regime. In the following years, using the KLM *fs* Ti:sapphire laser as the pump source, several SPOPOs were reported based on various nonlinear media such as KTP [18], KTA ($KTiOAsO_4$) [19], [20], CTA ($CsTiOAsO_4$) [21], [22], RTA ($RbTiOAsO_4$) [23], [24], LBO (LiB_3O_5) [25] for accessing the spectral regions from *near-to-mid-infrared* (1-5 μm) under critical and non-critical phase-matching conditions. The spectral range of KLM Ti:sapphire-pumped *fs* SPOPOs has also been extended into *visible* region either by intracavity SHG of the SPOPO signal pulses [26], [27] or through intracavity SFG between the pump and oscillating signal pulses [28] in a suitable nonlinear media like β-barium borate, (β-BaB_2O_4 or BBO). Both approaches exploited the high intracavity oscillating signal intensities inside the SPOPOs. A *visible fs* SPOPO was reported by Driscoll [29] in 1994 based on BBO as the nonlinear medium pumped by the second harmonic of the KLM Ti:sapphire laser at $\sim$400 nm.

The early 1990's can be considered as a culmination of two important technologies that paved the way for development of ultrafast *fs* SPOPOs. One being the invention of KLM Ti:sapphire in the laser technology and the other being the matured crystal growth technology for periodically poling the ferroelectric materials like $LiNbO_3$. While the KLM *fs* Ti:sapphire established itself as reliable and robust all-solid-state laser, the periodic poling [30], [31] enabled the possibility of bringing QPM into action, nearly three decades after the first postulation in 1962 [6]. In 1997, there were two independent demonstrations of Ti:sapphire-pumped SPOPOs based on periodically poled

lithium niobate (PPLN), and periodically poled RTA (PPRTA) by Burr [32] and Reid [33], respectively. This was followed by several SPOPOs based on PPKTP and its isomorphs [34], [35], [36].
Later in 2006, a *fs* SPOPO was reported by our group [37] based on bismuth triborate (BiB_3O_6) as nonlinear medium. However, this SPOPO was pumped by second harmonic of the Ti:sapphire laser at ∼400 nm and provided a gap-free tuning all the way from 350 nm in the UV to 2500 nm in the *near-infrared* region. After this, a *fs* SPOPO directly pumped by KLM Ti:sapphire was reported by Kalyan [38] based on periodically poled stoichiometric lithium tantalate ($PPSLT$). Quite recently, in 2011 we demonstrated a *fs* SPOPO directly pumped by a Ti:sapphire laser based on BiB_3O_6 [39]. Thus, one can clearly see the progress achieved in the ultrafast *fs* SPOPOs based on various nonlinear media by using solid-state KLM Ti:sapphire *fs* laser as the pump source over the last 23 years.

1.2 Overview

This thesis presents various ultrafast SPOPOs based on different nonlinear crystals. This includes systems, designs, techniques and novel concepts that have enabled access to spectral regions from 1 μm in the *near-infrared* to as far as 8 μm in the deep mid-infrared (MIR) region. Throughout this thesis, the KLM Ti:sapphire was used as the pump source for developing various *fs* SPOPOs except in one chapter where we have used a picosecond Yb-fiber laser.

The thesis has been organised as follows:

Chapter 2 includes the basic theory of nonlinear optics with a focus on second-order nonlinear optical processes such as SHG, SFG, DFG, OPG and OPOs. Also, some important phenomena like group velocity, group velocity mismatch, group velocity dispersion and compensation are described, which are vital in the *fs* regime.

In chapter 3, we describe a *fs* SPOPO based on BiB_3O_6. This system can be rapidly tuned from 1420 to 1580 nm in the *near-infrared* region just by changing the cavity length of the OPO. Though several SPOPOs have been developed previously in our group based on BiB_3O_6, this is the first demonstration of such a *fs* SPOPO based on BiB_3O_6 directly pumped by KLM Ti:sapphire laser.

In chapter 4, we describe a technique of synchronous retro-reflection of the pump. This technique involves retro-reflection of the undepleted pump back into the SPOPO cavity for signal amplification and pump threshold reduction even before the onset of the oscillation. This technique is particularly important for the ultrafast SPOPOs while deploying the birefringent nonlinear media with relatively low nonlinear coefficients and limited available pump powers.

In chapter 5, we demonstrate the first self-phase-locked degenerate *fs* SPOPO based on a birefringent nonlinear crystal - BiB_3O_6. By exploiting the inherent and unique optical properties of BiB_3O_6 under *type I(e→oo)* phase-matching, we have generated a stable degenerate output spectrum of 46 nm, when pumped with a 7 nm bandwidth Ti:sapphire laser pulses centred at 800 nm. The true phase-locking mechanism was verified using f-$2f$ interferometer along with the RF measurements.

In chapter 6, we describe a novel and universal technique to couple two SPOPO cavities using Anti Resonant Ring (ARR) or Sagnac interferometer. Using this technique, we have coupled two separate *fs* SPOPOs that can provide independent and arbitrarily tunable wavelengths without any coherent coupling between the two nonlinear media. The technique has a potential impact especially in the context of terahertz (THz) generation through difference frequency mixing inside an optical cavity by exploiting the high intracavity intensities of the two independently oscillating fields inside the ARR. This technique can be employed in any time domain from *cw* to ultrafast *fs*, irrespective of the operating wavelengths.

In chapter 7, we have designed and demonstrated a double-crystal, dual-synchronously-pumped SPOPO system in picosecond regime that has facilitated independent and arbitrary tuning of wavelengths. This system could provide Watt level signal output and can be used to generate THz radiation external to the cavity by doing DFG in a suitable nonlinear medium like DAST or ZnTe.

In chapter 8, we present a dual-crystal, dual-synchronously-pumped *fs* SPOPO for intracavity signal amplification based on MgO:PPLN as a nonlinear medium. Two MgO:PPLN crystals are deployed in a single cavity and are pumped synchronously with a common pump source. This scheme shows how the interaction length can be increased without compromise on the gain bandwidth.

Finally, in chapter 9, we have devised and developed a new, simple, novel and universal concept of developing an OPO within another OPO. This novel concept and design has the potential to develop all-solid-state-pumped tunable OPOs that can provide wavelength tunability from 1 μm in the *near-infrared* to as far as 18 μm in the *mid-infrared* region depending upon the careful selection of the nonlinear media.

Chapter 10 consists the overall summary and an outlook of the presented work.

Chapter 2

Basic principles of nonlinear optics

2.1 Introduction to nonlinear optics

The description of nonlinear optical effects is based on the extension of the motion of linear propagation of the *electromagnetic fields* in a dielectric medium. It relies on the use of Maxwell's equations in which the polarisation of the medium is expressed by means of a power series expansion of the amplitude field present in the medium. In the same manner as the linear properties of the medium are described by the quantity called *susceptibility*, the nonlinear properties are characterised by certain number of nonlinear susceptibilities. To modify the properties of material, it is necessary to use a coherent light source like laser that is sufficiently intense. The first observation of nonlinear optical effects dates back to 1961, when Franken demonstrated optical second harmonic generation in a quartz crystal. Previously it was thought that linear properties of a medium are described by means of one complex quantity only - *The susceptibility.* The induced polarisation of a medium in presence of applied electric field is defined as

$$P = \epsilon_o \chi^{(1)} E \tag{2.1}$$

where $\chi^{(1)}$ is the linear susceptibility of the medium and this relation shows the linear dependence of polarisation (dipole moment per unit volume) on the strength of the applied *electromagnetic field*. When the applied electric field is intense enough, the induced polarisation is no longer linear and the non-linear properties of the medium are characterised by higher order nonlinear susceptibilities. Thus, the polarisation term can be expressed as

$$P = \epsilon_o[\chi^{(1)}E + \chi^{(2)}E.E + \chi^{(3)}E.E.E + ...] \tag{2.2}$$

where $\chi^{(2)}$, $\chi^{(3)}$ are the second- and third-order nonlinear optical susceptibilities. As a consequence of the nonlinear dependence of the polarisation, the orientation of the induced polarisation differs from that of the applied optical electric field. Also, for an anisotropic medium to exhibit the second-order nonlinearity, the material must be non-centrosymmetric as proved below. In case of centrosymmetric medium, the inversion symmetric operation is defined as

$$I_{op}(F) = -F \tag{2.3}$$

where F is a material property and from equation 2.2, one can write that

$$-P = \epsilon_o[-\chi^{(1)}E - \chi^{(2)}E.E - \chi^{(3)}E.E.E + ...] \tag{2.4}$$

If the medium is centrosymmetric, then the following relations are applicable:

$$I_{op}(P) = -P \tag{2.5}$$

and

$$I_{op}(E) = -E \tag{2.6}$$

Applying the symmetry operation on 2.2 gives

$$I_{op}(P) = -P = \epsilon_o[-\chi^{(1)}E + \chi^{(2)}E.E - \chi^{(3)}E.E.E + ...] \tag{2.7}$$

By comparing 2.4 and 2.7, consistency exits only if

$$\chi^{(2)}E.E = -\chi^{(2)}E.E \tag{2.8}$$

Hence, $\chi^{(2)}$ must be zero and any media with inversion symmetry has $\chi^{(2n)}$ = 0. Thus, to exhibit a second order non-linearity, the medium must be non-centrosymmetric.

In this thesis, we restrict ourselves to various optical processes related to second-order nonlinear susceptibility. More commonly, the susceptibility is represented by the so-called d-coefficients given by $\chi^{(2)}_{ijk} = 2d_{ijk}$. The susceptibility ($\chi_{ijk}$) and the nonlinear coefficient (d_{ijk}) are tensors of rank 3 containing 3^{n+1} elements with n being the order of susceptibility. The index i can have values 1, 2, 3 corresponding to the respective crystal axes *x, y, z,* and *jk* can have values 1, 2, 3, 4, 5, 6 corresponding to the combinations of axes *xx, xy=yx, yy, yz=zy, zx=xz, and zz.* In practice, the d-coefficients are used to analyse the nonlinear interactions by using the d-matrix depending on the crystallographic point group. Also, the effective nonlinear coefficient (d_{eff}) depends on the direction of propagation of light within the crystal, polarisation direction, and the orientation of the crystal as well.

2.2 Optical parametric processes and devices

If we consider an optical field consisting of two distinct frequency components, ω_1 and ω_2, incident upon the nonlinear medium, which can be represented by

$$E(t) = E_1(t)\exp(-i\omega_1 t) + E_2(t)\exp(-i\omega_2 t) + c.c \tag{2.9}$$

Then, the second-order nonlinear polarisation can be expressed as

$$P^{NL} = \chi^{(2)}E^2(t) \tag{2.10}$$

Substituting equation 2.9 in 2.10, we get

$$P^{NL} = \epsilon_o \chi^{(2)}[E_1^2(t)\exp(-2i\omega_1 t) + E_2^2(t)\exp(-2i\omega_2 t) + 2E_1E_2\exp(-i(\omega_1+\omega_2)t + 2E_1E_2^*\exp(-i(\omega_1-\omega_2)t + c.c.] + 2\epsilon_o\chi^{(2)}[E_1E_1^* + E_2E_2^*] \quad (2.11)$$

Thus, from the above equation, we can conclude that an optical parametric process of three-wave interaction consists of the following frequency mixing processes. The first two terms describe the SHG processes, the third term describes the SFG, while the fourth term describes the DFG, and the last term describes the OR process. SHG can be considered as a special case of SFG in which ω_1=ω_2. The various second-order nonlinear optical processes are depicted in the *Fig.* 2.1.

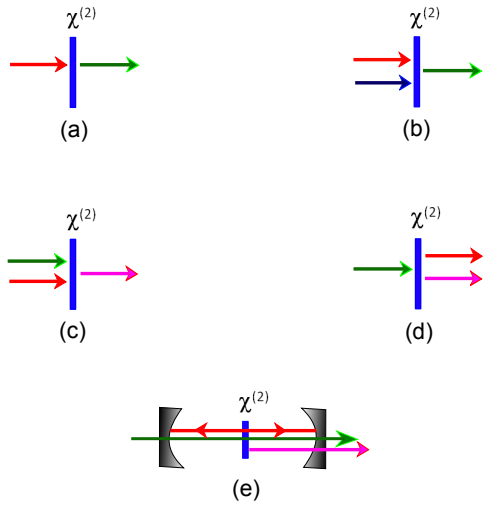

Figure 2.1: Various second-order nonlinear optical processes in a non-centrosymmetric medium (a) SHG (b) SFG (c) DFG (d) OPG (e) OPO.

Optical parametric generation (OPG) is a process in which an input pump photon at high frequency ω_p is split into two photons of lower frequencies in the nonlinear medium. The field at ω_p generally corresponds to an intense input optical field called *pump*, giving rise to a pair of generated fields at frequencies ω_s and ω_i. The generated field at the higher frequency is referred

to as *signal*, while the field at lower frequency is termed as *idler*. This process is also known as *parametric down-conversion*. In all the three wave interaction processes, both conservation laws - energy and momentum (or phase-matching) must be satisfied such that

$$\omega_p = \omega_s + \omega_i \tag{2.12}$$

$$\Delta k = k_p - k_s - k_i = 0 \quad \text{or} \quad n_p\omega_p - n_s\omega_s - n_i\omega_i = 0 \tag{2.13}$$

where $n_{p,s,i}$ are the respective refractive indices of *pump*, *signal* and *idler*. The generated *signal* and *idler* wavelengths are governed by the above two conservation conditions. The down-conversion process generates a very weak *signal* called *parametric fluorescence*. To obtain appreciable amount of conversion efficiency, either we need a very strong pump intensity or the nonlinear medium should posses very high nonlinear coefficient under proper phase-matching conditions. Thus, to increase the conversion efficiency, two parametric sources or devices are generally used for practical applications.
One being the *optical parametric amplifier* (OPA), the other is called *optical parametric oscillator* (OPO). OPAs are pumped by high-power lasers like regenerative amplifiers which possesses very large peak intensity (GW/cm^2) and hence *parametric super-fluorescence* can be generated in a single pass configuration. However, OPAs consists of multiple stages through which the generated parametric fluorescence is amplified in successive stages with a proper delay between the generated *signal* and the *pump* pulses inside the nonlinear crystal. On the other hand, if we deploy the nonlinear crystal inside an optical resonator that could provide feedback for amplification, such a device is known as *optical parametric oscillator* (OPO). The major difference between an OPA and OPO can be described as follows:
An OPA requires extremely powerful (mJ) pump pulses in *ps* or *fs* duration and operate in a single pass configuration with very low repetition rate typically at 1 *KHz*. On the other hand, OPOs can be operated at much low pump energy (nJ pulses) and at high repetition rates (76 to 100 *MHz*).
Also, one has to note the major difference between a laser and an OPO. While both laser and OPO consist of optical cavities, the gain in an OPO is

instantaneous unlike in the laser where the emission is governed by population inversion. *Thus, in OPOs there is no storage of energy.* In a laser, the tunability depends on the bandwidth of the electronic transitions whereas in OPOs the tunability is achieved by phase-matching conditions in conjunction with the energy conservation laws. Especially in the ultrafast *fs* regime, since gain is instantaneous, it is necessary to use the scheme of *synchronous pumping* in which the cavity length of the OPO needs to be matched exactly with the repetition rate of the pump laser.

2.3 Coupled wave equations

The coupled wave equations are the important tools to investigate the various optical parametric processes involving any three-wave interactions like - SHG, SFG and DFG in a nonlinear medium. For a lossless, non-conducting, and non-magnetic medium, the coupled equations with *slowly varying envelope approximation (SVEA)* can be written as follows:

$$\frac{\partial}{\partial z}E_1(z) = \frac{2id_{eff}\omega_1^2}{k_1c^2}A_3A_2^*exp(i\Delta kz) \tag{2.14}$$

$$\frac{\partial}{\partial z}E_2(z) = \frac{2id_{eff}\omega_2^2}{k_2c^2}A_3A_1^*exp(i\Delta kz) \tag{2.15}$$

$$\frac{\partial}{\partial z}E_3(z) = \frac{2id_{eff}\omega_3^2}{k_3c^2}A_1A_2exp(-i\Delta kz) \tag{2.16}$$

where E_i(z) are the amplitudes of the electric fields of interacting waves, d_{eff} is the effective nonlinear coefficient, and $\Delta k = k_3$ - k_2 - k_1 is the momentum or wave vector mismatch between the interacting fields.
The three basic equations imply that the amplitude of the newly produced wave is coupled to the incoming waves through the nonlinear coefficient (d_{eff}) [40], [41]. There is energy flow from waves at frequencies ω_1 and ω_2 to the wave at frequency ω_3. At the same time, inverse process can also take place, i.e.,

the process in which the newly generated frequency ω_3 mixes with one of the two incoming waves called difference frequency mixing ($\omega_1 = \omega_3$ - ω_2).

2.4 Phase-matching

Phase-matching or conservation of *electromagnetic* momentum was proposed separately by Giordmaine [4] and Maker [5] in 1962. *It is a technique in which the phase velocity mismatch between the interacting waves could be offset by exploiting the inherent characteristics of an anisotropic nonlinear medium.* In a three-wave interaction process, physically it represents that the value of Δk should somehow be made equal to zero (k_1 - k_2 - $k_3 = 0$). Phase-matching can be realized by different methods which will take the advantage of the fact that the refractive index changes as a function of incident angle, temperature and wavelength. The case in which $\Delta k = 0$ is known as perfect phase-matching.

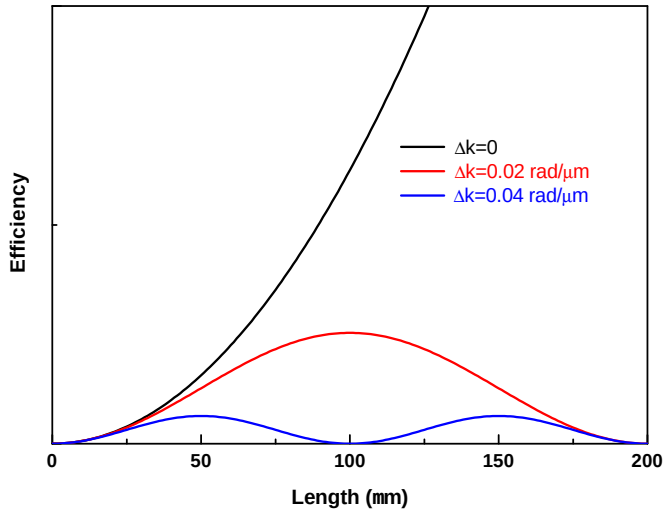

Figure 2.2: Dependence of efficiency on phase-mismatch between the interacting waves along the crystal length for SHG process.

However, in general, due to dispersion, optical waves at different frequencies travel with different phase velocities as they propagate through the nonlinear medium. Thus, after travelling a short distance known as the coherence length ($l_c = \frac{\pi}{\Delta k}$), the relative phase of the interacting waves slips by 180°. So, along the propagation direction inside the nonlinear medium, the

waves step in and out of phase periodically, resulting in exchange of energy back and forth. This periodic oscillation along the propagation length is shown in *Fig.* 2.2. To offset the phase-mismatch, two techniques are widely used in nonlinear optics:

1. Birefringent phase-matching (BPM)
2. Quasi-phase-matching (QPM)

2.4.1 Birefringent phase-matching (BPM)

This is the most commonly known and widespread technique for achieving phase-matching in which the birefringence of a nonlinear crystal is exploited to offset the phase-velocity-mismatch. Birefringence is the property of anisotropic optical materials, where the refractive index of the material depends on the polarisation and propagation direction of light. When the interacting waves at different frequencies are polarised differently, their corresponding phase velocities can be adjusted, such that the index difference due to dispersion is balanced through the birefringence. In anisotropic materials, there exists normal modes of propagation for each frequency. These waves are orthogonally polarised and travel with different phase velocities. One of these waves, called *ordinary* wave, experiences a constant index of refraction independent of the direction of propagation known as *ordinary* index (n_o). The second wave, experiences different refractive index depending upon the direction of propagation, hence is called as *extraordinary* index (n_e). The angle θ describes the direction of propagation relative to one of the principal axes of the medium. Depending upon the number of optical axes, a birefringent crystal can be divided into two categories, *uniaxial* (single optical axis) and *biaxial* crystals (two optical axes). With θ being the angle between wave-vector and the optic axis, the refractive index of *extraordinary* wave is given by

$$\frac{1}{n_e^2(\theta)} = \frac{cos^2\theta}{n_o^2} + \frac{sin^2\theta}{\bar{n_e}^2} \tag{2.17}$$

From the above equation, one can deduce the following:

$$at \;\; \theta = 0^\circ \;\; ; \;\; n_e(0) = n_o \tag{2.18}$$

$$at \;\; \theta = 90^\circ \; ; \;\; n_e(90) = \bar{n_e} \tag{2.19}$$

Depending upon the polarisation of the interacting waves, the BPM can be classified into two types known as *type I* and *type II*. For OPO - *type I* phase-matching refers to the situation where the *signal* and *idler* have the same polarisations, whereas in *type II* phase-matching, the *signal* and *idler* have orthogonal polarisations. For SHG process - in *type I* phase-matching, the *pump* wave has either *ordinary* or *extraordinary* polarisation, while the generated SHG field is orthogonal to the input *pump* field *(ee→o or oo→e)*. In *type II* phase-matching, the *pump* is polarised in such a way that one of its orthogonal components is *ordinary* and the other is *extraordinary (eo→e or oe→o)*.
The birefringence Δn is defined as $n_e - n_o$. Depending upon the magnitude of this Δn, anisotropic crystals are divided into *positive* ($\Delta n > 0$) and *negative* ($\Delta n < 0$) uniaxial crystals, as shown in the *Fig.* 2.3.

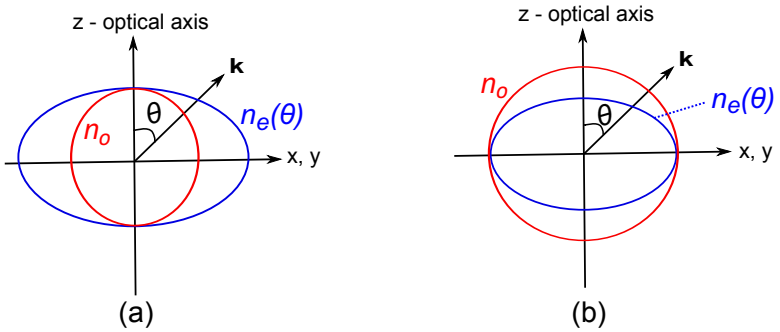

Figure 2.3: Index ellipsoid for (a) positive and (b) negative uniaxial crystal.

Also depending upon the angle θ with respect to the optical axis, the phase-matching is categorised into two types.

1. Non-critical phase-matching (NCPM)
2. Critical phase-matching (CPM).

If $\theta = 90°$, it is called non-critical phase-matching (NCPM), otherwise it is known as critical phase-matching (CPM). Whenever the angle θ between the propagation direction and the optical axis has a value other than 90°, the Poynting vector **S** and the propagation vector **k** are not parallel for *extraordinary* rays. As a result, *ordinary* and *extraordinary* rays with parallel propagation vectors quickly diverge from one another as they propagate through the crystal. This phenomenon is known as *spatial walk-off (or) Poynting vector walk-off.* This effect limits the spatial overlap of the two interacting waves and decreases the efficiency of any nonlinear frequency conversion process. The walk-off angle (ρ) is given by

$$\tan \rho = \frac{-1}{n_e} \frac{dn_e}{d\theta} \tag{2.20}$$

Thus, after a distance, denoted as the walk-off distance, the interacting beams will be completely separated from each other, causing a reduction in the intensity of the generated beam. Further, if the crystal length is much longer than the walk-off distance or aperture length (l_a), walk-off will severely hamper the growth of the generated beams. The relation between the walk-off angle ρ and aperture length l_a is given by

$$l_a = \frac{\sqrt{\pi}\omega}{\rho} \tag{2.21}$$

where ω is the radius of the Gaussian beam spot of *signal* or *idler* in an OPO.

The difference between the non-critical and critical phase-matching is depicted in the *Fig.* 2.4. In the case of critical phase-matching, a small deviation from perfect phase-matching will reduce the conversion efficiency considerably. While in the case of non-critical phase-matching, a small angle mismatch (induced by small angle tuning of the crystal) will only have minor effect on the conversion efficiency.

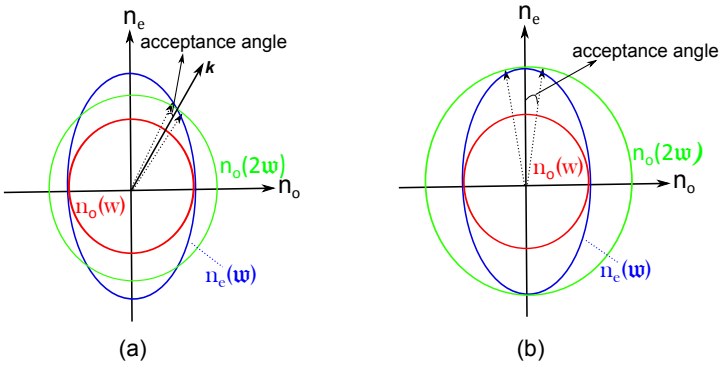

Figure 2.4: Phase-matching in a uniaxial birefringent crystal for a SHG process showing the distinction between (a) critical and (b) non-critical phase-matching.

The acceptance angle $\delta\theta$ is defined as follows: If the phase-matching angle θ_{PM} is tuned to $\theta_{PM} + \delta\theta$, the intensity of the generated field shall drop to half of its peak intensity, i.e., the acceptance angle gives the deviation from the phase-matching angle θ_{PM} for which the generated field intensity decays to half of its peak value. This deviation is characterized by the quantity $\Delta kL/2$ for which the function $\text{sinc}^2(\Delta kL/2) = 0.5$ for $\theta = \theta_{PM} + \delta\theta$ with L being the crystal length.

Thus NCPM is always advantageous over critical PM for two reasons. First, it is less sensitive to the acceptance angle and second, the walk-off angle is zero, which reduces the constraint on beam size and the effective crystal length.

In biaxial crystals, there exists two optical axes, which by convention are taken to lie in the optical xz plane. The optical axes are situated symmetrically about the z-axis as shown in *Fig.* 2.5. The optical axes makes an angle of Ω with respect to the z-axis, given by

$$\sin\Omega = \frac{n_z}{n_y}\sqrt{\frac{n_y^2 - n_x^2}{n_z^2 - n_x^2}} \tag{2.22}$$

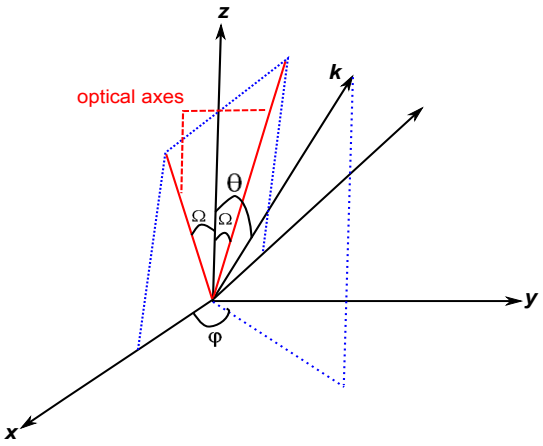

Figure 2.5: Crystallographic coordinate system for a biaxial crystal.

By convention, it is taken as $n_z > n_y > n_x$ and for the light propagating along the optical axes, the refractive index is independent of polarisation. The refractive indices of the two allowed modes of propagation are determined by solving the Fresnel's equation given by:

$$\frac{sin^2\theta cos^2\phi}{n^{-2} - n_x^{-2}} + \frac{sin^2\theta sin^2\phi}{n^{-2} - n_y^{-2}} + \frac{cos^2\theta}{n^{-2} - n_z^{-2}} = 0 \tag{2.23}$$

where θ is the angle with respect to the z-axis and ϕ is the azimuthal angle with respect to x-axis. More detailed description about the phase-matching for various nonlinear frequency processes in biaxial crystals can be found in [42].

2.4.2 Quasi-phase-matching (QPM)

Quasi-phase-matching is an alternative technique to birefringent phase-matching postulated by Armstrong [6] in 1962 for compensating the phase velocity mismatch in various frequency conversion processes. For birefringent materials, even though we have the major problem of walk-off, it is still possible to fulfil both the energy conservation and phase-matching under certain conditions since the refractive index depends on the polarisation of the nonlinear media. In addition to the phase-matching conditions to be satisfied for various frequency conversion processes, efficient nonlinear conversion also requires large

nonlinear optical coefficient (d_{eff}). But there exists many nonlinear materials in which the phase-matching and the energy conservation can be fulfilled simultaneously but the largest nonlinear coefficient could not accessed for frequency conversion processes. As an example, is the well known negative birefringent nonlinear material $LiNbO_3$. Its largest nonlinear coefficient is d_{33}, which implies that the polarisations of the three interacting beams need to be the same. In birefringent phase-matching, this coefficient cannot be accessed either by *type I* or *type II* phase-matching. Thus, an alternate method is necessary to access the largest nonlinear coefficient and this is made possible through the process called quasi-phase-matching.

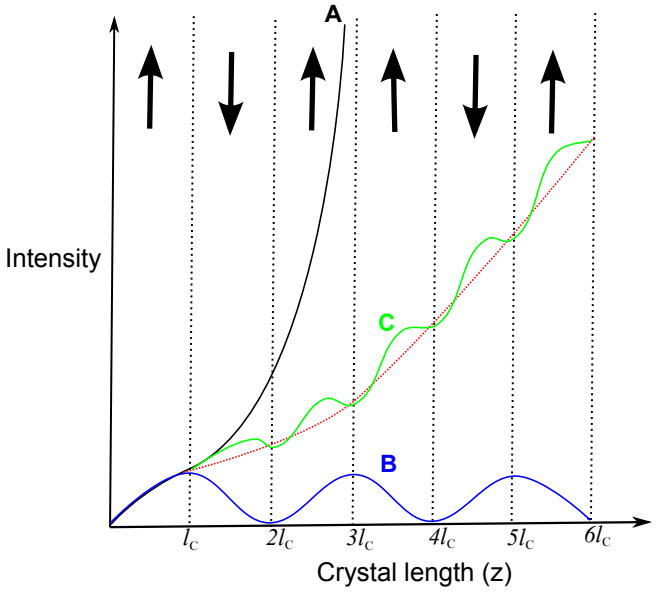

Figure 2.6: Quasi-phase-matching in a periodically poled nonlinear optical material. (A) Perfect phase-matching, (B) Non-phase-matched, and (C) Quasi-phase-matching.

In QPM, the nonlinear coefficient is modulated using a technique called periodical poling, as shown in *Fig.* 2.6. Using this technique, the nonlinear coefficient is modulated with a period twice the coherence length given by $l_c = \frac{\pi}{\Delta k}$. In other words, the nonlinear coefficient changes its sign after each coherence length. Thus, the polarisation is shifted by 180 ° after each coherence length, making the interacting waves propagate in phase along the

crystal length. The relative phase is adjusted by modulating the sign of the nonlinear coefficient of the medium with a period given by $\Lambda = 2l_c$.
From *Fig.* 2.6, although the efficiency in a QPM process is lower than the perfect phase-matching in birefringent materials, QPM is not restricted to *type I* or *type II* phase-matching. Especially with the type 0 (e→ee) process, the largest nonlinear coefficient (d_{33}) for many nonlinear materials can be accessed, which inturn enhances the conversion efficiency to a greater extent. The nonlinear coefficient in the QPM process is given by the relation:

$$d = \frac{2d_{eff}\sin(Dm\pi)}{m\pi} \tag{2.24}$$

where m is the order of QPM and D is the duty cycle ($D = l/\Lambda$).
Another advantage is that QPM usually operates in non-critical phase-matching and hence walk-off angle is zero (as all the involved polarisations are parallel to each other).

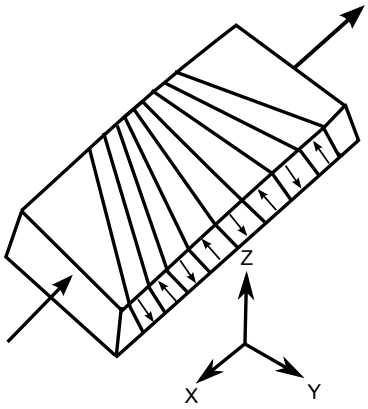

Figure 2.7: Fan-out grating design.

With the development of crystal growth technology of periodic poling since 1990's, periodically poled lithium niobate (popularly known as PPLN) has become most commonly used nonlinear material for various frequency conversion process throughout its transparency range from 400 *nm* in the *visible* region to 5400 *nm* in the *mid-infrared* region. Nowadays fan-out grating poling in the PPLN is used for many OPO applications ever since the design was first used by P. E. Powers [43] in 1998.

The design of the fan-out grating is shown in *Fig.* 2.7. Fabrication of quasi-phase-matched crystals is done by periodic reversal of the domains in ferroelectric materials such as $LiNbO_3$ and $LiTaO_3$. By applying a strong periodic electric fields ($\sim$21 kV/mm), the spontaneous electronic polarisation of these materials are inverted at room temperature.

2.5 Ultrafast synchronously-pumped optical parametric oscillators

An OPO essentially consists of a nonlinear medium deployed within an optical cavity pumped by a suitable laser source. In analogy, an OPO can be treated as a tunable coherent source but is not a laser by itself. Because in a laser, transitions are governed by the population inversion through energy storage and the tuning depends on bandwidth of the electronic or atomic transitions. On the other hand, in OPOs, there is no storage of energy and the gain is instantaneous. Also, the wavelength tunability is attained by the phase-matching condition in conjunction with the energy conservation laws. Due to this instantaneous nature of the parametric gain, operation of ultrafast pulse OPOs is attainable only under synchronous pumping conditions. The temporal window of the pump pulses is very narrow to allow a sufficient number of round-trips for the build up of the parametric waves over the pump pulse envelope, even for OPO cavity lengths as short as a few millimetres. To circumvent this difficulty, the OPO cavity length is matched exactly to the repetition rate of the pump laser, and hence is known as synchronously-pumped OPO (SPOPO). Thus, the round-trip transit time in the OPO cavity is equal to the repetition period of the pump pulse train. In this way, the resonated parametric waves experience amplification after each round trip through the nonlinear crystal. In practice, the most widely used solid-state KLM Ti:sapphire *fs* laser has a repetition rate (RR) typically between 76 to 100 *MHz*. This corresponds to a SPOPO standing wave cavity length ($L = c/2RR$) of 197.4 cm to 150 cm, respectively.

SPOPOs offer a number of advantages over the conventional mode-locked lasers. In addition to the broad wavelength tuning, the output pulses from SPOPOs exhibit lower timing jitter relative to the pump pulses. This makes SPOPOs highly suitable for many applications like time resolved spectroscopy, confocal microscopy, pump-probe spectroscopy, etc. The first report of a *fs* SPOPO was made by Edelstein [12] in 1989, based on KTP as the nonlinear medium pumped by a colliding pulse-mode-locked dye laser. However, progress in *fs* SPOPO technology has experienced an unprecedented upsurge with the invention of the Kerr-lens-mode-locked (KLM) Ti:sapphire laser. In today's technology, ultrafast *fs* SPOPOs pumped by solid-state Ti:sapphire laser represent the most advanced class of reliable and robust tunable coherent sources. In this thesis, the main focus or theme is projected in the direction of all solid-state Ti:sapphire-pumped SPOPOs and their potential impact for accessing various spectral regions from *near to mid-infrared*.
The configuration of a commercially available solid-state KLM Ti:sapphire laser used for pumping various SPOPOs is shown in the *Fig.* 2.8.

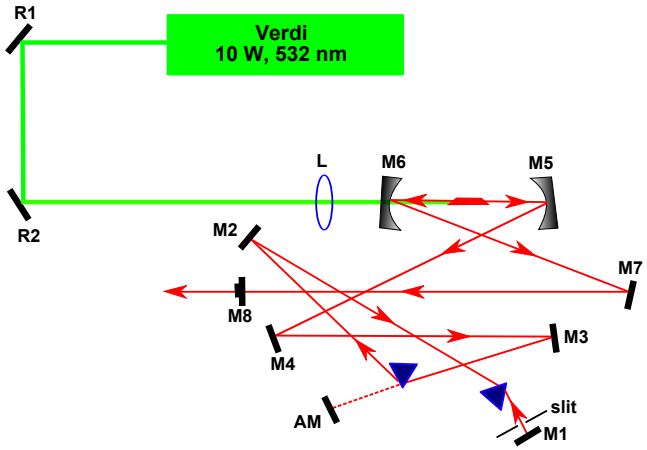

Figure 2.8: Schematic of a commercially available solid-state KLM Ti:sapphire laser system used to pump the SPOPOs.

The KLM Ti:sapphire has a repetition frequency of 76 *MHz* and is tunable from $700-980$ *nm*. At a central wavelength of 800 *nm*, it delivers an average power of 1.2 W with a spectral bandwidth of 7 *nm* and has a measured interferometric autocorrelation time duration of $\sim$150 *fs*. Also the schematic

of the Ti:sapphire pumped SPOPO is shown in the *Fig.* 2.9 in a simple standing-wave V-cavity design.

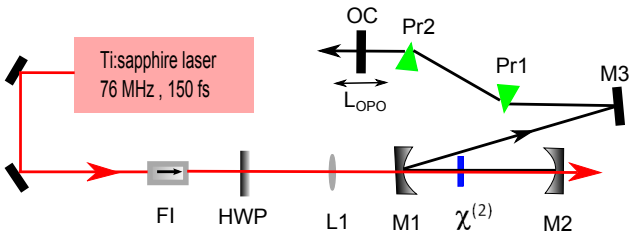

Figure 2.9: Schematic of the SPOPO in standing-wave V-cavity design. The cavity length of the SPOPO is equal to the repetition rate (76 *MHz*) of the pump laser source.

2.6 Gain and amplification in parametric devices

In case of nonlinear optical parametric process, the single-pass amplification in a crystal of length L, is given by

$$G_s(L) = \frac{E_s^2(L)}{E_s^2(o)}) - 1 \simeq \Gamma^2 L^2 \frac{\sinh^2[\Gamma^2 L^2 - (\Delta k L/2)^2]^{1/2}}{[\Gamma^2 L^2 - (\Delta k L/2)^2]} \tag{2.25}$$

where Δk is the phase-mismatch. With I_p as the pump intensity, the gain factor Γ is defined as

$$\Gamma^2 = \frac{8\pi^2 d_{eff}^2}{c\epsilon_o n_s n_i n_p \lambda_s \lambda_i} I_p \tag{2.26}$$

Under perfect phase-matching $\Delta k = 0$, the single-pass amplification in *equation* 2.25 reduces to

$$G_s(L) = \sinh^2(\Gamma L) \tag{2.27}$$

For low gain, $\Gamma L \leq 1$, the *equation* 2.27 can be approximated to

$$G_s(L) = \Gamma^2 L^2 \tag{2.28}$$

and for high gain, $\Gamma L >> 1$, the *equation* 2.27 becomes

$$G_s(L) = \frac{1}{4} e^{2\Gamma L} \tag{2.29}$$

Thus, one can infer that under perfect phase-matching, the single pass amplification is proportional to square of the crystal length (L^2) in case of low gain and increases exponentially in case of high gain.

2.7 Design issues of the OPO

While designing OPOs, the underlying principle is the maximisation of parametric gain through suitable choice of nonlinear medium. Other important parameters are pump laser, favourable phase-matching conditions for obtaining the wavelength tunability, cavity design and optimum focusing. Each of the above mentioned parameters play a crucial role in the process of developing an OPO to make it operate at optimum performance.

2.7.1 Nonlinear material

The selection of the nonlinear material is the heart of the whole OPO system. This selection is governed by many factors such as broad transparency range, phase-matchability in the wavelength of interest, high optical damage threshold, low spatial and temporal walk-off, availability in bulk form, low loss, and if possible, the capability of NCPM. Another important material parameter is the large nonlinear coefficient (d_{eff}), because the parametric gain is directly proportional to the square of the nonlinear coefficient. One often describes the efficiency of the nonlinear medium in terms of *figure of merit (FOM)* defined as

$$FOM \equiv \frac{d_{eff}}{\sqrt{n_p n_s n_i}} \tag{2.30}$$

However, the *FOM* is a convenient parameter to compare nonlinear media for a particular spectral range, but it neglects the effects of absorption and group-velocity mismatch.

2.7.2 Pump laser

The selection of the pump laser plays a major and crucial role in the process of developing any OPO. Because for each nonlinear material, depending upon the phase-matching conditions and for the wavelengths of interest to be generated, it may require a pump source operating at a different wavelength other than the commercially existing lasers. In this case, other alternative methods like cascaded OPOs have to be deployed in which the output of an OPO is used to pump the next consecutive OPO. One obvious criterion is that the pump laser should lie within the transparency range of the nonlinear medium. The pump source must also have sufficient peak intensity (I_p) and low beam divergence to obtain the optimum focussing.

2.7.3 Phase-matchability

The phase-matching behaviour and tuning characteristics of the material can be derived from the conservation of *electromagnetic* momentum or the phase-matching condition ($\Delta k = k_p - k_s - k_i = 0$) by using the dispersion relations or Sellmeier equations of the nonlinear materials. Also, since the parametric gain has its maximum value at $\Delta k = 0$, the generated wavelengths are determined by the energy conservation, defined as $\omega_p = \omega_s + \omega_i$. And the wavelength tuning is achieved commonly by changing one of the parameter of the nonlinear crystal like angle, temperature, grating, or even by varying the pump wavelength.

2.7.4 Cavity design

Different cavity designs can be configured while deploying the SPOPOs as shown in the *Fig.* 2.8. Extreme care should be taken to determine the stability region of the cavity and for mode-matching the pump beam and the oscillating signal inside the optical resonator. Also due to synchronous pumping, precision within a few micrometers plays a vital role in the process of developing SPOPOs. In general, the optical cavities can be classified into two types.

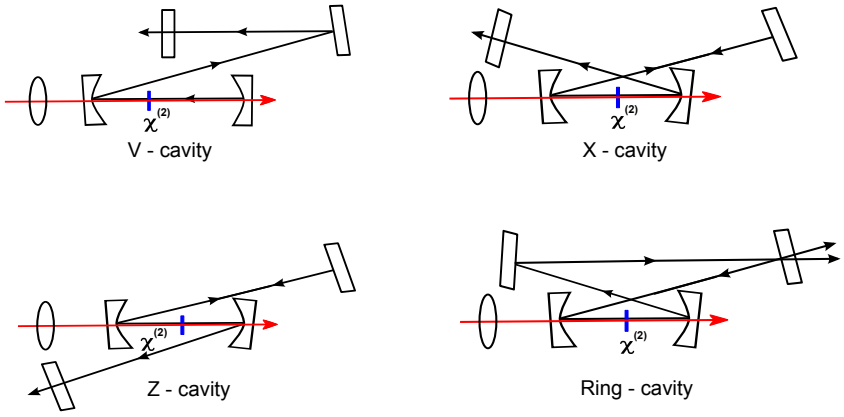

Figure 2.10: Different cavity designs for deploying the SPOPOs. The designs of V, X, Z are known as standing-wave cavities while the ring design is known as travelling-wave cavity.

First one is the standing-wave cavity like V, X, and Z. In these designs, the oscillating fields transits twice through the nonlinear medium in a round trip. The second one is travelling-wave ring cavity in which the oscillating field transits only once through the nonlinear crystal per round trip thus providing extra reduction in the losses due to absorption and crystal coatings. One particular advantage of using ring cavity design is that it avoids the optical feedback into the laser system.
Also for attaining optimum performance of an OPO, the confocal parameter of the pump beam, b_p, which is twice the Rayleigh range, needs to be equal to that of the resonating beam b_s ($\sim b_p$). For more information on stability criteria, ABCD and transformation matrices, one can refer to *Laser electronics* [44] by Verdeyen and *the classic paper* of Kogelnik and Li [45].

2.8 Dispersion characteristics

Dispersion characteristics like group velocity, group velocity mismatch (GVM) and group velocity dispersion (GVD) play very important role in the ultrafast *fs* regime [46], [47].

2.8.1 Group velocity

An ultrafast pulse can be imagined as quasi-monochromatic, and hence is composed of several frequencies clustered about some central frequency ω_o that can be considered as the *carrier frequency* of the wave. Under the condition where dispersion in the refractive index cannot be ignored with the pulse propagation inside the medium, the concept of unique phase velocity becomes meaningless, and the pulse itself should be treated as superposition of monochromatic waves lying under a *carrier wave envelope*. This is characterised by the group velocity defined as

$$v_g = \frac{d\omega}{dk}|_{\omega_o} \tag{2.31}$$

The group velocity of a pulse propagating in a medium is defined as

$$v_g = \frac{c}{n - \lambda \frac{dn}{d\lambda}} \tag{2.32}$$

where c is the velocity of light in vacuum, n is the refractive index of the nonlinear medium, and λ is the central wavelength.

2.8.2 Group velocity mismatch (GVM)

In various nonlinear frequency mixing processes and devices such as SHG, SFG, DFG, OPO and OPA, two or more waves interact with each other while propagating through the nonlinear medium. Due to the dispersion of the nonlinear medium, different waves propagate at different group velocities and thus the interacting pulses will get completely separated after a certain distance in the medium. This physical temporal separation between the pulses thus causes a reduction in effective interaction length between the interacting waves. In *fs* regime, while propagating through a nonlinear medium, the quantitative evaluation of this temporal pulse separation with distance is characterised by group velocity mismatch (GVM). The GVM is

defined as

$$GVM = |(\frac{1}{v_{g,i}} - \frac{1}{v_{g,j}})|^{-1} \tag{2.33}$$

where $v_{g,i}$ and $v_{g,j}$ are the group velocities of the interacting waves i and j, respectively.

The GVM dictates the phase-matching bandwidth and the maximum effective interaction length that can be used for any frequency conversion process. As an example, we derive here the dependence of phase-matching bandwidth on the GVM in a SHG process [48].

2.8.3 Phase-matching bandwidth

Consider that the pulse at fundamental wavelength λ_o is propagating through a nonlinear crystal and the generated SHG is at wavelength $\lambda_o/2$. Since both the fundamental and SHG waves have different group velocities, there will be a mismatch between these two interacting waves. The two pulses cease to overlap after propagating some distance L inside the crystal. We can calculate the bandwidth of the SHG pulses when GVM is taken into consideration. Assuming that a very short pulse enters the crystal, the time lapse for the SHG pulse, δt, can be determined by the difference between the time durations of the fundamental and SHG waves given by:

$$\delta t = \frac{L}{v_g(\lambda_o/2)} - \frac{L}{v_g(\lambda_o)} = L\ GVM \tag{2.34}$$

where GVM $= \dfrac{1}{v_g(\lambda/2)} - \dfrac{1}{v_g(\lambda)}$. Rewriting this equation in terms of group velocity defined as

$$v_g(\lambda) = \frac{c/n(\lambda)}{1 - (\lambda/n(\lambda))n'(\lambda)} \tag{2.35}$$

and substituting for the group velocities in equation 2.34, we get

$$\delta t = L\frac{n(\lambda_o/2)}{c}[1 - \frac{\lambda_o/2n'(\lambda_o/2)}{n(\lambda_o/2)}] - L\frac{n(\lambda_o)}{c}[1 - \frac{\lambda_o n'(\lambda_o)}{n(\lambda_o)}] \tag{2.36}$$

Now considering the fact that under perfect phase-matching, $n(\lambda/2) = n(\lambda)$, the above equation can be rewritten as

$$\delta t = \frac{L\lambda_o}{c}[n'(\lambda_o) - \frac{1}{2}n'(\lambda_o/2)] \tag{2.37}$$

Assuming that the second-harmonic pulse has a Gaussian intensity, for which $\delta t \delta\nu = 0.44$, in terms of wavelength it becomes

$$\delta t \delta\lambda = \delta t \delta\nu [\frac{d\nu}{d\lambda}]^{-1} = -0.44\frac{\lambda^2}{c} \tag{2.38}$$

The minus sign can be neglected since we are computing the bandwidth, which is inherently positive. So the phase-matching bandwidth can be written in terms of wavelength as follows:

$$\delta\lambda = \frac{0.44\lambda_o/L}{[n'(\lambda_o) - \frac{1}{2}n'(\lambda_o/2)]} \tag{2.39}$$

Therefore, from the above equation, we can infer the following:
The phase-matching bandwidth $\delta\lambda$, is inversely proportional to the length of the nonlinear crystal.
Since an ultrashort pulse can have extremely broad bandwidth (as an example a 10 *fs* pulse centred at 800 *nm* will have a bandwidth of ∼100 *nm*), to achieve efficient phase-matching for the entire bandwidth of the pulse, it is necessary to use extremely thin (as thin as 5 μm) SHG crystals.
Also, recalling from *equation* 2.28 the parametric gain of the phase-matched process is directly proportional to L^2, so a very thin crystal yields a lower output intensity or conversion efficiency.
Thus in the ultrafast fs *regime, there always exists a trade-off between efficiency and bandwidth.*
The phase-matching bandwidth can also be computed in frequency domain by expanding phase-mismatch (Δk) as a function of wavelength in Taylor's series expansion [48].

2.8.4 Effective interaction length

As mentioned before, the crystal length is limited by the GVM between the interacting waves. In case of OPO, we mainly take into account the GVM between the pump and the oscillating signal pulses. Assuming that the signal and pump have the similar pulse duration, τ_p, the effective crystal length can be computed by using the following formula:

$$L_{eff} \leq 2\ \tau_p \mid \Delta v_g \mid \leq 2\tau_p |\frac{1}{v_{g,p}} - \frac{1}{v_{g,s}}|^{-1} \tag{2.40}$$

where L_{eff} is the effective interaction length and $v_{g,p}$, $v_{g,s}$ are the group velocities of pump and signal pulses, respectively. The practical crystal length is normally longer than L_{eff}. In case of sub-100 *fs* pulses, the crystal length should be chosen as thin as $L_{eff}/4$ [49].
Thus in any nonlinear frequency conversion process, GVM between the interacting waves is an important factor leading to pulse broadening in ultrafast fs *regime. Together with the pump pulse duration and the expected signal pulse duration, it determines the effective interaction length.*

2.8.5 Spectral acceptance bandwidth

The spectral acceptance bandwidth (SAB) is another important parameter to be considered in ultrafast *fs* regime. The large spectral bandwidth of *fs* pulses imposes severe restrictions on the maximum usable crystal length. Also, it sets an upper limit to the maximum allowable pump bandwidth before the parametric gain severely diminishes. In general SAB depends on the type of phase-matching and the dispersion properties of the nonlinear medium. For an OPO, the SAB can be computed using the GVM between the interacting waves given by

$$\Delta\lambda L = \frac{\lambda^2}{2\pi c}\ \frac{2.78}{(GVM)_{i,j}} \tag{2.41}$$

SAB has the units of *nm.cm*. *Thus, the SAB provides the information about the maximum usable length of the nonlinear medium and the maximum allowed pump spectral bandwidth for attaining optimum parametric gain in a frequency conversion process.*

2.8.6 Group velocity dispersion (GVD)

When dispersion cannot be ignored, the propagating pulse will no longer have the simple form and the dispersion will cause the pulse amplitude to decrease and spread out as the pulse propagates. Then the group velocity itself will exhibit dispersion, which is characterised by the group velocity dispersion coefficient defined by

$$k'' = \frac{d(v_g)^{-1}}{d\omega} = \frac{d^2k}{d\omega^2} \tag{2.42}$$

In terms of wavelength, it can be written as :

$$k'' = \frac{\lambda^3 L}{2\pi c^2}\frac{d^2n}{d\lambda^2} \tag{2.43}$$

In ultrafast *fs* regime, GVD is an important parameter to evaluate the dispersion characteristics of gain media or in this case the nonlinear medium to be deployed inside the optical resonator. Based on GVD, we can estimate the degree of pulse broadening, and thus can design a proper dispersion compensation mechanism. Also, the pulse broadening induced by the GVD, when the pulses propagate through a nonlinear material of length (z), is given by

$$\tau_p(z) = \tau_o\sqrt{1 + (\frac{z}{z_d})^2} \tag{2.44}$$

where τ_o is the original pulse duration before entering the dispersive medium, τ_p is the pulse duration after passing through the dispersive material, and z_d is the characteristic length defined as

$$z_d = \frac{1}{4ln2}\frac{\tau_0^2}{\frac{d^2k}{d\omega^2}} \tag{2.45}$$

Thus, control of dispersion is an important key to obtain short and transform-limited pulses.

Two commonly used methods for manipulating the GVD are prism sequence and grating pairs. Both of these methods involve optical components with angular dispersion. Alternative methods include chirped mirrors [50] or wedges made up of materials which inherently possesses the negative GVD, can also be used for GVD compensation. Here we describe the dispersion compensation using a prism pair [51], [46] which is the most common method used in ultrafast optics. Compared to gratings, the main advantage of using prisms is the low loss, which makes them suitable for dispersion compensation control inside the optical resonators, as well as easy tuning of the sign and magnitude of the dispersion.

2.8.7 GVD compensation using a prism pair

The configuration consists of a pair of anti-parallel prisms. The various frequencies in the collimated input beam emerge from the first prism with different angles, but travel in parallel directions after the second prism. While the angular dispersion between the prisms contributes anomalous or negative GVD, the passage through the prism material is also a source of normal dispersion. The overall dispersion can be tuned by translating one of the prisms in a direction perpendicular to its base, which varies the material path length without affecting the angular dispersion.

As shown in the *Fig.* 2.9, the first prism is oriented at Brewster angle for the beam to incident at its apex (P_o). The dispersed beam after the first prism is made to be incident at the apex of the second prism (Q_o), which is also oriented at Brewster angle.

Both the prisms are arranged in such a manner that their apexes are aligned in opposite direction. The angular dispersion occurring between the two prisms is designated by the angle $\alpha(\lambda)$, which is a function of wavelength. Since $\alpha(\lambda)$ is very small, the wavefront at $\overline{P_1P_2}$ has approximately the same phase at $\overline{P_1'P_2'}$. The optical path length of $\overline{P_0P_1}$ corresponds to the shortest spectral component of the incident beam. At point P_1, the optical path

length of any other spectral components can be expressed as

$$l(\lambda) = \overline{P_0P_1}cos\alpha, \tag{2.46}$$

and the phase delay can be written as :

$$\psi_\alpha = \frac{2\pi}{\lambda}\overline{P_0P_1}cos\alpha \tag{2.47}$$

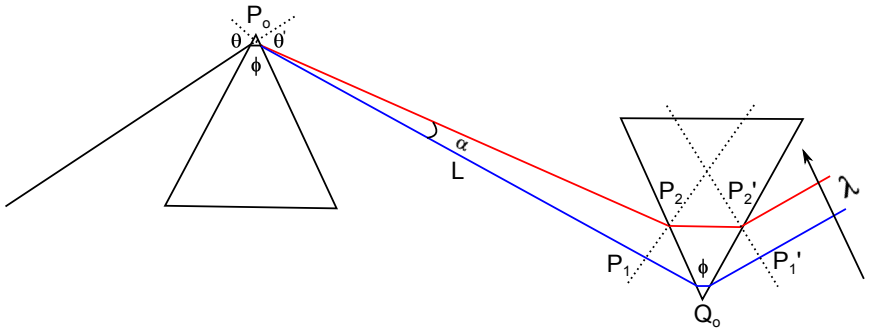

Figure 2.11: Schematic of the prism pair for GVD compensation in ultrafast *fs* regime.

As α is very small and the distances between the two prisms, $\overline{P_0P_1} >> \overline{P_1Q}$, $\overline{P_0P_1}$ can be approximated to the distance between the prisms (L), and the above equation can be rewritten as

$$\psi_\alpha = \frac{2\pi}{\lambda}Lcos\alpha = \frac{\omega}{c}Lcos\alpha. \tag{2.48}$$

Then, the GVD induced by the angular dispersion by prisms can be derived from following *equation*.

$$\frac{d^2\psi_\alpha}{d\omega^2} = -\frac{L}{c}\{\sin\alpha[2\frac{d\alpha}{d\omega} + \omega\frac{d^2\alpha}{d\omega^2}] + \omega\cos\alpha(\frac{d\alpha}{d\omega})^2\} \tag{2.49}$$

Since α is very small, we can assume that $\sin\alpha \sim 0$ and $\cos\alpha \sim 1$.

Then the GVD can be rewritten as

$$\frac{d^2\psi_\alpha}{d\omega^2} = -\frac{\omega L}{c}(\frac{d\alpha}{d\omega})^2 \tag{2.50}$$

From the above equation, we can infer that the GVD induced by the prism pair is negative, and thus can be used to compensate the positive GVD induced by the nonlinear gain medium.
To compute the value of $(\frac{d\alpha}{d\omega})$, consider

$$\frac{d\alpha}{d\omega} = \frac{d\alpha}{dn}\frac{dn}{d\alpha} \quad and \quad \frac{dn}{d\alpha} = -\frac{\lambda^2}{2\pi c}\frac{dn}{d\lambda} \tag{2.51}$$

where n is the refractive index of the prism material. To calculate $\frac{d\alpha}{dn}$, consider the geometry of the prism as shown in $Fig.$ 2.10.

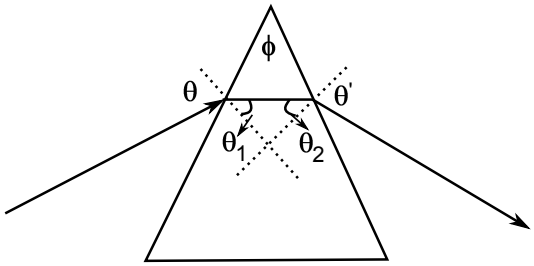

Figure 2.12: Geometry of a single prism showing the apex angle, angle of incidence and refracted rays.

The following relationships can be written from the geometry of the prism

$$\sin\theta = n\sin\theta_1 \tag{2.52}$$

$$\sin\theta' = n\sin\theta_2 \tag{2.53}$$

$$\theta 1 + \theta 2 = \phi \tag{2.54}$$

From the above equations we can obtain

$$\cos\theta\frac{d\theta}{dn} = \sin\theta_1 + n\cos\theta_1\frac{d\theta_1}{dn} \tag{2.55}$$

$$\cos\theta' \frac{d\theta'}{dn} = \sin\theta_2 + n\cos\theta_2 \frac{d\theta_2}{dn} \tag{2.56}$$

$$\frac{d\theta_1}{dn} = -\frac{d\theta_2}{dn} \tag{2.57}$$

Since θ is fixed, $\frac{d\theta}{dn} = 0$, we can derive that

$$\frac{d\theta_1}{dn} = -\frac{d\theta_2}{dn} = \frac{1}{n}\tan\theta_1 \tag{2.58}$$

and we can compute

$$\frac{d\theta'}{dn} = \frac{\sin\theta_2}{\cos\theta'} + \frac{\cos\theta_2}{\cos\theta'}\tan\theta_1 \tag{2.59}$$

Considering the Brewster angle of incidence at λ_o, $\theta' = \theta$ and $\theta_1 = \theta_2$, and substituting in equation 2.59, we get

$$\frac{d\theta'}{dn} \mid_{\lambda_o} = 2 \tag{2.60}$$

From *Figs.* 2.9 and 2.10, we can conclude that, $\frac{d\alpha}{dn} = \frac{d\theta'}{dn}$, and substituting in equation 2.50 for GVD, we get

$$\frac{d^2\psi_\alpha}{d\omega^2} \mid_{\lambda_o} = -4L\frac{\lambda^3}{2\pi c^2}(\frac{dn}{d\lambda})^2 \tag{2.61}$$

This is the final expression for the single-path negative GVD created by the prism pair.

As the beam propagate through some amount of the prism material, an additional GVD will be induced by the prisms, which should also be taken into account while calculating the total amount of GVD created by the prism pair. Assuming l to be mean amount of glass material path through the prisms, the positive GVD introduced by prism pair can be written as

$$\frac{d^2\psi_p}{d\omega^2} \mid_{\lambda_o} = \frac{\lambda^3 l}{2\pi c^2}\frac{d^2n}{d\lambda^2} \tag{2.62}$$

If we know the material of prisms, $\frac{d^2n}{d\lambda^2}$ can be determined. Therefore, we need to find the mean path length (l) of glass that the pulses propagate through. If the beam diameter is D, ϕ is the apex angle of the prisms, θ is the Brewster angle for the prism material and $\Delta\lambda$ is the spectral bandwidth of the incident pulses, the mean path length l is given by

$$l = \frac{2[D + \Delta\lambda L\frac{dn}{d\lambda}]\sin\frac{\phi}{2}}{\cos\theta} \tag{2.63}$$

Thus, the equation for the positive GVD induced by the prism pair can be written as

$$\frac{d^2\psi_p}{d\omega^2}\,|_{\lambda_o} = \frac{\lambda^3 l}{2\pi c^2}\frac{2[D + \Delta\lambda L\frac{dn}{d\lambda}]\sin\frac{\phi}{2}}{\cos\theta}\frac{d^2n}{d\lambda^2} \tag{2.64}$$

Therefore, the final expression for the total GVD can be written as

$$\frac{d^2\psi_T}{d\omega^2}\,|_{\lambda_o} = \frac{d^2\psi_\alpha}{d\omega^2}\,|_{\lambda_o} + \frac{d^2\psi_p}{d\omega^2}\,|_{\lambda_o} \tag{2.65}$$

Thus, the overall dispersion can be tuned by translating one of the prisms in a direction perpendicular to its base, which varies the material path length without affecting the angular dispersion.

2.9 SPOPO tuning methods

As mentioned before, the main strength of an OPO is its tunability. Traditionally known wavelength tuning methods are carried out by changing one of the parameter of the nonlinear medium like:

1. Angle
2. Temperature
3. Grating

Pump tuning can also be achieved by tuning the wavelength of pump laser source. *Besides the above traditional methods, in the ultrafast* fs *regime, the wavelength tunability can also be achieved by varying the cavity length of the SPOPO.*

2.9.1 Cavity length tuning

The cavity length tuning is mainly governed by the dispersion characteristics of the nonlinear material. The cavity length tuning can be understood as follows:
For the case of positive GVD, when the cavity length is increased, the signal wavelength has to shift to a longer wavelength side to maintain the synchronization with the pump pulse. Similarly, a shorter signal wavelength oscillates at a shorter cavity length.
For the case of negative GVD, the opposite process will take place. [33]

Chapter 3

Ti:sapphire-pumped femtosecond OPO based on BiB_3O_6

3.1 Motivation

Bismuth triborate, BiB_3O_6 or BIBO is a relatively new nonlinear material introduced by *Hellwig* [52] in early 2000. It possess unique and interesting optical properties for the frequency conversion processes in the *UV*, *visible* and *near-infrared (NIR)* spectral regions. It has an optical transmission from ∼280 nm in the UV to ∼2600 nm in the IR region. Owing to the non-centrosymmetric monoclinic space group C_2, BIBO is a biaxial crystal that exhibits versatile phase-matching characteristics in the three optical planes (xy, yz, xz). Although the UV transmission cut-off of BIBO is at longer wavelength (270 nm) than BBO (190 nm), it offers substantially larger effective nonlinearity (d_{eff}), measured to be as high as ∼3.7 pm/V, which is larger than the traditional nonlinear materials such as BBO and LBO, and is comparable to that of KTP. Also, it possesses low spatial walk off, broadband angle tuning at room temperature along with large angular and spectral acceptance bandwidths. This combination of properties makes BIBO highly attractive for various frequency conversion processes in the *visible*, UV and

in the *NIR* regions. Based on BIBO cut in yz plane, various ultrafast *fs* SPOPOs have been developed that have provided gap-free wavelength tuning all the way from 350 nm in the UV to the 2300 nm in the NIR spectral regions [37], [53], [54]. Nevertheless, these systems are pumped by the second harmonic of the KLM Ti:sapphire laser at ∼410 nm.
However, BIBO cut at θ=11.4°, (ϕ=90°) in the optical xz plane exhibits interesting optical properties for various parametric generation processes under *type I (e→oo)* phase-matching when pumped at 800 nm [55], [56]. In addition to high nonlinear coefficient d_{eff} (∼2.9 pm/V), it provides wide spectral acceptance bandwidth since the group velocity mismatch (GVM) between *signal* and *idler* pulses is very small and vanishes near degeneracy. In particular, for signal wavelength range of 1400 to 1600 nm, the $pump - signal$ and $pump - idler$ GVM are very close and is less than 11 fs/mm, giving rise to a $signal - idler$ GVM less than 1.2 fs/mm. Moreover, the group velocity dispersion (GVD) varies from 35 fs^2/mm at 1400 nm to nearly zero at degeneracy (1600 nm). These features make BIBO an attractive birefringent material for broadband parametric generation processes in the *NIR* region under *type I (e→oo)* phase-matching in the xz optical plane. By exploiting the above properties, we developed a *fs* SPOPO based on BIBO pumped directly by the KLM Ti:sapphire laser [39] at ∼800 nm.

3.2 Optical properties of BIBO

The phase-matching properties of the BIBO for parametric generation with different pump wavelengths are shown in $Fig.$ 3.1. BIBO cut at an angle of θ=11.4°, (ϕ=90°) shows the broadest phase-matching bandwidth and weakest angular dependence when pumped at 800 nm under *type I (e→oo)* interaction in optical xz plane. This allows broad and rapid tuning across the bandwidth from 1300-1600 nm without changing the crystal angle.

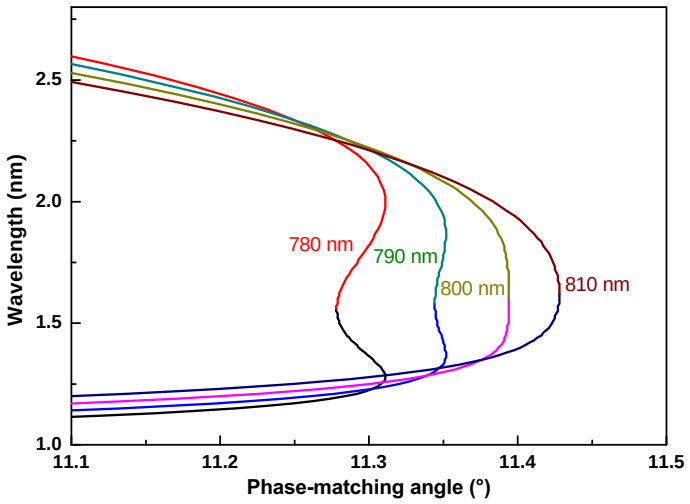

Figure 3.1: Phase-matching curves for parametric generation in BIBO cut at θ=11.4°, (ϕ=90°) in optical xz plane under *type I (e→oo)* interaction for different pump wavelengths.

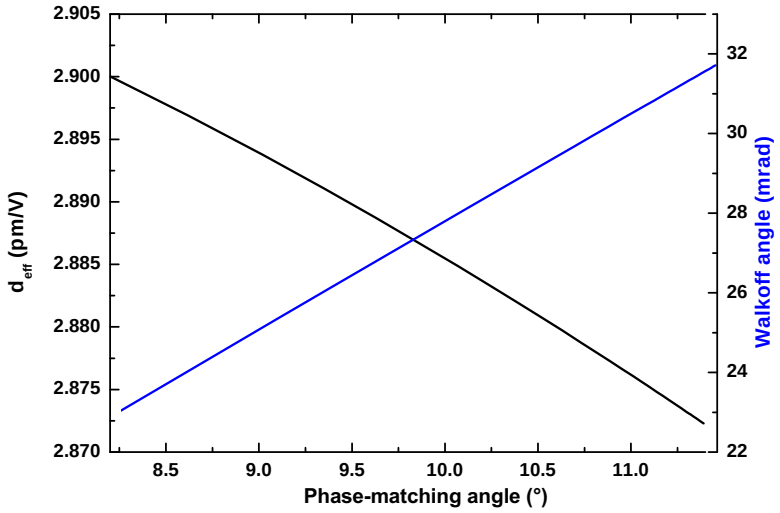

Figure 3.2: Variation of (d_{eff}) and walk-off angle with respect to phase-matching angle in BIBO under *type I (e→oo)* interaction.

The dependence of the nonlinear coefficient and the walk-off angle with respect to the phase-matching angle and the signal wavelength in the optical

xz plane under *type I* ($e \rightarrow oo$) interaction are shown in *Fig.* 3.2 and 3.3 respectively. BIBO possesses an effective nonlinear coefficient of $\sim$2.9 pm/V across the tuning range and has a minimal spatial walk-off of $\sim$32 *mrad*. These special properties makes it an excellent candidate to access the *NIR* region by pumping with the traditionally well-established KLM Ti:sapphire laser systems.

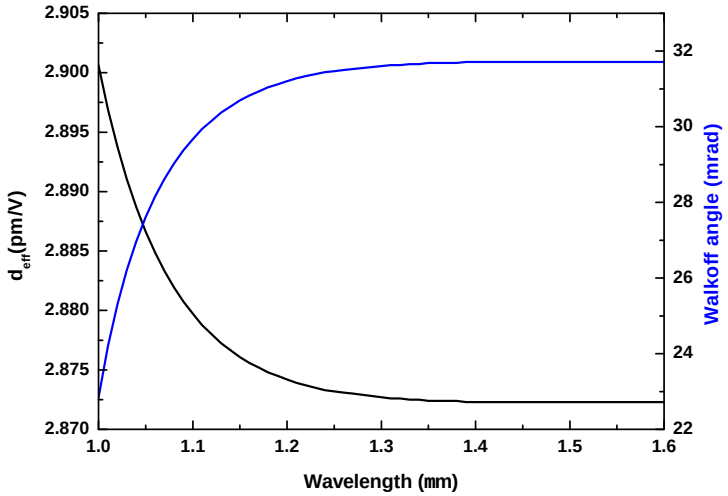

Figure 3.3: Variation of d_{eff} and walk-off angle with respect to signal wavelength.

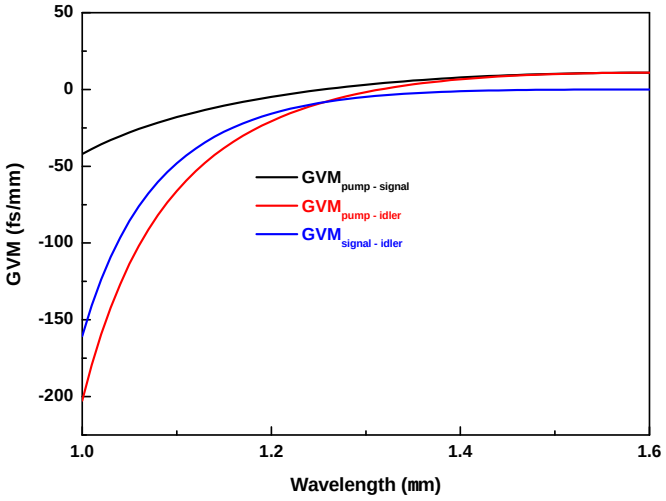

Figure 3.4: Variation of GVM between the interacting waves in the wavelength range of 1.0 to 1.6 μm.

The GVM between the $pump - signal$, $pump - idler$, and $signal - idler$ are plotted in $Fig.$ 3.4, while the group velocity dispersion (GVD) across the wavelength region between 1000 to 1600 nm is plotted in $Fig.$ 3.5. As one can notice that the group velocity mismatch between the $pump - signal$ and $pump - idler$ are almost equal across the spectral range from 1400 to 1600 nm. Additionally, the GVD is very small $\sim$35 fs^2/mm at 1400 nm and is approaching to zero at degeneracy as shown in $Fig.$ 3.5.

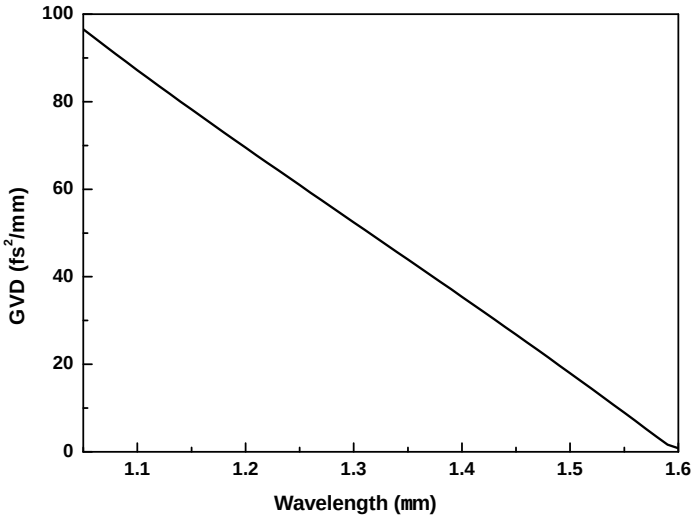

Figure 3.5: Group Velocity Dispersion of BIBO cut at θ=11.4°, (ϕ=90°) in optical xz plane under *type I (e→oo)* interaction in the *NIR* region.

3.3 Experimental Setup

The configuration of the SPOPO is shown in $Fig.$ 3.6. The pump laser provides transform-limited pulses of $\sim$150 *fs* at 76 *MHz* repetition rate centred at 800 nm. After the optical isolator, an average pump power of 1 W is available to pump the SPOPO. The SPOPO uses a 1.5-mm-long BIBO crystal cut for collinear *type I (e→oo)* phase-matching in the xz optical plane at an internal angle of θ=11.4°, (ϕ=90°) at normal incidence.

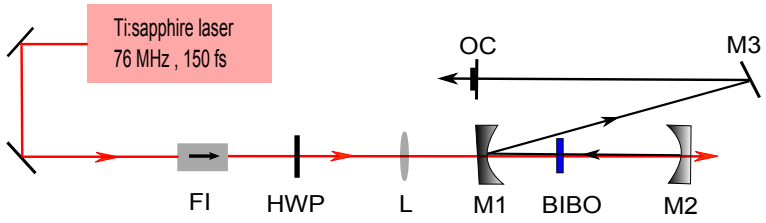

Figure 3.6: Configuration of the experimental setup. FI: Faraday isolator, HWP: Half-wave plate, L: Focussing lens, M1-3: Mirrors, OC: Output-coupler.

The end-faces have broadband anti-reflection (AR) coating (R<1%) for the pump wavelength over 800-840 nm and for signal wavelength over 1400-1600 nm. A lens L (f=8 cm) AR coated (R<1%) at 800 nm was used to focus the pump to a beam waist radius ω_o ~16 μm inside the BIBO crystal. A half-wave plate (HWP) provides the required extraordinary pump polarisation for *type I (e→oo)* interaction. The SPOPO is configured in a standing-wave cavity comprising two concave high reflectors, M1 and M2 (r=100 mm), one plane highly reflecting mirror, M3, and one plane mirror as a 5% output coupler (OC) mounted on a translation stage to allow variation of the cavity length with micrometre precision to match the cavity length of SPOPO to the pump laser repetition rate. The mirrors M1, M2, and M3 are highly reflecting (R>99%) over 1.40-1.58 μm and highly transmitting (T>90%) at 800 nm.

3.4 Results and Discussion

For wavelength tuning, we used two independent mechanisms, both resulting in signal coverage across the entire range of $1.42 - 1.56$ μm. In the first method, rapid and continuous tuning was achieved by adjustment of the cavity length delay without varying any other parameters, where the BIBO crystal was maintained at a fixed angle near normal incidence (θ=11.4°) and

the pump wavelength remained fixed at 800 nm. The static cavity length tuning is shown in $Fig.$ 3.7. In the second method, continuous tuning across the full range could be obtained by changing the pump wavelength, while keeping all other parameters including the crystal angle, cavity delay, and SPOPO alignment unaltered. The static pump wavelength tuning is also shown in $Fig.$ 3.8, and the corresponding output power through the 5% OC in both cases are also shown in $Figs.$ 3.7 and 3.8, respectively. Therefore, one can see that the SPOPO can be tuned across 1420-1560 nm, either by varying the SPOPO cavity length over 110 μm or by tuning the pump wavelength over 7.5 nm. Moreover, the performance of the SPOPO output power across the tuning range remains the same in both cases.

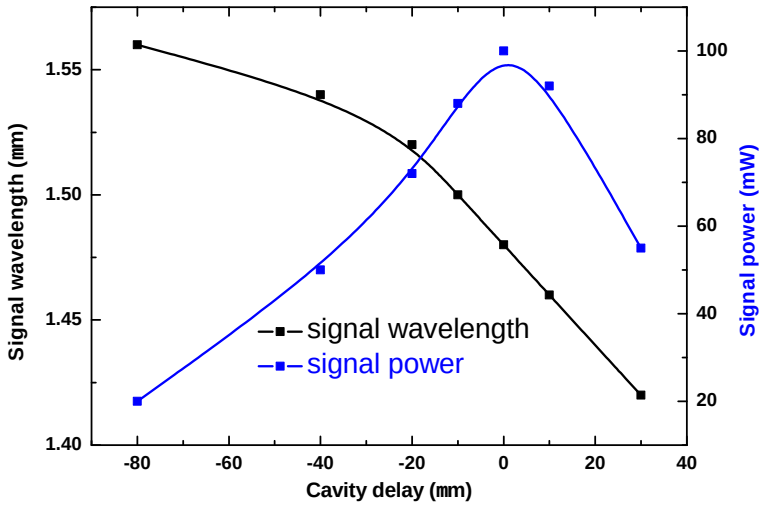

Figure 3.7: Cavity length tuning.

For a fixed pump wavelength, the cavity length tuning avoided the need for realignment of the SPOPO, resulting in simplified and rapid tuning. The total obtained tuning range for the signal wavelength is 1.42-1.56 μm, with a corresponding idler tuning from 1.64-1.83 μm. This tuning was only limited by the reflectivity of the SPOPO mirrors at the signal wavelength and the crystal coating. With optimized broadband coatings, we expect to be able to exploit the large phase-matching bandwidth, that could provide continuous coverage in the signal and idler from $\sim$1 μm to the IR transmission cut-off

in BIBO at $\sim$2.6 μm, using rapid static tuning. The signal power extracted through the 5% OC reaches 100 mW at the maximum available pump power of 1 W, corresponding to a conversion efficiency of 10%.

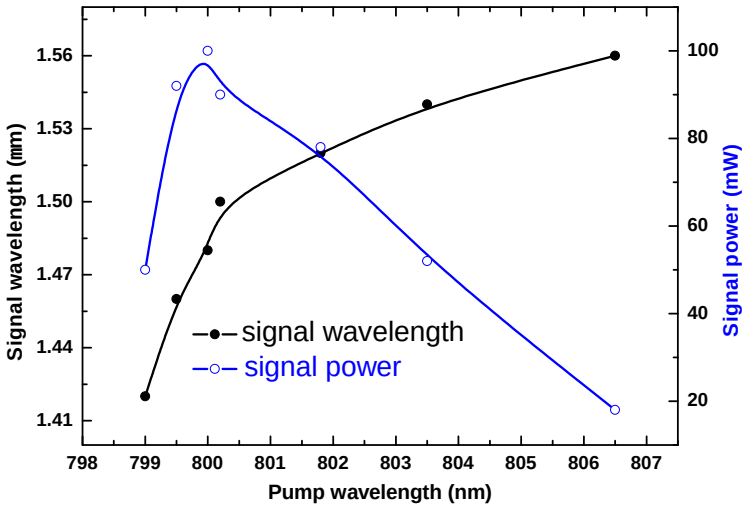

Figure 3.8: Pump wavelength tuning.

In the absence of more suitable output couplers, no attempt was made to maximize the extracted power. The pump depletion is 40% at the maximum input pump and the typical pump power threshold for the SPOPO with the 5% OC is 325 mW. The absence of saturation, no evidence of optical damage, and quite moderate level of depletion, suggest the possibility of increasing the output power by increasing the pump power as well as by optimizing the output coupling.

3.5 Spectral and Temporal measurements

Spectral measurements for the pump and the SPOPO output signal pulses were obtained using an optical spectrum analyser, whilst temporal characterization was performed using fringe-resolved intensity autocorrelation based on two-photon absorption in Si and $GaAsP$ photo-detectors for the signal and pump, respectively. A typical autocorrelation profile and spectrum of the

pump at 800 nm are shown in $Fig.$ 3.9(a), indicating 144 fs pulses, and thus confirming a time-bandwidth product of 0.47 (assuming $sech^2$ pulse shape).

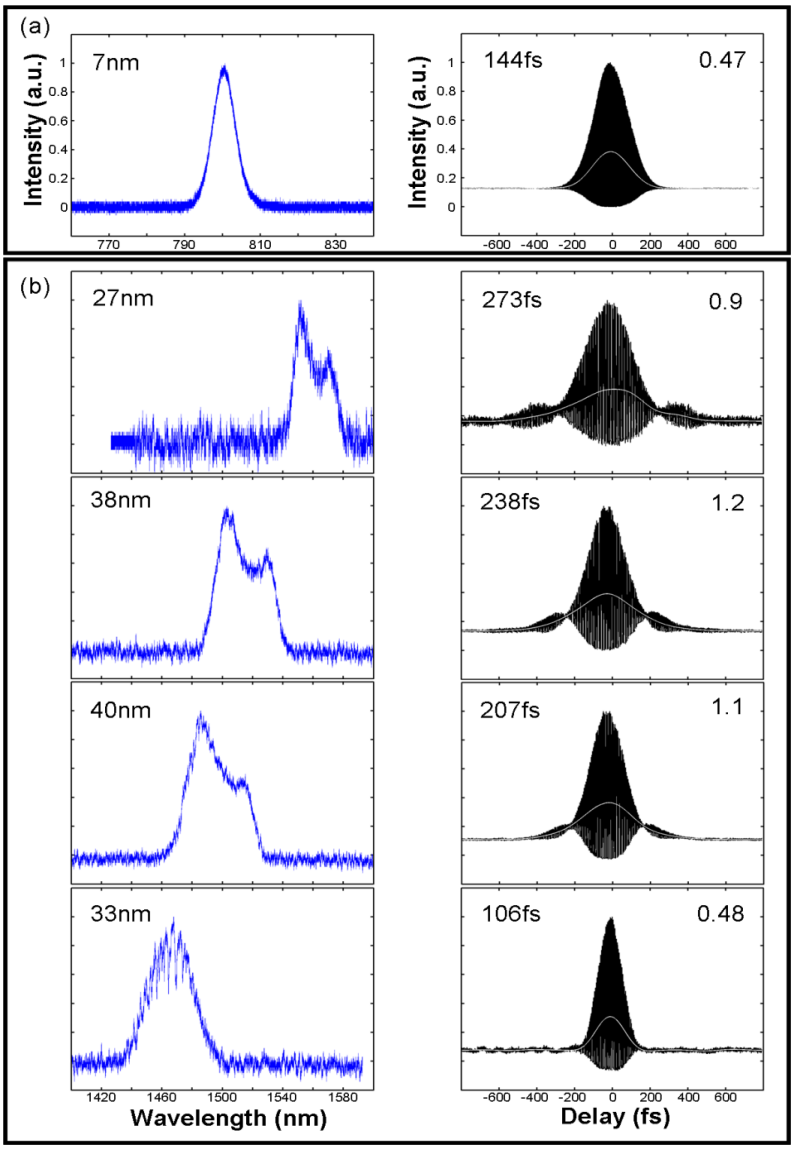

Figure 3.9: Spectral and Temporal characteristics of (a) pump laser, and (b) SPOPO signal.

In the absence of dispersion compensation in the SPOPO, spectral bandwidths for the signal pulses range from ∼20 nm to ∼40 nm, but the pulses are chirped across most of the tuning range. However, the signal spectrum

showed a smoother profile in the vicinity of 1.46 μm, while maintaining a broad bandwidth of 33 nm. Pulse durations from 206 *fs* to 273 *fs* were measured within the tuning range of 1.50-1.58 μm, with time-bandwidth products from 0.9 to 1.2, implying near-transform-limited pulses. The variation in pulse duration across the tuning range is consistent with the variation in the corresponding spectra, where shorter wavelengths exhibit broader spectra, and consequently, shorter pulse durations.

Interestingly, we find that the pulses around 1.46 μm showed no evidence of chirp and the measured pulse duration is as short as 106 *fs*, being near-transform-limited with a time-bandwidth product of 0.48 and shorter than the pump pulse duration, as shown in *Fig.* 3.9(b). It is worthwhile to note that the spectrum between 1.46 and 1.48 μm was even broader than 40 nm, but is extremely unstable, making it impossible for reliable characterization. Therefore, the tuning range was divided into two regions with different performance. In one region, from 1.50 μm, where pulses are affected by chirp and the spectrum is broad. In another region, below 1.48 μm, where the pulses are smooth and self-compressed. This unusual self-compression effect has been previously observed in a *visible* SPOPO based on BBO pumped by the second harmonic of a Ti:sapphire laser [29], and is attributed to cascaded nonlinear effects [57], where the parametric signal and SHG of the signal occur simultaneously. Indeed, with the crystal used in our experiment, we observed a collinear SHG in the neighbourhood of pulse compression region at signal wavelength around 1.5 μm. We expect that with the use of suitable chirped mirrors with controlled GVD, the tuning range can be extended and will enable the generation of even shorter pulses, making use of the broadband spectrum supported by this SPOPO.

3.6 Conclusions

We have demonstrated a direct Ti:sapphire-pumped *fs* SPOPO based on BIBO, providing wide, continuous, and rapid static tuning across $1.4 - 1.6$ μm by only varying the cavity delay or the pump wavelength. The use of collinear *type I (e→oo)* phase-matching with a pump wavelength range in the

vicinity of 800 *nm* leads to a large spectral acceptance bandwidth, resulting from near-zero GVM between signal and pump pulses, and enabling the generation of near-transformed signal pulses down to 106 *fs*. The obtained tuning range is currently limited only by the reflectivity of available mirrors and can be readily extended using more suitable coatings. The static cavity delay tuning could be attractive for rapid wavelength scanning or modulation using piezoelectric control of the SPOPO cavity length. To our knowledge, the rapid, broadband, and static tuning features of BIBO exploited here have not been previously demonstrated in any *fs* SPOPO directly pumped by the KLM Ti:sapphire laser based on other birefringent materials such as BBO, LBO, or KTP and its isomorphs.

Chapter 4

Synchronously-retro-reflection pumped femtosecond OPO

4.1 Motivation

Over the past twenty years, many SPOPOs have been developed either based on birefringent nonlinear crystals such as KTP and its isomorphs, BBO, LBO and BiBO or with quasi-phase-matched materials, like PPLN, PPLT and their combinations as well, covering spectral regions from the *UV* to the *mid-infrared (MIR)*. An important parameter in successful attainment of SPOPO operation is the threshold pump power. In particular, when employing birefringent crystals offering relatively low nonlinear gain, operating the SPOPO at high harmonic repetition rates with increased intracavity signal losses, or while deploying intracavity second harmonic of the signal-the utilization of maximum available input pump power becomes a critical factor in achieving oscillation threshold. Typically, the depletion of input pump power in SPOPOs is below 50%, suggesting that efficient re-utilization of the undepleted pump can be a valuable tool for the reduction of input pump power required to reach threshold, and consequently, enhancing the output power. The most direct method is to deploy double-pass-pumping to return the undepleted pump back into the crystal, but critical to success of this technique in a SPOPO is the attainment of optimum spatial mode-matching

as well as temporal synchronism of the returned pump with the circulating signal pulses in the crystal for minimum threshold. It is well known that use of one cavity mirror to reflect the pump together with the oscillating signal can provide threshold reduction, as used in *cw* OPOs [58]. However, the technique is not flexible, since the focal length of the mirror is designed for the signal wavelength, and cannot be adjusted to provide optimum spatial mode-matching for the returned pump with the signal in the crystal. This technique also places additional constraints on the mirror coating, resulting in higher complexity and cost. One may consider the use of an external concave mirror of suitable radius of curvature to achieve spatial mode-matching of the undepleted pump in the second pass through the crystal. However, in the context of SPOPOs, this technique also suffers from lack of flexibility in maintaining optimum spatial mode-matching while simultaneously permitting temporal synchronization of the returned pump with the signal pulses inside the crystal through translation of the external mirror. Such a scheme has been previously deployed in a SPOPO pumped by a high-energy pulsed mode-locked laser, where the effects of spatial mode-matching are not critical due to high gain and large mode volume [59]. However, in SPOPOs pumped by *cw* mode-locked lasers, where the substantially lower peak pump intensities require tight focusing, the attainment of optimum spatial mode-matching as well as temporal synchronism is vital in achieving oscillation threshold. In this case, a more flexible retro-reflection system of the pump to achieve the optimum spatial mode-matching and temporal synchronism for minimum threshold will be necessary. Moreover, in many practical situations, it would be highly desirable to deploy double pass pumping to ensure SPOPO threshold minimization from the outset, prior to oscillation, for example when dealing with limited input pump power and/or low nonlinear gain in birefringent crystals. However, previous attempts based on external double-pass-pumping provide amplification and threshold reduction only after the oscillation is established, not taking full advantage of the technique to achieve SPOPO operation. In this context, we developed a practical and flexible technique for optimum double-pass-pumping of SPOPOs that circumvents the above limitations, enabling simultaneous adjustment of spatial

and temporal overlap of the retro-reflected undepleted (residual) pump with the circulating signal pulses inside the crystal, and thus facilitating threshold reduction prior to oscillation.

4.2 Experimental Setup

The configuration of the experimental setup is shown in *Fig.* 4.1. The SPOPO is pumped by 150 *fs* pulses at 800 *nm* at a repetition rate (RR) of 76 *MHz*. The SPOPO uses a 1.5-*mm*-long BIBO crystal cut for collinear *type I (e→oo)* phase-matching in the *xz* optical plane at an internal angle of θ=11.4°, (ϕ=90°) at normal incidence. A lens, L1 (f=8 *cm*), AR-coated (R<1%) at 800 *nm*, is used to focus the pump beam to a waist radius, ω_o ∼16 μm, inside the crystal.

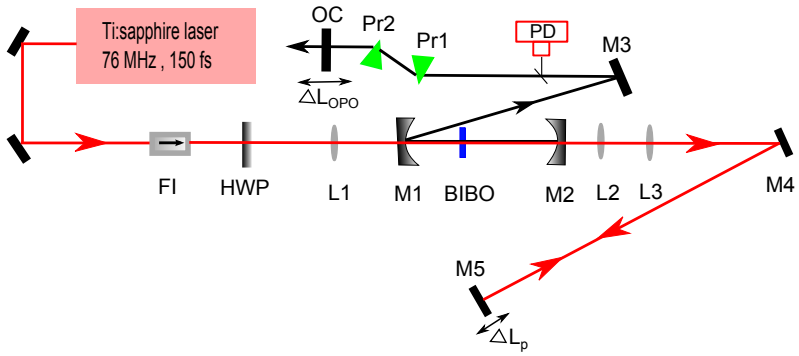

Figure 4.1: Schematic of the experimental setup. FI: Faraday isolator, HWP: Half-wave plate, L1-3: Lenses, M1-5: Mirrors, PD: Photo-detector, Pr1-2: Prism pair, OC: Output-coupler.

The SPOPO is configured in a four-mirror, standing-wave cavity comprising two concave high reflectors M1 and M2 (r=100 mm), a plane mirror M3, with reflectivity (R>99%) at the signal wavelengths, and a 5% output coupler (OC) mounted on a translation stage to allow variation of the cavity length (ΔL_{OPO}) with micrometer precision. Intracavity dispersion compensation is implemented using a pair of SF-11 prisms with a tip-to-tip separation of

15 *cm*. The new section consists of a double-pass scheme that retro-reflects the undepleted pump beam to amplify the intracavity signal, while providing independent adjustment of the spatial and temporal overlap between the reflected pump and intracavity signal pulses. In more detail, the pair of lenses L2 (f=15 *cm*) and L3 (f=5 *cm*) form a telescope that collimates the undepleted pump beam and can be fine-adjusted with the translation (ΔL_{lens}) of L3. After collimation, the beam is steered via M4 to a delay line mirror M5 mounted on a micrometer translation stage (ΔL_p). L2 and L3 are anti reflection coated, and M4, M5 are highly reflecting (R>99%) for the pump . Finally, the total optical length of the retro-reflected pump beam is synchronized to the SPOPO cavity length by adjusting ΔL_p.

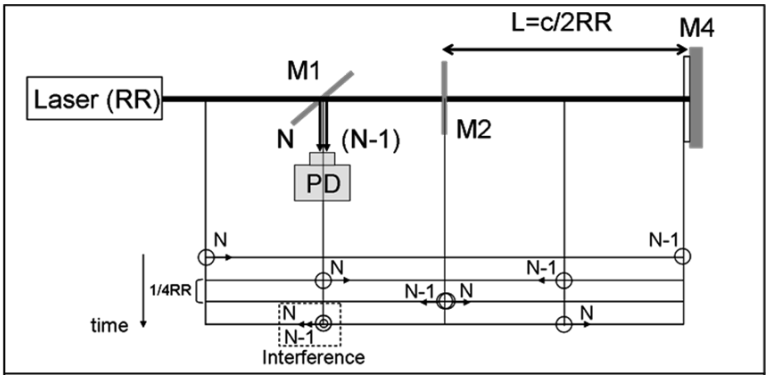

Figure 4.2: Interferometric analogy of the experimental setup between the pump pulses.

Figure. 4.2 represents the simplified equivalent interferometric scheme of the experimental setup in *Fig*. 4.1 to explain the initial pump synchronization, in which M1 and M2 can be regarded as high transmittance beam-splitters for the pump pulses. In the experimental setup, mirror M2 serves as beam-splitter for the pump. The distance travelled by the collimated pump beam after the mirror M2 via M4 was matched to the pump laser repetition rate by scanning the mirror M5 mounted on the micrometre precision translational stage. As a result, one can easily verify that the output of such an interferometer provides interference between a weak pump pulse (N) and

the earlier pulse in the train (N-1), which is delayed in the extended arm (L). Thus, by placing a photo-diode (PD) in the path between M1 and M3, the interference or beating effect between the pulse trains can be observed while the pump repetition rate can be precisely matched before the onset of SPOPO oscillation. This ensures that the undepleted pump has been directed back into the SPOPO under synchronization. The beating effect on the PD before and after synchronization can be seen clearly in *Fig.* 4.3.

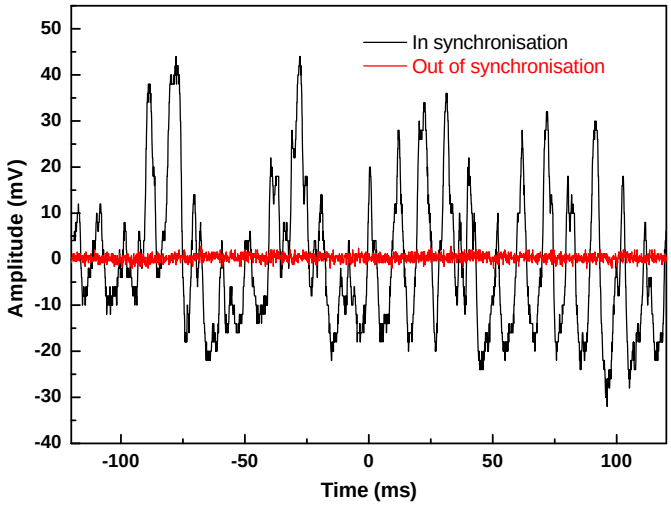

Figure 4.3: Beating signal of the retro-reflected pump with and without synchronization.

This interferometric technique allows perfect temporal synchronization of the retro-reflected pump, even before SPOPO oscillation is established. Thus, threshold reduction is achieved from the outset. It can be seen that when M5 is out of synchronization, the pump signal is near zero and flat. However, when M5 is scanned and eventually finds the position of synchronization, the pump signal on the PD shows a clear interference beating, thus confirming temporal overlap between first and second pump pulses. After obtaining this interference beat, we can remove the PD and scan the SPOPO cavity by translating OC to initiate oscillation assuring threshold reduction. It is worthwhile to point out that the signal amplification will be achieved through the retro-reflected pump delay line, ΔL_p.

4.3 Results and Discussion

We performed power measurements to evaluate SPOPO threshold reduction and signal power enhancement using the synchronized retro-reflected pump. *Figure*. 4.4 presents the recorded data for the SPOPO average signal power extracted through the 5% OC as a function of the delay (ΔL_p) applied to the retro-reflected pump beam.

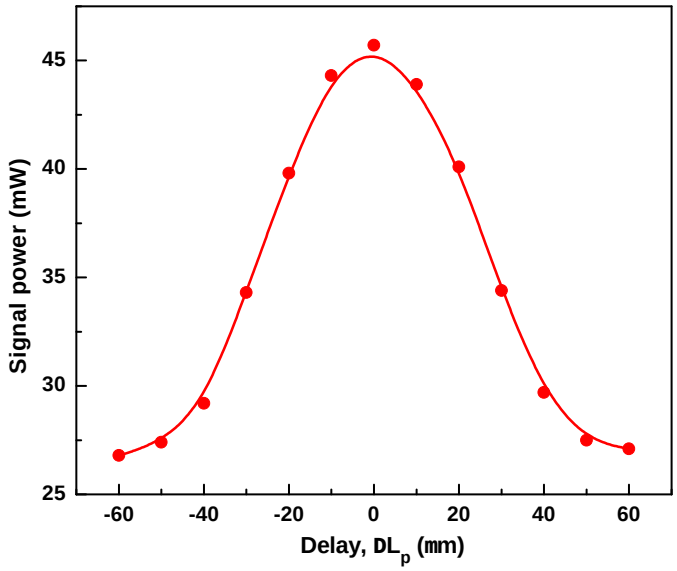

Figure 4.4: Average signal power extracted from the SPOPO depending on the retro-reflected delay line detuning.

As can be seen, the enhancement ($\Delta P/P_o$) in the signal output power, under perfect synchronism (ΔL_p), is >70%, reaching 46 mW at the maximum pump power of 850 mW. In the absence of suitable output couplers, no attempt was made to maximize the absolute extracted power. Moreover, a delay of 40 μm could still result in amplification of ∼28%, while beyond 50 μm delay retro-reflection of the pump has no effect on the signal output power. The effect of the synchronized reflection of the undepleted pump beam on the threshold reduction has been depicted in *Fig*. 4.5. It is clearly evident that with the perfect retro-synchronized pump, the threshold of the SPOPO reduced from 575 mW to 450 mW.

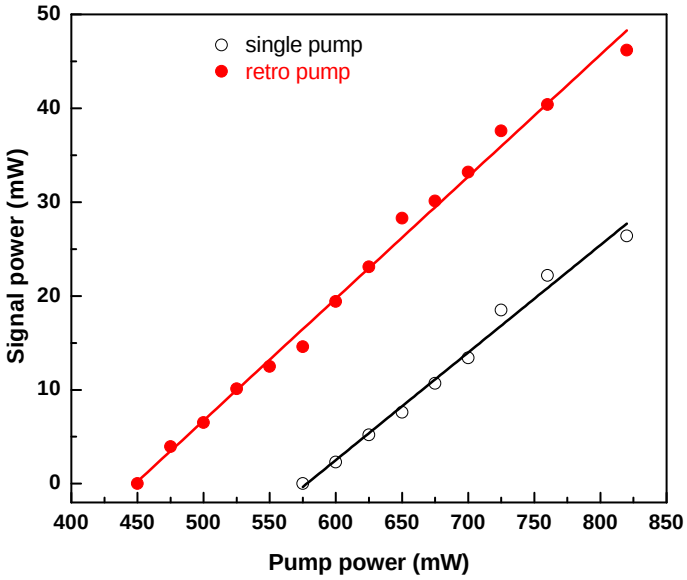

Figure 4.5: SPOPO signal power using single pump and retro-reflected pump with respect to input pump power.

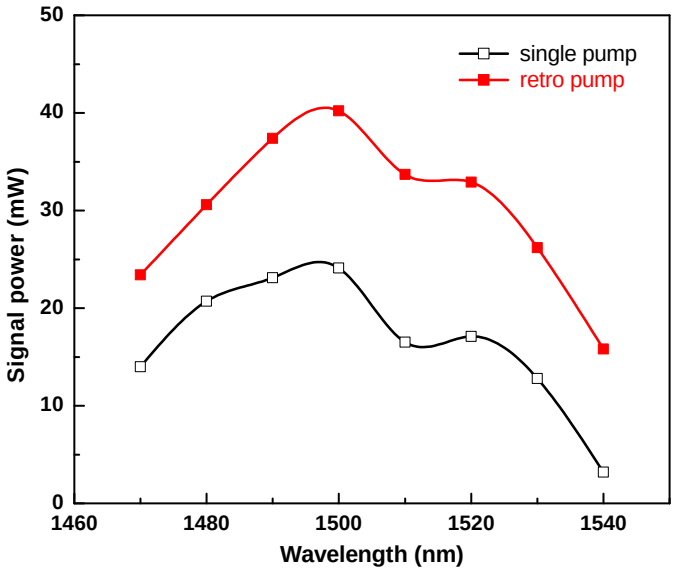

Figure 4.6: SPOPO signal power using single pump and retro-reflected pump with respect to change in wavelength.

Moreover, enhancement in the signal output power increases from moderate values around 70% to >700% when the input pump power approaches the threshold of the single-pass-pumped SPOPO near 600 mW. It should be noted that the enhancement in signal power is also clearly dependent on the input pump power. In order to evaluate the performance of synchronized retro-reflected pumping with signal wavelength, the SPOPO was continuously tuned by adjustment of the cavity delay (ΔL_{OPO}) without varying any other parameters. *Figure* 4.6 shows the comparison of SPOPO output power across the tuning range with the single pump fixed at 850 mW, and with synchronized retro-reflected pump using the 5% output coupler. With the synchronized retro-reflected pump, we were able to extract higher output power across the entire tuning range, and especially near the reflectivity edge of the mirrors. The total tuning range was limited only by signal reflectivity of the available SPOPO mirrors.
This clearly shows that the technique is universal and can be used for any temporal and spectral regimes for SPOPO output power enhancement and threshold reduction.

4.4 Spectral and Temporal Characterisation

We also studied the dependence of the spectral and temporal characteristics of the SPOPO without and with synchronised retro-reflection. *Figure* 4.7(a) and 4.7(c) show typical spectra of SPOPO signal pulses without and with retro-reflected pump beam, respectively, measured at 1.5 μm. In the presence of dispersion compensation, the signal spectra had a smooth profile with a FWHM bandwidth of $\sim$28 nm, as shown in *Fig.* 4.7(a). When the retro-reflected pump was perfectly synchronized, the spectra showed amplification without broadening and maintained the same smooth profile, as in *Fig.* 4.7(c). We also performed fringe-resolved autocorrelation measurements of the signal pulses using a two-photon absorption Si photo-detector. Typical autocorrelation profiles corresponding to the spectra of *Fig.* 4.7(a) and 4.7(c) are shown in *Fig.* 4.7(b) and 4.7(d), respectively. Without (with) retro-reflected pump, the average pulse duration is estimated as 230 fs (227

fs), assuming $sech^2$ pulse shape, resulting in a time-bandwidth product of 0.84 (0.85), indicating no variations in pulse characteristics with the deployment of the retro-reflected pump. Furthermore, we did not observe any evidence of asymmetry either in spectral amplification or autocorrelation for fine adjustments in delay of retro-reflected pump beam, confirming that the technique has no detrimental effect on SPOPO output pulse characteristics.

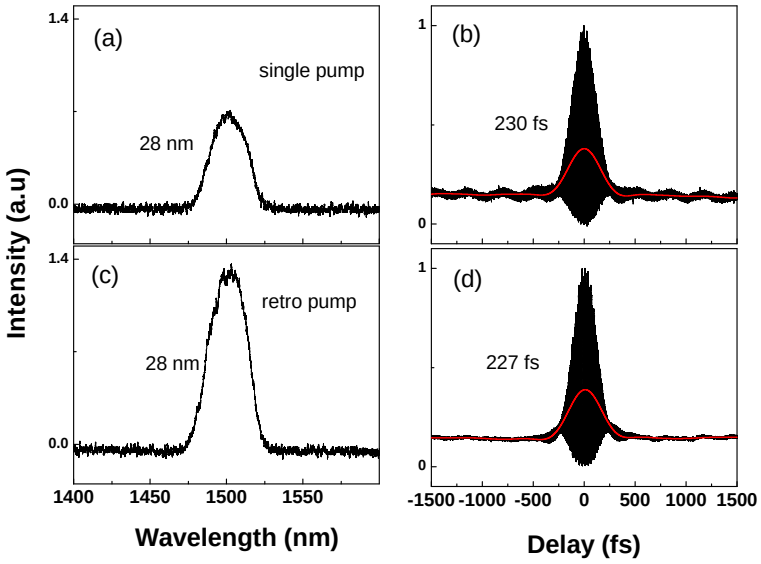

Figure 4.7: Spectral and temporal measurements of the SPOPO without (a)&(b) and with (c)&(d) retro-reflection pump.

Finally, we investigated output pulse train and repetition frequency stability of the SPOPO. The pulse train was monitored using an *InGaAs* photodetector ($NewFocus$ 1444, 20 GHz, 18.5 ps) and a fast oscilloscope ($LeCroy$, $Wavepro$ 735Zi, 3.5 GHz, 40 GS/s) with the results shown in $Fig.$ 4.8. Without the retro-reflected pump, the train shows a peak-to-peak amplitude variation of ∼5.7%, whereas the amplified pulse train shows a peak-to-peak amplitude variation of ∼6.4% when deploying the retro-reflected pump and under perfect synchronism. $Figure$ 4.9. further presents the measured RF spectra of the SPOPO output without and with the retro-reflected pump. As can be seen, the spectra, centred at 76.00 MHz, are of similar bandwidth, indicating no perturbation in the repetition frequency of the output signal

pulses due to retro-reflection pumping.

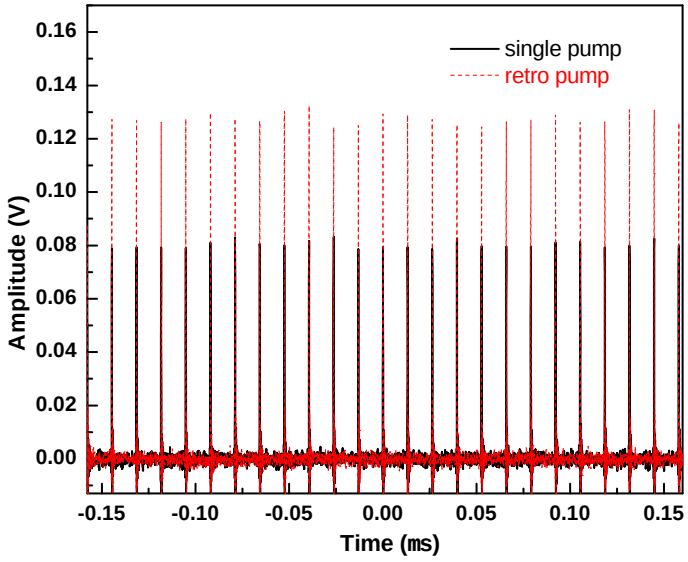

Figure 4.8: Stability measurements with fast photo-detector.

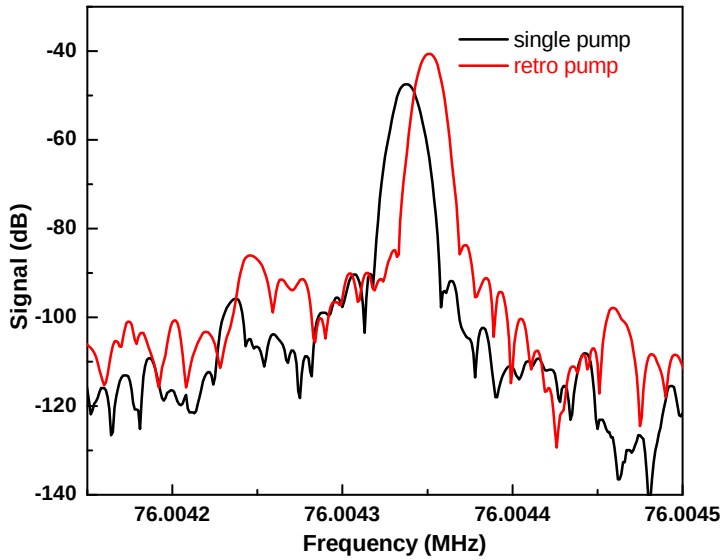

Figure 4.9: RF spectra of SPOPO operating at 76.00 *MHz*.

4.5 Conclusions

We have described a flexible and practical method for threshold reduction and signal power enhancement in SPOPOs based on synchronous-retro-reflection of the undepleted pump, with no detrimental effects on spatial and temporal output characteristics. The design permits initial synchronization by interferometry, enabling threshold reduction before the onset of oscillation. The scheme may be exploited in various birefringent crystals such as BBO and LBO, offering relatively low nonlinearities, or when using the harmonics of the pump, with limited input power, allowing operation at reduced pump powers. The technique also holds promise for materials that suffer optical damage, since the double pump amplification occurs at different times in the crystal, and may also be combined with cavity length extension schemes [54] to achieve high repetition rates.

Chapter 5

Self-phase-locked degenerate femtosecond optical parametric oscillator based on BiB_3O_6

5.1 Motivation

With the advent of ultrafast *fs* laser sources, optical frequency combs have revolutionized precise measurements of frequency and time, and have become enabling tools for demanding applications from high-resolution spectroscopy of molecules to calibration of astronomical spectrographs [60], [61]. Frequency combs have been traditionally generated by means of a mode-locked *fs* laser in which the pulses circulating inside the cavity are coupled out after every round-trip. When the carrier-envelope-phase (CEP) of the *fs* pulses is stabilized, the output spectrum constitutes a broadband comb of axial modes with exact frequency spacing corresponding to the round-trip time of the laser cavity, thus providing an accurate optical ruler for precise frequency measurements. Over past decade, tremendous progress has been made in optical frequency comb generation. By deploying Kerr-lens-mode-locked (KLM) *fs* Ti:sapphire and mode-locked fiber lasers, optical frequency combs have been generated for spectral regions from $\sim$700 nm to $\sim$2 μm [62], [63]. However, due to a scarcity of practical *fs* laser sources at longer wavelengths, effective

generation of frequency combs in the *MIR* has relied mainly on nonlinear down-conversion techniques. By the virtue of their phase-coherence properties, nonlinear frequency conversion processes offer an attractive approach for the expansion of optical frequency combs into new wavelength regions, preserving the phase characteristics of the input pump radiation in the down-converted output. In particular, *fs* SPOPOs based on quasi-phase-matched (QPM) nonlinear materials and synchronously-pumped by KLM Ti:sapphire, Cr:ZnSe, and mode-locked fiber lasers have proved highly effective tools for the expansion of frequency combs into the *visible* and *MIR*, covering spectral regions from ∼400 nm to ∼6 μm [64], [65], [66], [67], [68]. The generation of optical frequency combs using *fs* SPOPOs can be achieved using two different approaches. In the more conventional method, a singly-resonant oscillator (SRO) configuration is employed for the *fs* SPOPO, with only the signal wave resonant within the cavity. When pumped by a *CEP*-stabilized *fs* laser, the generated signal and idler combs inherit the mode spacing of the pump comb, and CEP frequencies of the interacting combs is subject to the condition

$$f_{\mathrm{CEP}}(signal) + f_{\mathrm{CEP}}(idler) = f_{\mathrm{CEP}}(pump) \tag{5.1}$$

The pump comb is thus directly transferred to signal and idler output combs through energy conservation and phase-matching, and the coherence properties of input pump are passed on to the down-converted signal and idler output at longer wavelengths with high conversion efficiency. Such *fs* SPOPOs have been extensively developed for the *near* to *MIR* using KLM Ti:sapphire and mode-locked fiber lasers in combination with PPLN as the nonlinear material. With active CEP stabilization, they have been shown to provide broadband frequency combs covering spectral regions from 400 nm to 4.8 μm [64], [65]. In the second approach, the *fs* OPO is configured as a doubly-resonant oscillator (DRO), with both signal and idler waves resonant in the cavity near degeneracy. If the signal and idler waves have the same polarisation (e.g. under *type I (e→oo))* phase-matching, they become indistinguishable at exact degeneracy and exhibit self-phase-locked behaviour through mutual injection, providing a single coherent broadband output centred at

degeneracy [66], [68], [67], [69]. Such sub-harmonic SPOPOs have been shown to inherit all coherence properties of the pump and are locked in frequency and phase to the input pump laser [69]. They thus offer a highly attractive method for frequency comb generation into the *MIR*. When pumped by a CEP-stabilized *fs* laser, the sub-harmonic SPOPO can produce an output comb with two possible values for the *CEP* frequency, given by

$$f_{\mathrm{CEP}}(sub) = (f_{\mathrm{CEP}}(pump)/2) \tag{5.2}$$

$$f_{\mathrm{CEP}}(sub) = (f_{\mathrm{CEP}}(pump) + f_{\mathrm{rep}})/2 \tag{5.3}$$

where f_{rep} is the pump pulse repetition frequency.
Thus, as the equations indicate, when the CEP of the input pump laser is stabilized, the degenerate SPOPO output comb is automatically stabilized. The advantage of the sub-harmonic SPOPO, therefore, lies in the fact that the self-phase-locking of the signal and idler occurs at degeneracy, in addition to energy conservation and phase-matching, imposes a further constraint on the conversion process by setting $f_{CEP}(signal)$=$f_{CEP}(idler)$, thus simplifying the task of stabilization. It thus substantially reduces the demands on active stabilization and electronic feedback loops compared to non-degenerate SPOPO schemes. Since its first demonstration in 2008 [70], several degenerate *fs* SPOPOs synchronously-pumped by KLM Ti:sapphire, Cr:ZnSe, and mode-locked fiber lasers have been developed, and their potential for broadband frequency comb generation in the *NIR* and *MIR* bas been demonstrated [67], [68]. To satisfy phase-matching condition for degenerate operation, such sub-harmonic SPOPOs have relied exclusively on QPM materials, in particular $PPLN$, and more recently orientation-patterned $GaAs$ (OP-$GaAs$), as the nonlinear gain media. The grating engineering capability available to QPM materials permits the design of suitable poling periods for degenerate parametric generation at a given pump wavelength, while taking advantage of the highest nonlinear gain coefficient under *type 0 ($e \rightarrow ee$)* non-critical phase-matching. On the other hand, the relatively high cost of $PPLN$ and similar QPM materials together with the need for temperature phase-matching, and restricted availability of OP-$GaAs$, can be significant

limitations for some practical applications. As such, the quest for new materials with more widespread availability, lower cost, and desirable nonlinear and phase-matching properties must continue for further development of sub-harmonic SPOPOs and the realization of practical and cost-effective frequency comb generators based on this concept. In this context, we describe here the first self-phase-locked degenerate *fs* SPOPO based on a birefringent nonlinear material.

5.2 Unique properties of xz BIBO

The nonlinear material, BIBO [52], is an optically biaxial crystal with unique properties for frequency conversion from the *UV* to the *NIR* [53], [54] [71]. It can offer different phase-matching configurations in the three principal optical planes for various frequency conversion processes, with non-vanishing nonlinear coefficients at room temperature. The effective nonlinear coefficient (d_{eff}) of BIBO is typically ∼2 to ∼3.7 pm/V for various conversion processes. Under collinear *type I (e→oo)* phase-matching in the optical xz plane, it possesses large spectral acceptance bandwidth for parametric generation when pumped at ∼800 nm. *Type I (e→oo)* phase-matching in the optical xz plane with d_{eff} ∼2.9 pm/V can be exploited to achieve broadband tuning [39]. As shown in $Fig.$ 5.1, the spectral acceptance bandwidth becomes very large, since the GVM between signal and idler pulses is very small and vanishes near degeneracy [55]. In particular, for signal wavelength range close to degeneracy at ∼1600 nm, the GVM between the pump and signal (idler) is <11 fs/mm, and the spectral acceptance bandwidth is ∼20 $nm.cm$. In addition, as shown in $Fig.$ 5.2, the group velocity dispersion (GVD) is ∼0 fs^2/mm at 1600 nm, resulting in minimal pulse broadening.

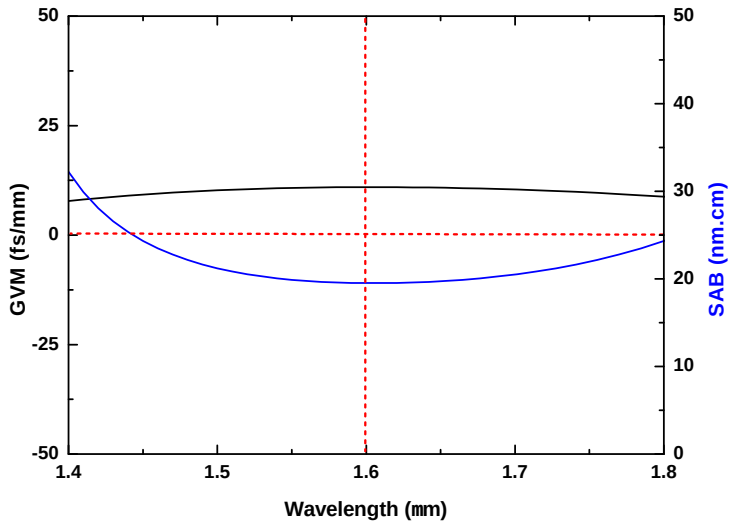

Figure 5.1: GVM between pump-signal and the respective spectral acceptance bandwidth (SAB). Dotted line shows the values at degeneracy.

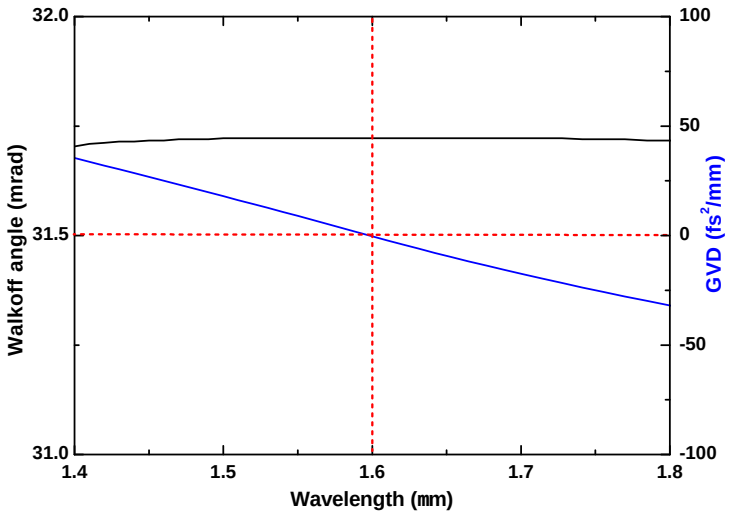

Figure 5.2: Walk-off angle and GVD of BIBO in optical xz plane for *type I* *($e \rightarrow oo$)* interaction. Dotted line shows the values at degeneracy.

Low spatial walk-off is another important advantage of BIBO. At 1600 nm, the walk-off between the pump and the degenerate signal (idler) beam

amounts to ∼32 *mrad*, as also shown in *Fig*. 5.2. This feature allows collinear interaction in a SPOPO under critical phase-matching, not possible with other birefringent crystals such as BBO, thus resulting in greatly simplified and practical design. These features make BIBO a uniquely attractive birefringent crystal for broadband frequency comb generation in the 1-2 μm spectral range based on degenerate SPOPOs using the KLM Ti:sapphire pump laser at ∼800 nm.

5.3 Experimental Setup

The configuration of the degenerate *fs* SPOPO based on BIBO is shown in *Fig*. 5.3. The SPOPO is pumped collinearly by a 76 *MHz fs* KLM Ti:sapphire laser centred at 800 nm. After transmission through an optical isolator, an average power of 750 mW in near-transform-limited pulses of ∼155 *fs* with a spectral bandwidth of 7 nm ($FWHM$) is available for pumping the SPOPO. A half-wave plate after the isolator provides extraordinary pump polarisation for phase-matching in the BIBO crystal.

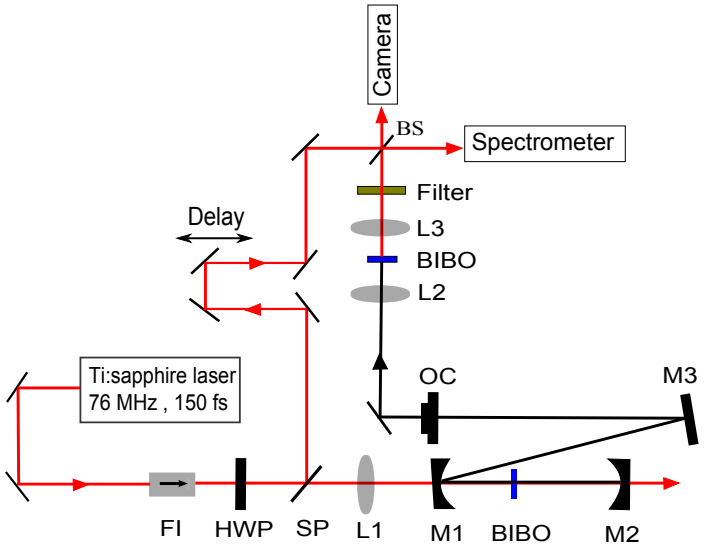

Figure 5.3: Schematic of the experimental setup. FI: Faraday isolator, HWP: Half-wave plate, SP: Sampling plate, L1-3: Lenses, M1-3: Mirrors, OC: Output-coupler, BS: Beam-splitter.

The SPOPO is configured in a standing-wave cavity comprising two concave reflectors M1 and M2 (r=100 mm), one plane high reflector folding mirror, M3, and a plane ∼5% output coupler (OC) mounted on piezoelectric transducer (PZT) and on a translational stage. The mirrors, M1, M2, M3, are all highly reflecting (R>99%) centred at 1600 nm and highly transmitting (T>90%) at 800 nm. The BIBO crystal is 1.5-mm-long and cut at $\theta = 11.4°$, ($\phi = 90°$) in the optical xz plane for *type I ($e \rightarrow oo$)* phase-matching. A lens, L (f=8 cm), AR-coated (R<1%) at 800 nm, is used to focus the pump beam to a waist radius, ω_o ∼16 μm inside the BIBO crystal, resulting in an effective interaction length of ∼1.4 mm for a walk-off of ∼32 *mrad*, almost equal to the full crystal length used. Given the near-zero GVD of the BIBO crystal in the degenerate wavelength region, no dispersion compensation was deployed in the SPOPO cavity. For synchronous pumping, the SPOPO resonator length was matched to the repetition frequency of the pump laser by coarse adjustment of OC mirror on the micrometer translation stage. To obtain degenerate self-phase-locked operation, the position of the OC was finely scanned using PZT control. We achieved successful operation of the non-degenerate SPOPO in free-running condition at an average threshold pump power of 325 mW. With further fine adjustment of the cavity length by PZT control, SPOPO operation was gradually transferred to a degenerate, self-phase-locked state, and stable oscillation was obtained. In this state, SPOPO operation could be maintained with a reduced pump power threshold of 200 mW, and we were able to extract an average output power of 40 mW through the 5% OC for the maximum available input pump power of 750 mW.

5.4 Results and Discussion

We performed spectral characterization of the SPOPO output in near-degenerate and degenerate operation, with the results presented in *Fig.* 5.4. As can be seen, the SPOPO output spectra undergo a gradual transition from near-degenerate operation, 5.4(a)-(c), to an exact degenerate state, *Fig.* 5.4(d), by careful adjustment of the cavity length using the PZT controller. In non-

degenerate operation, there are clearly two distinct signal and idler spectra, which exhibit some spiking and modulation, but progressively merge into a single broadband and smooth spectrum centred at 1600 nm with fine adjustment of the cavity length. The SPOPO cavity length required for the transition from $Fig.$ 5.4(a) to 5.4(d) is 8 μm.

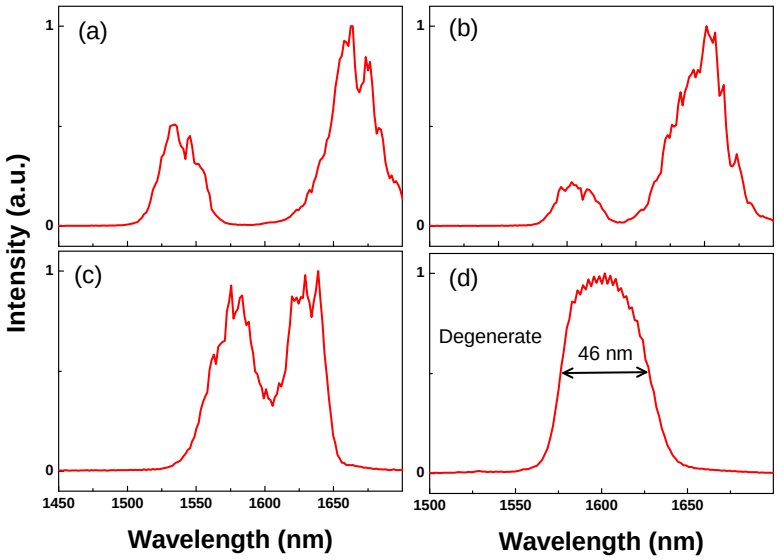

Figure 5.4: Spectral tuning between non-degenerate and degenerate modes

We find that in non-degenerate operation with the signal and idler spectra well separated ($Fig.$ 5.4(a)-(b)), the SPOPO is more susceptible to instabilities until the cavity length is adjusted towards degeneracy. In the degenerate state ($Fig.$ 5.4(d)), the SPOPO exhibits improved output stability and oscillation can be maintained for long periods of time (>40 minutes) in the absence of external perturbations. In the intermediate case, where the spectra of signal and idler begin to overlap, $Fig.$ 5.4(c), the SPOPO oscillates between the degenerate and non-degenerate states. But with a slight perturbation, it switches back to the degenerate case and remains more stable. To verify self-phase-locked operation, we determined the phase coherence between the pump laser and the SPOPO output using f-2f interferometry, as

used previously [70]. The SPOPO output was frequency-doubled in a 0.4-*mm*-long BIBO crystal also cut at $\theta = 11.4^\circ$ ($\phi = 90^\circ$) in the optical xz plane for *type I (oo→e)* SHG. As shown in *Fig.* 5.3, a portion of the fresh pump was extracted using a thin glass sampling plate (SP) and the beam was steered to a delay line. The optical path length of the pump beam and the frequency-doubled SPOPO output were matched using this delay line and combined at a beam-splitter (BS). The spatial interference pattern between the two beams was then recorded using a pyroelectric camera *(Spiricon, Pyrocam III*) beyond the beam-splitter, while the spectra were simultaneously monitored using a spectrometer *(Ocean Optics, NIR QUEST)* on reflection from the beam- splitter. In non-degenerate operation, corresponding to the spectra in *Fig.* 5.4(a)-(c), we observed no spatial interference pattern in the output beam, as can be seen in the inset of *Fig.* 5.5(a). However, as we tuned the SPOPO cavity length to exact degeneracy using the PZT controller, we observed a stable fringe pattern appearing on the camera, as evident in the inset of *Fig.* 5.5(b). Re-adjusting the cavity length to any of the non-degenerate states, *Fig.* 5.4(a)-(c), again resulted in the washing off of the fringe pattern. This on and off switching of the fringe pattern in the degenerate and non-degenerate states of SPOPO with the change in cavity length delay clearly establishes the phase coherence between the pump and OPO output, confirming self-phase-locked operation at degeneracy. To further verify the most favourable regime for self-phase-locked operation, we performed radio frequency (RF) measurements of the OPO output pulses in both degenerate and non-degenerate states. The OPO output was coupled into an *InGaAs* fast photo-diode *(New Focus 1444, 20 GHz, 18.5 ps)* and the spectra were recorded using a RF spectrum analyser *(Agilent, EXA Signal Analyser, 10 Hz to 44 GHz).* With the SPOPO in non-degenerate operation, we observed satellite peaks at 67.5 and 85.5 *MHz*, respectively, on either side of the fundamental peak at 76 *MHz*, as shown in *Fig.* 5.5(a). These are due to the non-overlapping of the CEP frequencies of pump and the oscillating signal/idler combs [66], [69]. When the SPOPO cavity length was finely adjusted to degeneracy, a single peak oscillating at a frequency of 76 *MHz* was always observed, as shown in *Fig.* 5.5(b). This further confirms

self-phase-locking of all oscillating modes in the SPOPO under degenerate operation.

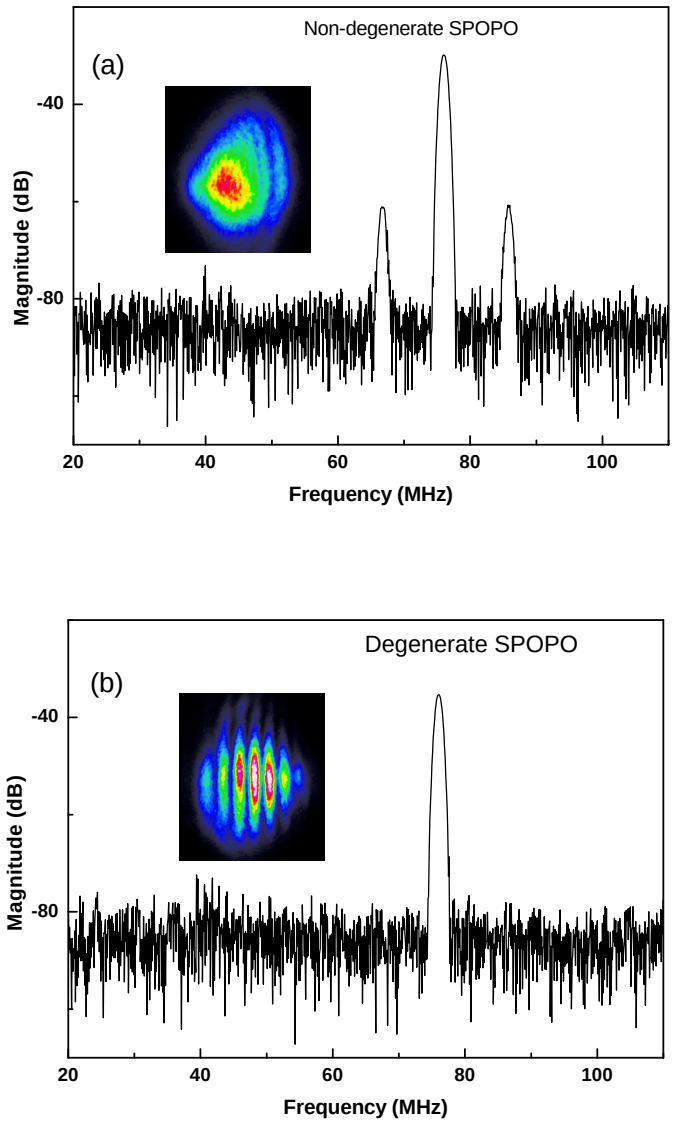

Figure 5.5: RF measurements in (a) non-degenerate and (b) degenerate modes. Inset shows the corresponding fringe patterns.

We also studied the temporal behaviour of the SPOPO in degenerate self-phase-locked state using interferometric autocorrelation measurements of the output pulses based on two-photon absorption in a Si photo-detector. The

resulting autocorrelation trace and the corresponding spectrum of SPOPO output pulses in degenerate operation are shown in *Fig.* 5.6(a) and 5.6(b), respectively. Also shown for comparison are the autocorrelation measurement of the input pump pulses and the corresponding spectrum in *Fig.* 5.6(c) and 5.6(d), respectively. As can be seen from *Fig.* 5.6(a), the autocorrelation trace of the self-phase-locked OPO has a smooth profile with some evidence of chirp. Given the near-zero GVD of the BIBO crystal at ∼1600 *nm*, we attribute this extra chirp to additional GVD introduced by the dielectric cavity mirrors used, which is unknown, thus leading to broadening of the SPOPO output pulses.

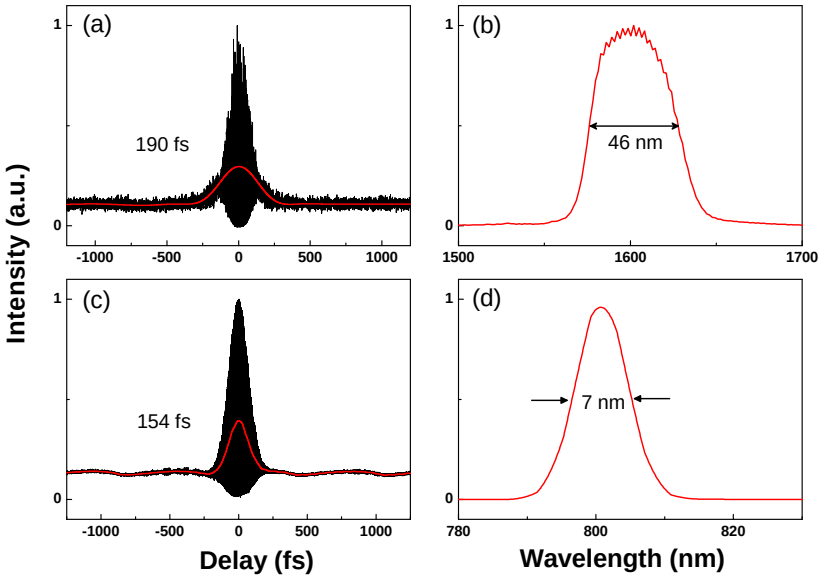

Figure 5.6: Spectral and temporal measurements SPOPO at degeneracy (a), (b); (c), (d) correspond to the Ti:sapphire pump laser.

The deconvoluted pulse duration deduced from the autocorrelation measurement is 190 *fs* (assuming $sech^2$ profile). The corresponding spectrum in *Fig.* 5.6(b) has a FWHM bandwidth of (46 *nm*) ∼5.4 THz centred at 1600 *nm*, resulting in a time-bandwidth product of ∼1.02, well above the transform limit. This value could be significantly improved by deploying dispersion-controlled mirrors for the SPOPO to reduce the output pulse du-

ration. The degenerate bandwidth of 46 nm could potentially support pulses as short as $\sim$75 fs with optimum dispersion management using near-zero GVD mirrors.

5.5 Conclusions

By exploiting the unique phase-matching properties of BIBO under *type I (e→oo)* phase-matching in the optical xz plane when pumped at 800 nm by a KLM Ti:sapphire laser, we have demonstrated what is to our knowledge the first self-phase-locked sub-harmonic *fs* SPOPO based on a birefringent nonlinear crystal. The OPO can provide a 46 nm-wide self-phase-locked output spectrum in pulses of $\sim$190 *fs*, for 155 *fs* input pump pulses of 7 nm bandwidth. The large spectral acceptance, low spatial walk-off, near-zero GVD and room-temperature phase-matching in BIBO resulted in a simplified and practical SPOPO design in collinear pumping geometry. Given the wide spectral acceptance bandwidth of $\sim$20 $nm.cm$ and relatively high nonlinearity (d_{eff} $\sim$2.9 pm/V) of BIBO, the use of an ultrashort pulse ($<$20 *fs*) Ti:sapphire laser with broad bandwidth ($>$50 nm) in crystals as long as 4 mm will enable efficient self-phase-locked broadband generation potentially extending across the entire 1-2 μm region. Such a possibility, together with the low cost and widespread availability of BIBO, a simple and practical SPOPO design, high passive stability, and room-temperature operation, will make the described system a viable alternative to mode-locked Er and Yb fiber lasers for frequency comb generation in the *NIR* for a wide range of applications in spectroscopy and frequency metrology.

Chapter 6

Dual-wavelength, femtosecond optical parametric oscillator using antiresonant ring interferometer

6.1 Motivation

Intrinsic to the operation of an OPO is the three-wave parametric interaction involving pump (ω_p), signal (ω_s) and idler (ω_i) fields. In this process, the generation of output signal and idler frequencies from the input pump frequency is governed by energy conservation (ω_p=ω_s+ω_i,) and phase-matching ($k_p = k_s + k_i$). The coupling of the three optical fields and their inter-dependence through these two conditions, however, dictates that, while broadly tunable signal and idler frequencies can be obtained from a fixed input pump frequency, the generation of truly arbitrary output frequencies with independent tuning is not permissible. This can have consequences, for example, in providing closely matched wavelengths, where the only solution is to tune the OPO to near degeneracy [72], with the concomitant disadvantages of doubly-resonant oscillation and requirements for active output power and frequency control. Even in cases when stable degenerate operation can

be achieved, tuning of the wavelength degeneracy is only possible by tuning of the pump, so that a fixed pump wavelength will only provide a single degenerate wavelength. On the other hand, the provision of multiple output wavelengths with independent tuning can be of great interest for applications such as coherent anti-stokes Raman spectroscopy (CARS) and pump-probe spectroscopy, whereas intracavity access to arbitrarily close wavelength pairs near degeneracy, together with the ability to tune the degenerate wavelength, would be highly desirable for the generation of widely tunable radiation in different bands across the THz spectrum. There have been some previous attempts to provide two different signal and idler wavelength pairs in OPOs by employing two nonlinear crystals in series [73], [74] or a single crystal in cascaded parametric process [75], [76] and in non-collinear double-pass configuration [77]. However, in such schemes, the high pump depletion in the first crystal or the first pass, generating the first signal-idler pair, can deteriorate the pump beam quality available for the succeeding crystal or pass, hence affecting overall OPO performance in terms of threshold and output power in the second signal-idler pair. Additionally, thermal effects and crystal damage issues in such schemes at higher pump powers are significant challenges to overcome. In an effort to circumvent the limitations of these techniques and overcome the intrinsic tuning constraints of OPOs, we recently demonstrated a *cw* singly-resonant oscillator (SRO) based on a novel two-crystal architecture [78], which provided flexible and arbitrary wavelength tuning across 850-1430 nm by generating two independent signal-idler pairs in a common optical cavity. Since in this scheme the two crystals share the same resonant cavity, we observed coherent coupling of the signal waves in degenerate operation, and achieved a frequency separation between the resonant signal waves down to 0.55 THz. As a result of coherent coupling, the minimum signal frequency separation near degeneracy was limited by the spectral acceptance bandwidth for phase-matching. In this context, we have developed a novel and universal technique for coupling two OPOs using Sagnac or antiresonant ring interferometer circumventing the problem of coherent coupling between the gain media even at exact degeneracy.

6.2 Antiresonant Ring (ARR) interferometer

The Sagnac or ARR interferometer is a well-known classical optical element that was proposed nearly a century ago [79], and has been suggested for many applications in lasers [80] such as cavity dumping, Q-switching, mode-locking, nonlinear spectroscopy, and fiber optics. The basic concept of exploiting the ARR interferometer for coupling two optical cavities is schematically shown in *Fig.* 6.1.

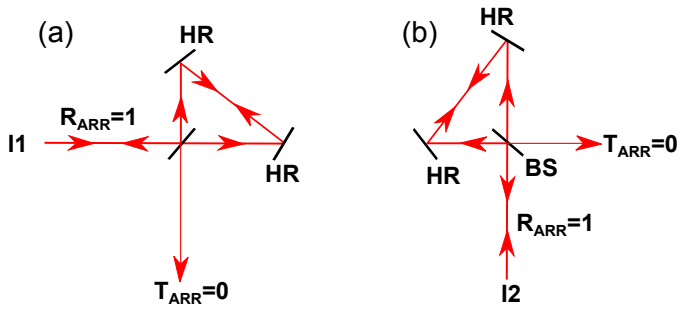

Figure 6.1: (a) The input optical beam, I1, incident on the 50:50 beam-splitter (BS) is split into clockwise and counter-clockwise beams. After propagation inside the ring and recombination, I1 is totally reflected backwards. (b) Total backward reflection when the optical beam, I2, is injected into the second input port of the ARR.

The optical cavity of the interferometer consists of a beam-splitter (BS) with transmittance, T, and reflectance, R, and a pair of high reflectivity mirrors (HR), which form the ring. The power reflected back towards the input beam (R_{ARR}) and the power transmitted out of the ring (T_{ARR}) are given by R_{ARR}=$4RT$ and T_{ARR}=$|R-T|^2$, respectively. Hence, if the T:R ratio is exactly 50:50, then T_{ARR}=0 and all the power is reflected back, making the ARR function as a highly reflecting mirror. Under this condition, two beams, I1 and I2, incident on the first and second port of the ARR will be totally reflected back, as shown in *Fig* 6.1(a) and 6.1(b),respectively. If I1 and I2 are the resonant beams corresponding to two independent optical oscillators, the

ARR will allow propagation of both beams inside the ring without any coupling outside. The architecture thus provides an intracavity common path for the two resonant signal fields, while avoiding inter-coupling between the nonlinear gain crystals. As a result, only inside the ARR both wavelengths are present, whilst outside the ring, in the part of the resonator including the nonlinear crystal, a single wavelength is oscillating. Therefore, the two OPOs can be independently tuned due to the absence of inter-coupling and, at the same time, high intracavity power at both signal wavelengths is available inside the common section, the ARR. This can be particularly attractive for efficient mixing of the two beams for applications such as THz generation.
We previously demonstrated the use of an ARR interferometer for optimum output coupling in ultrafast OPOs [81] [82] and mode-locking of *cw* OPOs [83]. In this work, we extend the potential of ARR for coupling two OPO cavities, for the first time. We demonstrate the technique using two *fs* SPOPOs, but it can be readily extended to any time-scale, and to other types of optical oscillators including lasers. The new method allows resonance of two independent signal waves in separate SRO cavities, while providing high intracavity circulating fields at both wavelengths. A particular feature of this approach is the absence of any coupling between the two resonant signal fields close to, or even at exact, wavelength degeneracy. This permits unrestricted and uninterrupted tuning of circulating signal waves across degeneracy, which can be a limitation in other methods due to parametric gain coupling and overlap of spectral acceptance for phase-matching. Moreover, the approach is particularly attractive in *fs* SPOPOs, where the limitations of group velocity mismatch and dispersion under synchronous pumping preclude the use of alternative methods based on a single optical cavity. In addition, the absence of gain coupling in the new scheme is of particular relevance in *fs* SPOPOs where the finite signal bandwidths can confine the range for independent tuning and minimum attainable wavelength separation near degeneracy. We also note that while dual-wavelength operation of *fs* SPOPOs based on a single crystal has been demonstrated by exploiting special dispersion properties in the nonlinear material within a particular wavelength range [84], [85], such methods are not generic, do not provide in-

dependent tuning, and cannot be universally deployed in different materials and in arbitrary spectral regions.

6.3 Experimental Setup

The configuration of the experimental setup is shown in *Fig.* 6.2. Two *fs* SPOPOs based on identical MgO:PPLN crystals are synchronously-pumped at 800 *nm* by a Kerr-lens-mode-locked (KLM) Ti:sapphire laser providing 150 *fs* pulses at 76 *MHz* repetition rate, and are connected by an ARR interferometer.

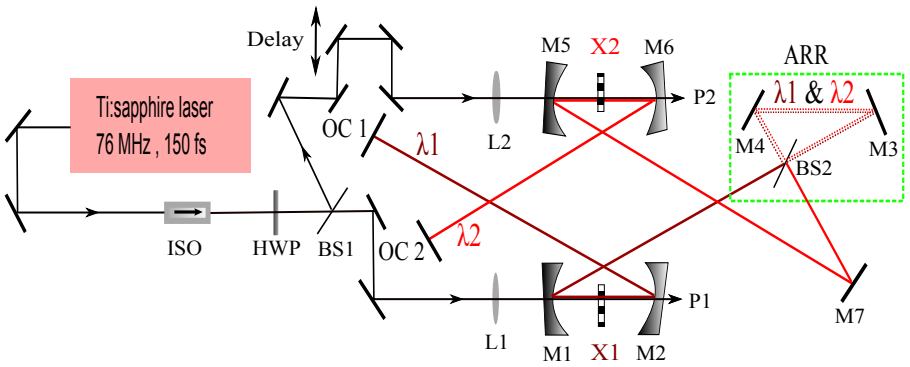

Figure 6.2: Schematic of the experimental setup. FI: Faraday isolator, HWP: Half-wave plate, BS1-2: Beam-splitters, L1-2: Lenses, M1-6: Mirrors, X1-2: MgO:PPLN, OC1-2: Output-couplers.

The crystals are 0.5-*mm*-long, 1-*mm*-thick, and incorporate fan-out gratings with continuously variable period from Λ=16 to 23 μm across the 3.4-*mm*-wide dimension. The crystal temperatures are maintained at ~100°C. A half-wave plate (HWP) provides the extraordinary pump polarisation for phase-matching in both SPOPOs. A nearly 50:50 beam-splitter (BS1) divides the laser power, providing two separate pump beams (P1 and P2). Identical lenses, L1 (f=8 *cm*) and L2 (f=8 *cm*), AR-coated (R<1%) at 800 *nm*, are used to focus the pump beams to waist radii, ω_o ~16 μm, inside the MgO:PPLN crystals. Both OPOs are singly-resonant for the signal and are deployed in standing-wave cavity configuration. The optical cavity of

SPOPO1 comprises two concave mirrors (M1, M2; r=10 cm), the ARR, and a plane 5% output coupler (OC1) mounted on a precision translation stage for synchronization with the pump laser. The cavity of SPOPO2 is formed by two concave mirrors (M5, M6; r=10 cm), a flat mirror (M7), the ARR, and a plane 5% output coupler (OC2) mounted on a translation stage. Except OC1 and OC2, all cavity mirrors are highly reflecting (R>99%) for the signal (1500-1580 nm) and highly transmitting (T>95%) for the pump (800 nm). The MgO:PPLN crystal faces are anti-reflection coated (R<0.7%) for the signal and pump (R<5%), with high transmission for the idler (T>98%). The fan-out grating structure allows smooth and continuous variation of the grating period through lateral translation of the crystal across the pump beam at a fixed temperature, enabling fine tuning of the signal wavelength within the reflectivity band of the SPOPO mirrors. The ARR interferometer consists of a commercially available 25 μm thin-film beam-splitter (BS2), coated for 1-2 μm spectral range, and two plane high reflectors (M3, M4). OC1 and OC2 provide single-wavelength signal extraction from SPOPO1 and SPOPO2, respectively, whereas dual-wavelength signal extraction is performed by introducing another film beam-splitter inside the ARR. The total optical length of each OPO cavity is 394.7 cm, including the linear part (L_{linear}=140.1 cm) and the ARR (L_{ring}=114.5 cm), ensuring synchronization to the pump laser repetition rate (RR=76 MHz), where $L_{OPO} = 2L_{linear} + L_{ring} = c/RR$, and c is the speed of light. Additionally, a delay line in one of the pump beams can be included to ensure synchronization of both signal pulses inside the ARR.

6.4 Results and Discussion

We fixed the beam-splitter angle of the ARR at 20° for minimum transmission (T_{ARR} = 1%), following earlier characterization [81], and optimized SPOPO1 and SPOPO2 to achieve equal output signal power of about 25 mW, while pumping simultaneously with an input power of 450 mW and 425 mW, respectively. Furthermore, we recorded the spectra from OC1 and OC2, as shown in *Fig.* 6.3, clearly verifying single wavelength operation of each SPOPO without any evidence of the presence of wavelengths from the other

SPOPO. In order to confirm dual-wavelength signal resonance inside the ARR, an additional beam-splitter was inserted at Brewster angle into the ring, so as to extract some of the circulating beams. The corresponding spectra are shown in *Fig.* 6.4, confirming dual-wavelength operation.

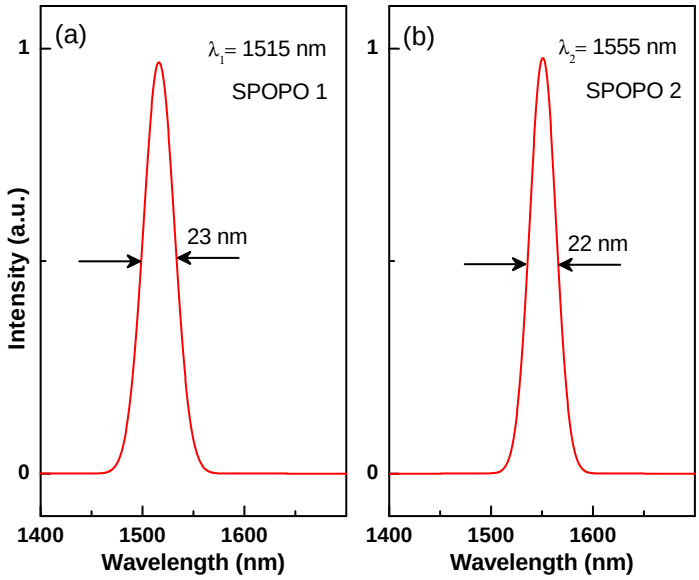

Figure 6.3: Signal output extracted through OC1 and OC2 of (a) SPOPO1, and (b) SPOPO2, respectively.

Moreover, independent tuning of the ARR-coupled *fs* SPOPOs was achieved by changing the cavity length, as commonly used in synchronously-pumped *fs* SPOPOs. In the example of *Fig.* 6.4, the cavity length of SPOPO2 was fixed, providing a spectrum centred at 1577 *nm*, whereas the cavity length of SPOPO1 was continuously varied to obtain a spectral shift from 1500 *nm* to almost degeneracy with SPOPO2, indicating clear central wavelength separations from 77 *nm* (*Fig.* 6.4(a)) down to 31 *nm* (*Fig.* 6.4(c)), resulting in broadband spectra with central frequency separations from 9.76 THz to 3.81 THz.

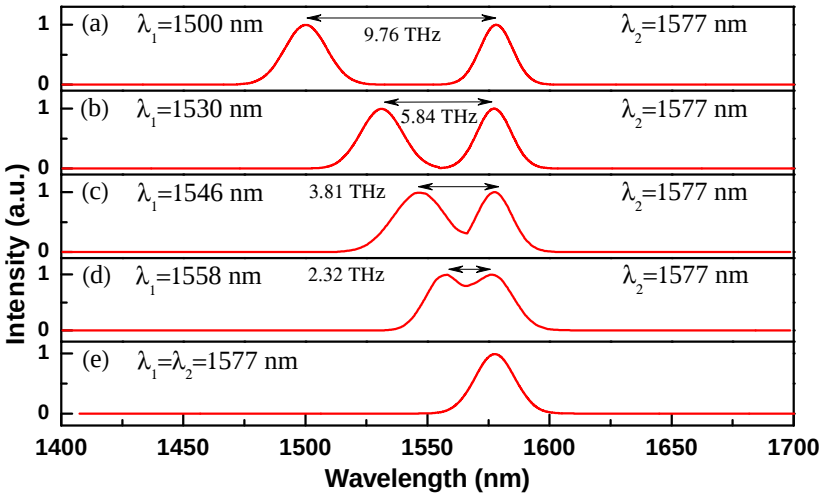

Figure 6.4: Independent and arbitrary spectral tuning of SPOPOs using cavity length delay.

Moreover, the central frequency difference can be further reduced where overlapping of the broad spectra starts. *Figure* 6.4(d) presents the overlapped spectrum with two central peaks separated by roughly 19 *nm*, corresponding to 2.32 THz. Eventually, degeneracy is achieved, resulting in two identical resonant signal wavelengths from both SPOPOs, without affecting one another, as shown in *Fig.* 6.4(e). Arbitrarily close wavelength separation of the two signal fields can be achieved at any value across the tuning range by simply varying the central wavelength of SPOPO2 and by scanning the SPOPO1.

6.5 Spectral and Temporal characteristics

We also performed temporal characterization of the output signal pulses extracted through OC1 and OC2 under degenerate and non-degenerate operation using fringe-resolved interferometric autocorrelation based on two-photon absorption in a *Si* photo-diode, with the results shown in *Fig.* 6.5. The interferometric autocorrelations for both pulses in the degenerate case

in the vicinity of 1500 nm are presented in $Fig.$ 6.5(a) and $Fig.$ 6.5(b).

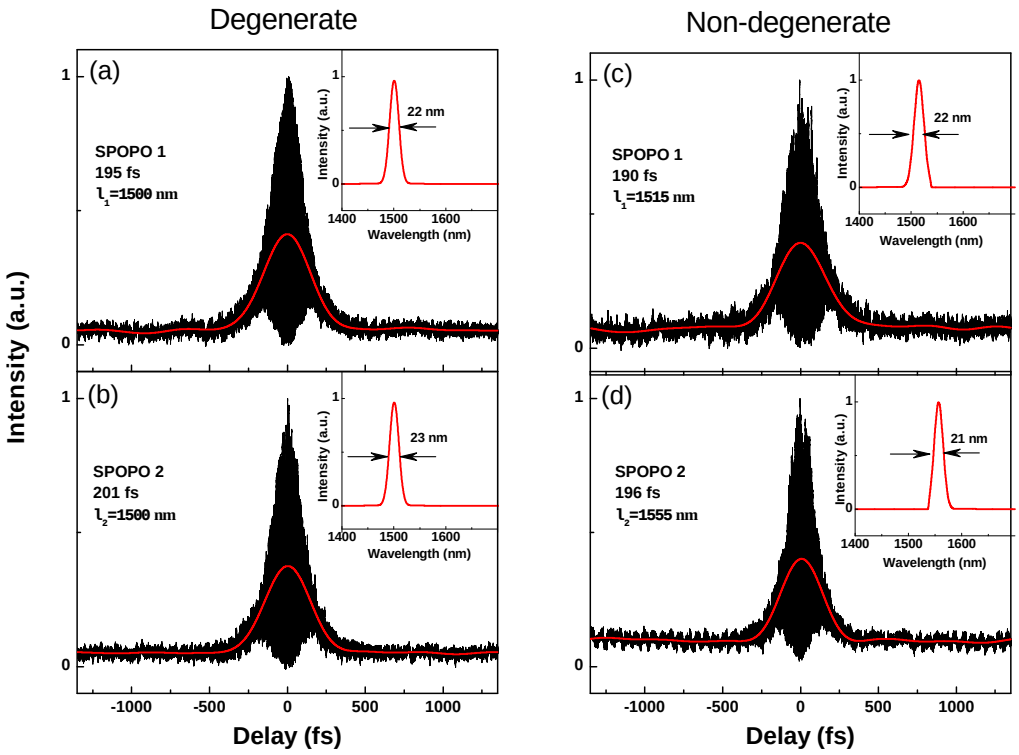

Figure 6.5: Interferometric autocorrelation of SPOPO1 (a), (b), and SPOPO2, (c), and (d) in degenerate and non-degenerate states.

They show pulses of ∼200 fs duration with smooth spectral profiles of similar FWHM bandwidth of ∼22 nm, resulting in time-bandwidth products of 0.57 and 0.61 ($sech^2$ pulse shape), close to the transform limit. There is also no evidence of any interference between the two pulses due to gain coupling. The results for non-degenerate operation are shown in $Fig.$ 6.5(c) and $Fig.$ 6.5(d). In this case, with peak spectral separation of 40 nm, the autocorrelations reveal similar pulse durations, the spectra also exhibit smooth profiles with nearly the same bandwidths, and the time-bandwidth products are 0.55 and 0.51, similarly close to the transform limit.

6.6 Conclusions

We have described and experimentally demonstrated a new technique for coupling of two optical oscillators using an intracavity ARR interferometer. This novel approach has been successfully implemented using two *fs* SPOPOs, enabling broadband dual-wavelength generation with arbitrary and independent tuning, but can be universally deployed in any optical oscillator and in any temporal regime from *cw* to *fs* time-scales, or their combinations. The new technique also holds promise for efficient generation of tunable THz radiation by intracavity difference frequency mixing in a suitable nonlinear element such as DAST, ZnTe, etc., deployed within the ARR and exploiting the high intensities available in the two circulating signal waves.

Chapter 7

Dual-wavelength picosecond optical parametric oscillator

7.1 Motivation

Dual-wavelength sources of picosecond radiation are of great interest for variety of application including CARS [86] and pump probe spectroscopy [87]. Many of these applications also ideally require the additional capability of arbitrary dual-wavelength tunability. Such tunable sources are key to access the THz spectral region through nonlinear optical processes, as well as the development of tunable THz sources [88] . In conventional ultrafast lasers, a variety of techniques have been devised to achieve dual-wavelength operation. Generation of two optical pulse trains operating at slightly different wavelengths has been demonstrated by using a programmable delay in a multichannel mode-locked grating cavity laser [89]. In another attempt, dual-wavelength picosecond pulses were generated from a gain-switched diode laser by controlling the optical paths on a diffraction grating [90]. Such techniques based on conventional laser sources provide very limited or no dual-wavelength tunability. Moreover, they offer no possibility for arbitrary and independent tuning of the two operating wavelengths, except in cases where two independent laser sources are deployed [91]. On the other hand, OPOs are viable sources of coherent radiation, which are inherently tunable, and

offer the potential for multiple wavelength generation over extended spectral regions. Recently, we have demonstrated the promise of such sources for dual-wavelength generation by deploying two-crystal architectures in *cw* [78] and *fs* SPOPOs [92]. While in *cw* operation, a single optical cavity was deployed for dual-wavelength generation, in *fs* operation an ARR interferometer was employed to couple the two SPOPO cavities, with both schemes providing arbitrarily tunable signal and idler wavelength pairs over a wide spectral range. Both techniques have been shown to provide arbitrary and independent tuning of the two signal-idler wavelength pairs, however, operation at identical wavelengths can lead to coherent coupling in the single-cavity *cw* OPO scheme, while this is circumvented in the double-cavity *fs* SPOPO with ARR interferometer. In this context, we have developed a dual wavelength picosecond SPOPO (DW-SPOPO) in a composite cavity design, that has provided independent and arbitrary tuning without coherent coupling even at degeneracy.

7.2 Experimental Setup

The DW-SPOPO employs two MgO:PPLN crystals and is pumped by a mode-locked Yb-fiber *ps* laser at 1064 *nm*, in a compact, robust, and practical architecture. The oscillator generates two pairs of signal-idler wavelengths that can be arbitrarily varied across the full tuning range of the SPOPO, even through degeneracy and beyond, irrespective of the operating wavelength. The schematic of the experimental setup is shown in *Fig.* 7.1. The pump source is mode-locked Yb-fiber laser at 1064 *nm*, providing up to 20 W of average power in 20 *ps* pulses at 80 *MHz* repetition rate. A Faraday isolator at the output end of the output fiber protects the laser from any back-reflections. A combination of a polarizing beam-splitter and a half-wave plate is used as a variable power divider, where the total available pump power is split into two arms in a controlled manner. A second half-wave plate in each arm provides the required polarisation for phase-matching in each crystal.

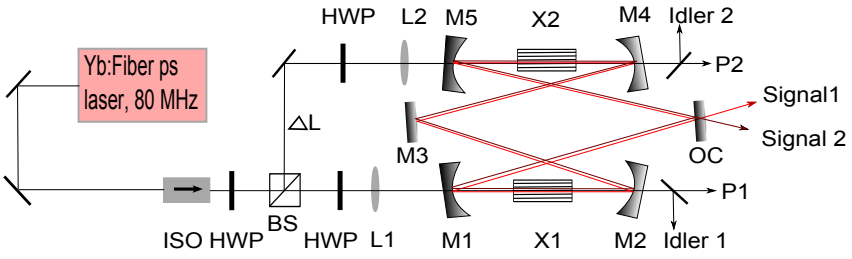

Figure 7.1: Schematic of the experimental setup. FI: Faraday isolator, HWP: Half-wave plate, BS: Beam-splitter, L1-2: Lenses, M1-5: Mirrors, X1-2: MgO:PPLN, OC: Output-coupler.

The DW-SPOPO constitutes two synchronously-pumped SPOPOs sharing the same optical cavity. The nonlinear gain media are two MgO:PPLN crystals with identical grating periods ranging from Λ=28.5 to 31.5 μm, in steps of 0.5 μm. However, in the present experiment, we only used a single grating period, Λ=30.5 μm. The pump beam in both the arms is focused using two lenses (L1 and L2) at the centre of the respective nonlinear crystals to beam waist radii of $\omega_{1,2}$ $\sim$65 μm. The DW-SPOPO resonator is configured in a folded ring cavity formed by four plano-concave mirrors (M1, M2, M4, M5) with radius of curvature, r=200 mm, a plane mirror (M3) and an output coupler (OC). All mirrors (M1-M5) are highly reflecting (R>99%)for the signal over 1.3-2.2 μm, and highly transmitting for the pump (T>90%) at 1064 nm and idler (T>87%) over 2.2-4 μm, ensuring singly resonant signal oscillation in both SPOPOs. A conventional plane OC with partial transmission (T$\sim$80%) over 1100-1630 nm is used to extract the signal power from the DW-SPOPO and a dichroic mirror separates the generated idler from the pump.

While a 48-mm-long, MgO:PPLN-1 serves as the nonlinear gain medium for SPOPO-1, a 50-mm-long MgO:PPLN-2 provides the gain for SPOPO-2. Both nonlinear crystals are housed in two identical ovens, which can be controlled from room temperature to 200°C with a stability of 0.1°C. The total optical length of the DW-SPOPO ring cavity is ∼186 cm, corresponding to a repetition rate of 160 MHz, ensuring synchronization with the second harmonic of the pump laser repetition-rate. It is to be noted that the pump pulses travel an additional path length of ΔL ∼42 cm, corresponding to a temporal delay of ∼1.4 ns, before entering SPOPO-2. Since the two SPOPOs share the same optical cavity, the resonant signal pulses traverse through both nonlinear crystals in each round-trip. However, due the temporal delay between the two input pump pulse trains, the generated signal pulses arrive at different times in each MgO:PPLN crystal, hence avoiding any possibility of coupling between the two SPOPOs, irrespective of the operating wavelengths. Further, the DW-SPOPO cavity design is different from our earlier demonstrations in the cw [78] as well as fs [92] time-scales. It is configured in such a way that the two SPOPOs are pumped through different arms and the corresponding signal pulses travel in opposite direction, again avoiding any coherent coupling, even when the resonant wavelengths are significantly close and ΔL∼0 or integral multiple of the cavity length corresponding to repetition rate of the pump laser. Moreover, the counter-propagating signal pulses result in the signal output from the OC in different directions, enabling us to monitor the output-coupled signal from each SPOPO separately.

7.3 Results and Discussion

In order to characterize the picosecond DW-SPOPO, we initially performed wavelength tuning measurements by varying the temperature of each nonlinear crystal individually, enabling arbitrary tuning of two independent signal-idler wavelength pairs generated by the two crystals. The signal wavelengths were measured using a *NIR* spectrometer (*Ocean Optics, NIRQUEST*). Since coherent coupling is completely avoided in the present cavity design, the signal-idler pairs from the two SPOPOs can be tuned indefinitely far or in-

finitesimally close, even through degeneracy and beyond, irrespective of the operating wavelength. The DW-SPOPO tuning behaviour, recorded at a fixed pump power of 8 W for each SPOPO, is shown in *Fig.* 7.2.

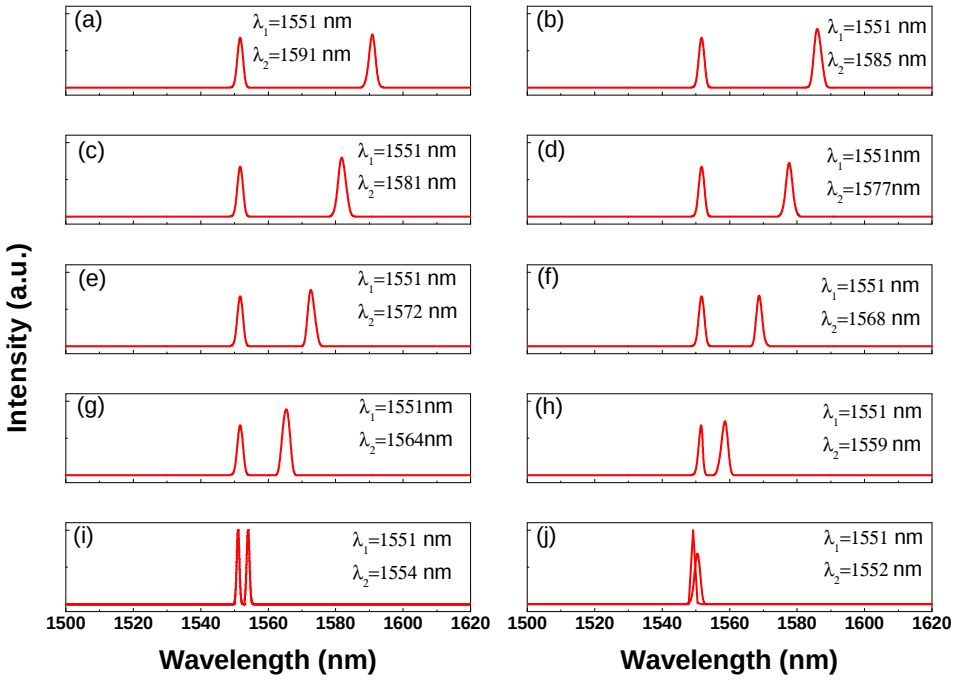

Figure 7.2: Independent arbitrary spectral tuning of the DW-SPOPO system by changing the temperature of the MgO:PPLN crystals.

By fixing the MgO:PPLN-2 crystal temperature at T2=50°C, generating a signal wavelength of 1550 *nm*, and varying the temperature of MgO:PPLN-1 from 150°C down to 50°C, the signal wavelength from OPO-1 could be continuously tuned from 1615 to 1551 *nm*, reaching a degenerate point where both the SPOPOs operate at nearly similar wavelengths. The difference of 1 *nm* between the two signal wavelengths, while operating at the same temperature, could be attributed to a small delay in the cavity length due to the 2-*mm* difference in the length for the two MgO:PPLN crystals. It is to be noted that the cavity of the DW-SPOPO is always optimized to achieve maximum output power. We also adjusted T1 slightly below 50°C in

order to operate at exact degeneracy, and observed no coherent coupling or perturbation between the two SPOPOs even at the degenerate point of 1550 nm. Further, by adjusting T1 and T2, the degenerate point of operation can be shifted arbitrarily within the full tuning range of the SPOPO, making it a highly attractive and viable source for applications such as tunable THz generation.

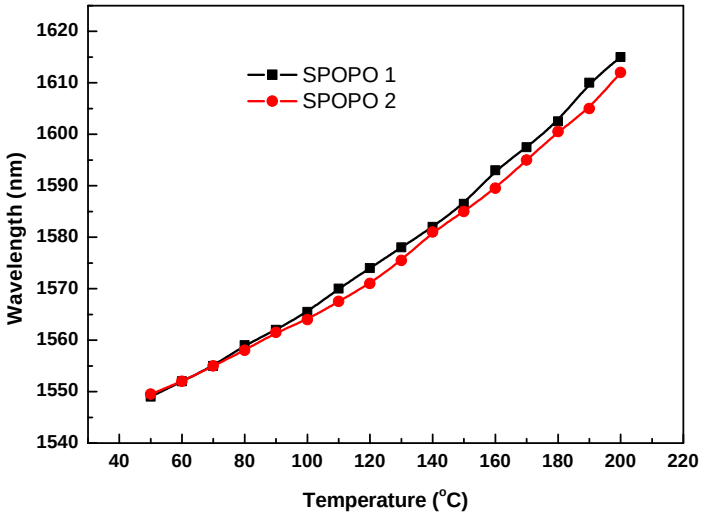

Figure 7.3: Variation of signal wavelength with crystal temperature.

The spectral tuning of the picosecond DW-SPOPO across the temperature range from SPOPO-1 and SPOPO-2, for a fixed grating period of Λ=30.5 μm and a constant pump power of 8 W at the input to each SPOPO, is shown in *Fig.* 7.3. As evident from *Fig.* 7.3, the two signal wavelengths generated from the SPOPO-1 and SPOPO-2 are almost identical in absolute value as well as tuning behaviour. We also performed simultaneous power scaling measurements of the signal output extracted through a 20% OC, as well as the idler, as function of the input pump power to each SPOPO, with the results shown in *Fig.* 7.4. With both SPOPO-1 and SPOPO-2 operating at a constant temperature of T1$\sim$T2$\sim$50°C, for the fixed grating period Λ=30.5 μm, corresponding to a signal wavelength of 1550 nm, we were able to extract as much as 1.35 W of average signal power from each SPOPO at

160 *MHz*, with a slope efficiency of ∼18%, for a maximum available pump power of 8 W to each crystal at 80 *MHz* repetition rate, as shown in *Fig.* 7.4(a).

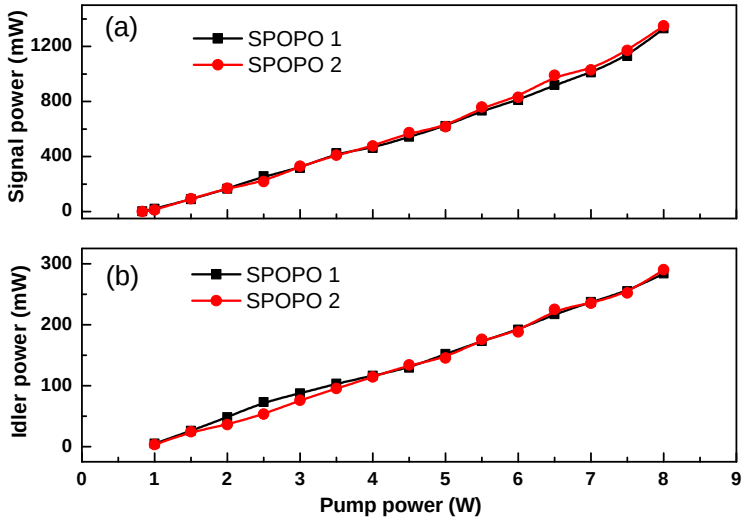

Figure 7.4: (a) Signal, and (b) Idler power extracted from the DW-SPOPO with change in input pump power.

The corresponding idler power is recorded to be 290 mW at a slope efficiency of ∼3.8% at 3393 nm, as shown in *Fig.* 7.4(b). This corresponds to an overall extraction efficiency as high as 44% for the picosecond DW-SPOPO. There is no evidence of saturation in the extracted signal and idler power, indicating the possibility of further power scaling by increasing the input pump power. Moreover, optimization and fine-adjustment of signal output coupling can lead to further improvements in the output power. Both SPOPO-1 and SPOPO-2 have similar threshold, recorded to be <830 mW. Although the resonant signal wavelength is the same in both the SPOPOs, no threshold reduction is observed due to the lack of coherent coupling between the two SPOPOs, as observed in *cw* DW-OPOs [78]. The long-term power stability measurement of the signal extracted from the each arm of the DW-SPOPO, together with the spatial beam profiles, when operating at signal wavelengths near 1550 nm, is shown in *Fig.* 7.5(a) and 7.5(b).

The SPOPO-1 and SPOPO-2 are recorded to exhibit a passive power stability better than 3.6% *rms* and 2.2% *rms*, respectively, over >5 hours under free-running conditions. The corresponding spatial beam profiles are shown in the insets, confirming a single-peak Gaussian intensity distribution.

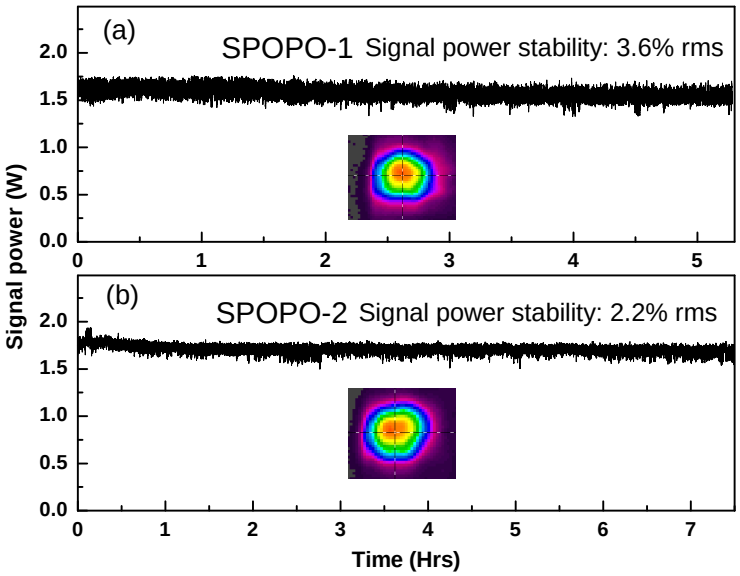

Figure 7.5: Passive power stability of (a) SPOPO-1, and (b) SPOPO-2.

We also performed spectral and temporal characterization of the signal pulses from the DW-SPOPO, with SPOPO-1 and SPOPO-2 operating at different temperatures of T1=50°C and T2=100°C. The signal pulse duration was measured using a home-made interferometric autocorrelator based on a two-photon absorption in a *Si* photo-detector. The results are shown in *Fig.* 7.6(a)-7.6(d). The signal pulses from SPOPO-1 and SPOPO-2 were both recorded to have a Gaussian temporal width of ∼18 *ps* and 15 *ps*, respectively. The pulse durations are consistent with the small difference in the operating wavelengths and crystal lengths. The corresponding spectra are shown in the *Fig.* 7.6(a), and 7.6(c) centred around 1550 *nm* and 1574 *nm*, respectively. The spectra have smooth clean profiles with a FWHM bandwidth of ∼2 *nm* for both SPOPO-1 and SPOPO-2.

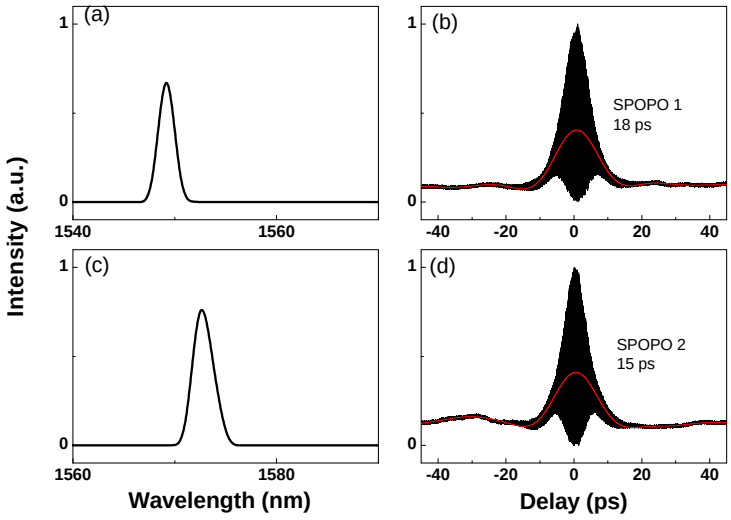

Figure 7.6: Spectral and temporal measurements of the SPOPO-1 and SPOPO-2 operating at different wavelengths.

Finally, we measured the time delay between the two oscillating signal pulses by performing simultaneous measurements of the two signal pulse trains emitted from the DW-SPOPO using an $InGaAs$ photo-detector (20 GHz, 18.5 ps) and a fast oscilloscope (3.5 GHz, 40 GS/s).

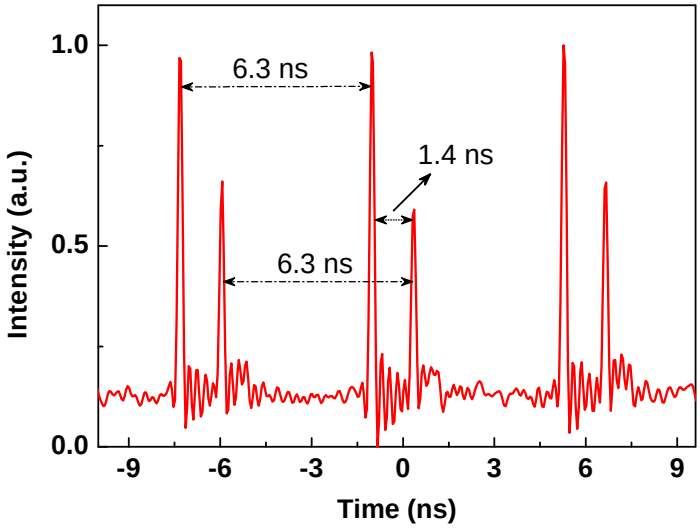

Figure 7.7: Pulse train delay between the two oscillating signals from SPOPO-1 and SPOPO-2.

The result is shown in *Fig.* 7.7, where it is evident that the pulses in each train are separated by 6.3 *ns*, corresponding to a repetition frequency of ∼160 *MHz*, while the two interleaved pulse trains from SPOPO-1 and SPOPO-2 are separated by 1.4 *ns*. This corresponds exactly to the spatial delay of ΔL∼42 *cm* between the pump pulses arriving at the input to SPOPO-1 and SPOPO-2, as shown in *Fig.* 7.1. Hence, another advantage of this configuration is that, by changing the delay between the input pump pulses, the signal pulses can be adjusted to operate at the desired time delay, maintaining the repetition frequency of the individual pulse train at the same cavity length, yet avoiding any coherent coupling between the two signal wavelengths resonating inside the same cavity. Alternatively, with a fixed delay between the input pump pulses, the output signal pulse trains from the DW-SPOPO can be synchronized using an external delay line, which would enable single-pass frequency mixing in suitable nonlinear crystals to access new wavelengths regions, with potential applications for THz generation using difference-frequency-generation.

7.4 Conclusions

In conclusion, we have described and experimentally demonstrated a simple, compact, picosecond DW-SPOPO at 160 *MHz* repetition rate based on two MgO:PPLN crystals in a single cavity, synchronously-pumped by a mode-locked Yb-fiber laser at 80 *MHz*. The DW-SPOPO provides two signal and idler pulse trains, which are independently and arbitrarily tunable in the *NIR* across 1550-1615 *nm*, and the *MIR* across 3118-3393 *nm*, using a single grating period. The signal and idler can be tuned through any degenerate wavelength pairs across the full DW-SPOPO tuning range without coherent coupling. The wavelength coverage of the signal and idler pairs can be readily extended using multiple grating periods of the MgO:PPLN crystals. We were able to extract signal power of up to 1.5 W from each SPOPO, at a total (signal plus idler) extraction efficiency as much as 44%, with a power stability better than 3.6% rms over >5 hours in excellent spatial beam quality. Interferometric autocorrelation measurements resulted in Gaussian pulse

duration of ∼18 *ps* from SPOPO-1 and ∼15 *ps* from SPOPO-2. The cavity design ensures no coherent coupling between the signal (idler) pairs, irrespective of the operating wavelength, enabling degenerate operation at any desired wavelength across the DW-SPOPO tuning range. Further, by adjusting the delay between the pump pulses through an external delay line at the input of two crystals, the delay between the pulse train from the DW-SPOPO can be tailored. The generic design can also be extended to new wavelength regions using alternative nonlinear materials and pump wavelengths. These characteristics make the described Yb-fiber-pumped DW-SPOPO a highly versatile and practical source of high-repetition-rate picosecond pulses for many applications.

Chapter 8

Double-crystal, dual-synchronously pumped femtosecond optical parametric oscillator

8.1 Motivation

Traditionally, ultrafast SPOPOs deploy a single nonlinear crystal as the gain element within a cavity that is synchronously driven by a single input pump pulse train. There have been some previous schemes involving more than one non-linear medium in an OPO for various purposes. For instance, non-resonant two-crystal OPO [93], tandem optical parametric oscillators (TOPO) [94], [95], [96] (in which the secondary OPO crystal uses the signal from the primary OPO as a pump source), two cascaded gratings on single non-linear crystal in a *fs* SPOPO [97] were demonstrated to achieve greater idler conversion efficiency. While two-crystal *cw* OPO for dual wavelength generation [78], SPOPO with intracavity difference-frequency mixing [98] and coupled TOPO were demonstrated for *MIR* generation [99]. Nevertheless, it would be desirable to exploit the possibility of deploying more than one non-linear crystal inside the SPOPO for the same optical parametric generation

process so as to achieve intracavity optical parametric amplification (IOPA) of the oscillating field. In more detail, if we would like to scale-up the average signal power, we may consider to deploy two nonlinear crystals instead of lengthening the single crystal to obtain significant SPOPO power scaling without detrimental effects imposed by parametric gain limitations such as spectral acceptance bandwidths (especially relevant when dealing with very broad pump sources) or spatial walk-off interaction. In this context, we propose and experimentally demonstrate an attractive scheme, in which the main pump beam is split into two and two identical non-linear media are pumped in synchronization to achieve signal IOPA in an ultrafast *fs* SPOPO. This method presents some additional advantages compared to that theoretically presented in [93] based on two crystals in cascade. Firstly, expensive custom-designed broad-band cavity mirrors are not required to reflect both pump and signal simultaneously. Secondly, the pump spectra available to the second non-linear crystal will be same as that of the one available to first non-linear crystal. Moreover, we have independent control of alignments and time delay to achieve the best overlapping between pump and signal pulses inside the nonlinear crystals.

8.2 Experimental Setup

The configuration of the experimental setup is shown in *Fig.* 8.1. The SPOPO is pumped by a KLM Ti:sapphire laser operating at 800 *nm* with a repetition-rate of 76 *MHz*. After transmission through an isolator, the pump pulses have durations of 150 *fs*, and a half-wave plate is used to control the beam polarization. Using a nearly 50:50 beam-splitter, the pump pulses are separated into two paths, P1 and P2. The path, P2, includes a delay line so as to synchronize both pump pulse trains inside the second crystal (X2). Two lenses, L1 and L2 (f=8 *cm*), AR-coated (R<1%) at 800 nm, are used to focus the two pump beams to identical waist radii (ω_o ∼16 μm) inside the two nonlinear crystals (X1 and X2). The SPOPO is singly-resonant and configured in a standing-wave resonator with two intracavity focal planes. The cavity comprises two pairs of identical concave mirrors (M1-M2 and

M4-M5) with radius of curvature, r=10 cm, a flat mirror (M3), and a ∼5% output coupler (OC) mounted on a translation stage to allow control of the cavity length for synchronization with the input pump pulse repetition rate. The SPOPO cavity is not symmetric with respect to the two focal planes, such that X1 is pumped as in a 3-mirror asymmetric cavity with an additional focus at X2, while X2 is pumped as in a 4-mirror symmetric cavity with an extra focus at X1. With the exception of the OC, all cavity mirrors are highly reflecting (R>99%) for signal wavelengths over 1420-1580 nm and highly transmitting (T>95%) for the pump at 800 nm, with >80% transmission for the idler over 3000-5000 nm.

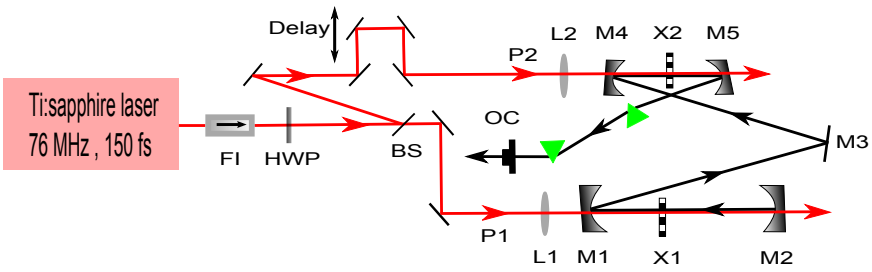

Figure 8.1: Schematic of the experimental setup. FI: Faraday isolator, HWP: Half-wave plate, BS: Beam-splitter, L1-2: Lenses, M1-5: Mirrors, X1-2: MgO:PPLN, OC: Output-coupler.

Two identical MgO:PPLN crystals (X1 and X2), 0.5-mm-long, 1-mm-thick, and incorporating fanned gratings with continuously variable period from Λ=16 to Λ=23 μm across the 3.4-mm-wide dimension, are used as nonlinear gain elements for the SPOPO. The crystal faces are anti-reflection-coated (R<0.75%) for the signal and the pump (R<5%), with high transmission (T>85%) for idler over 1600-3500 nm. Intracavity dispersion compensation is implemented using a pair of SF-11 prisms with a tip-to-tip separation of 15.4 cm, deployed between M5 and the OC.

8.3 Results and Discussion

To achieve successful operation of the dual-crystal SPOPO, oscillation was first initiated with only one crystal, X1, in the cavity, pumped by P1 (with P2 blocked). A grating period of $\Lambda \sim 21.4\ \mu m$ was used in X1 to obtain the phase-matching. Under this condition, oscillation was achieved at a pump threshold of 225 mW with $\sim$24 mW of signal power extracted through the $\sim$5% OC. With the deployment of the second crystal, X2, inside the cavity, a small drop in the signal output power of 4 mW is observed. The SPOPO oscillation is then initiated again only with the second crystal, X2, pumped by P2 (with P1 blocked), choosing the same grating period of $\Lambda \sim 21.4\ \mu m$ for phase-matching in X2. In this case, the average pump threshold was 200 mW, with 23.2 mW of average signal power extracted through the OC. To study the output power characteristics of the dual-crystal SPOPO, we measured the extracted signal power at different pumping levels.

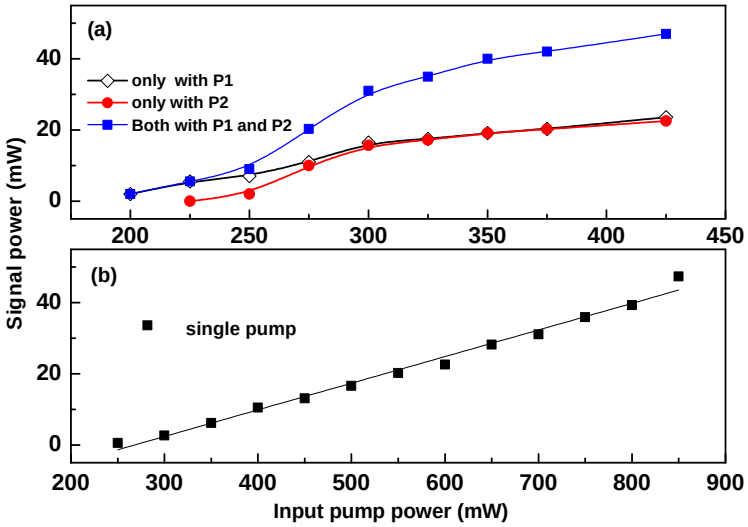

Figure 8.2: (a) Signal power with independent splitted pump beams and (b) Signal power without splitting the pump beam.

Figure 8.2(a) presents the recorded data for the SPOPO average signal power extracted through the $\sim$5% OC as a function of the input pump power, when X1 and X2 are pumped individually (with only P1 and P2). The

symmetric nature of the SPOPO with only P1 or with only P2 can be clearly seen from the power-scaling plot in *Fig.* 8.2(a). In order to evaluate the performance of the SPOPO using a single crystal at the maximum available pump power, we measured the variation of signal power without splitting the pump, with the resulting power scaling in crystal X1, (without X2 in the cavity). The result is shown in *Fig.* 8.2(b). In this case, the maximum signal power extracted was 47.4 mW at the highest available input pump power of 850 mW. With the deployment of second crystal (X2) at the intracavity focus between M4 and M5, the maximum extracted power was 44 mW. This small reduction in power of 3.4 mW indicates that the second crystal (X2) surfaces are nearly lossless. By comparing *Figs.* 8.2(a) and 8.2(b), we can infer that the sum of the extracted signal powers with P1 and P2 (see *Fig.* 2(a)) is nearly equal to the extracted signal power, when pumped with a single pump beam without splitting. Thus, the overall extracted signal power remained constant in both cases of pumping (with splitting and without splitting).
The presented data is the case where P2 pulse trains are not synchronized to P1 pulse trains. By using a delay line, P2 pump pulse train in X2 is synchronized to the signal pulse train generated by P1 in X1 circulating in the cavity. In this case, the signal from the first crystal X1 serves as a seed beam when passing through the second crystal X2, and since P1 and P2 are synchronized in time, intracavity amplification of the generated signal is achieved. Furthermore, P1 pulse trains are also synchronized in X1 with the signal pulse trains generated and are amplified in X2 by P2. As a result of this iterative OPO-IOPA process, a strong enhancement ($[P_{SPOPO}(syn) - P_{SPOPO}(unsyn)]/P_{SPOPO}(unsyn)$) in the oscillating signal power is observed. *Figure.* 8.3 presents the recorded data when both pump pulse trains, P1 and P2, are in and out of synchronization. When the pump pulse trains are out of synchronization, the SPOPO signal power is nearly equal to the sum of the signal powers from P1 and P2, individually. However, when both are synchronized, a strong enhancement in signal power from 47.4 mW to 74 mW is observed. Interestingly, under synchronization, the SPOPO signal power is not just the sum of the signal powers from P1 and P2, but is nearly two times higher at the maximum available pump power.

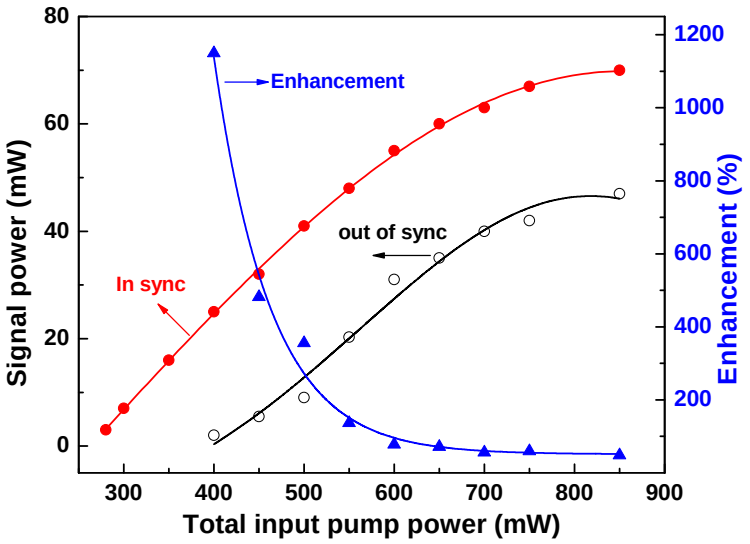

Figure 8.3: Signal power with splitted pumps in and out of synchronization with the corresponding enhancement.

Moreover, the enhancement is as high as 1150% at near threshold and is 56% at the maximum available pump power of 850 mW before separation by the beam-splitter into two beams, P1 (450 mW) and P2 (400 mW). In addition, we recorded the variation of signal power when the second pump pulse train was delayed with respect to the first pump pulse train as shown in *Fig.* 8.4. It can be seen that the signal power drops off gradually on either side of the zero delay. Also, one can clearly see that maximum signal power with substantial amount of enhancement has been achieved, only when both the pump pulse trains are exactly synchronized. Beyond 90 μm of delay, no enhancement in the signal power is observed due to the lack of overlap between the intracavity signal pulses and the pump pulses inside X1 and X2. We also measured the overall enhancement in the pump depletion at the maximum available pump power. The maximum pump depletion in the case when P1 and P2 are out of synchronization was 61%, whereas a significant enhancement in depletion of up to 91% was recorded under exact

synchronization, corresponding to the zero delay, as shown in *Fig.* 8.4.

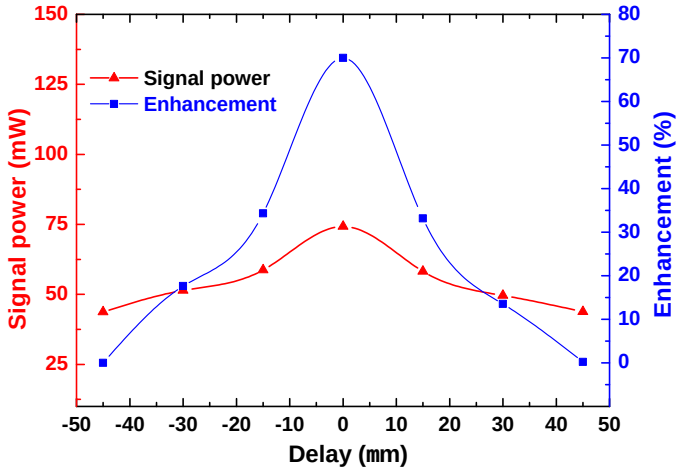

Figure 8.4: Variation of signal power with respect to synchronization between P1 and P2 pulse trains and the corresponding enhancement.

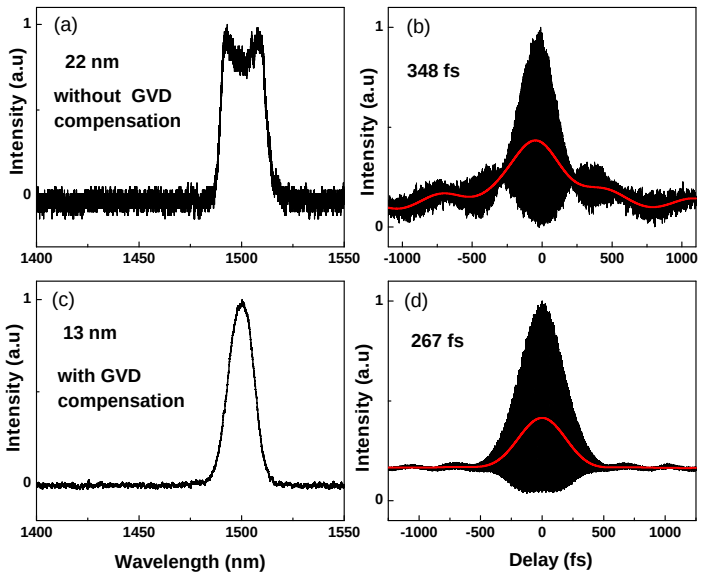

Figure 8.5: Spectra and Interferometric autocorrelation traces of signal pulses (a) and (b) without GVD compensation, (c) and (d) with GVD compensation.

Furthermore, we recorded the spectral and temporal profiles of the SPOPO signal pulses without and with GVD compensation. Spectral measurements

for signal pulses were obtained using an optical spectrum analyser, whilst temporal characterization was performed using fringe-resolved intensity autocorrelation based on two-photon absorption in a *Si* detector. The measured pulse width without deployment of prism pair for GVD compensation is 348 *fs* (linearly chirped as shown in *Fig.* 8.4(b)). The spectral profile has two peaks with a bandwidth of 22 *nm*. Assuming the pulses are $sech^2$, the time-bandwidth product value is 1.02, which is nearly three times longer than transform limited pulses. Using a SF11 prism pair with a tip-to-tip separation of 15.4 *cm* we were able to compress the pulses to as short as 267 *fs* with a corresponding bandwidth of 13 *nm*. With GVD compensation, the time-bandwidth product of the signal pulses is 0.46, which are near to the transform limit.

8.4 Conclusions

We have demonstrated a novel two crystal, dual-synchronously pumped *fs* SPOPO, to achieve intracavity signal amplification. We expect still higher average signal powers enhancements with optimized output coupling. The main advantage of this scheme is that the interaction length can be increased without compromise on the bandwidth of the nonlinear crystal. Also this concept can be cleverly used in case of birefringent nonlinear media where walk-off is a major problem. By introducing the second nonlinear crystal in place of X2, the walk-off can be compensated effectively while simultaneously achieving efficient pump to signal conversion. Furthermore, this technique provides an additional degree of flexibility to ensure higher output powers using less pump intensities per crystals, which can facilitate working well below the damage threshold of the crystals when significant power scaling is attempted.

Chapter 9

Ti:sapphire pumped deep-mid-infrared femtosecond optical parametric oscillator based on $CdSiP_2$

9.1 Motivation

With the lack of availability of practical ultrafast solid-state lasers, SPOPOs offer a viable route to the generation of ultrashort pulses in the *MIR*. By exploiting oxide-based birefringent nonlinear materials such as $LiNbO_3$, $KTiOPO_4$, $RbTiOAsO_4$ and $LiTaO_3$, and their quasi-phase-matched (QPM) counterparts, PPLN, PPKTP, PPRTA and PPLT, many *fs* SPOPOs pumped by the KLM Ti:sapphire laser have been realized covering spectral regions from ∼250 nm in UV up to ∼4.5 μm in *MIR* [11]. However, access to deep-*MIR* wavelengths beyond ∼4.5 μm in oxide-based crystals is fundamentally limited by multi phonon absorption, placing a practical upper limit of ∼4 μm in all such SPOPOs. As an alternative, non-oxide QPM materials, such as OP-GaAs, can be used for wavelength generation beyond ∼4 μm, but this requires pump sources above ∼2 μm to avoid two-photon absorption. Chalcopyrite crystals such as $AgGaSe_2$ (AGSe), $AgGaS_2$ (AGS), and the most

developed $ZnGeP_2$, can generate deep-*MIR* radiation up to ∼10 μm, but must be pumped above ∼1 μm to avoid two-photon and residual absorption, and material quality still remains a major practical limitation yet to be overcome. In an effort to extend the wavelength reach of Ti:sapphire-pumped *fs* SPOPOs beyond ∼4 μm, external cascaded pumping using two SPOPOs in series, based on *CTA* and *AGSe*, was previously deployed, providing spectral coverage up to ∼8 μm [100]. However, such external tandem pumping schemes result in relatively complex architectures involving two SPOPO cavities synchronized in series to one another, and to the pump laser, leading to increased output instabilities, which are not desirable for many practical applications.

The new nonlinear material, $CdSiP_2$ (CSP) [101], has the important capability to generate radiation beyond ∼6 μm under NCPM at room temperature with direct pumping at ∼1 μm [102], [103]. Using CSP, a number of ultrafast parametric sources have been recently demonstrated by deploying mode-locked solid-state and fiber pump lasers at ∼1 μm, providing spectral coverage from ∼6.1 to ∼6.7 μm [104], [105], [106], [107], [108]. However, the development of ultrafast SPOPOs based on CSP using the KLM Ti:sapphire laser, the workhorse of ultrafast technology, is precluded by the short-wavelength cut-off below ∼1 μm in this material. In this context, we describe the first SPOPO for the deep-*MIR* based on CSP, pumped by a KLM Ti:sapphire laser using a novel internal cascaded scheme that circumvents the fundamental short-wavelength material absorption. In this new scheme, the CSP is synchronously pumped internal to a MgO:PPLN *fs* SPOPO in a composite cavity geometry.

9.2 Experimental Setup

The schematic of the experimental setup is shown in *Fig.* 9.1. The KLM Ti:sapphire laser provides an average power of 900 mW at 796 nm and ∼155 *fs* pulses with a 7 nm bandwidth at 76 *MHz* for synchronously pumping the intracavity cascaded SPOPO (IC-SPOPO). The IC-SPOPO is arranged in a composite bifocal standing-wave cavity comprising a primary SPOPO based

on a 0.5-mm-long MgO:PPLN, and a secondary SPOPO based on a 0.5-mm-long CSP crystal. The MgO:PPLN crystal incorporates fanned gratings with periods of Λ=16-23 μm. The CSP crystal is cut at $\theta = 90\,^{\circ}$, ($\phi = 45\,^{\circ}$) for *type I (e→oo)* NCPM.

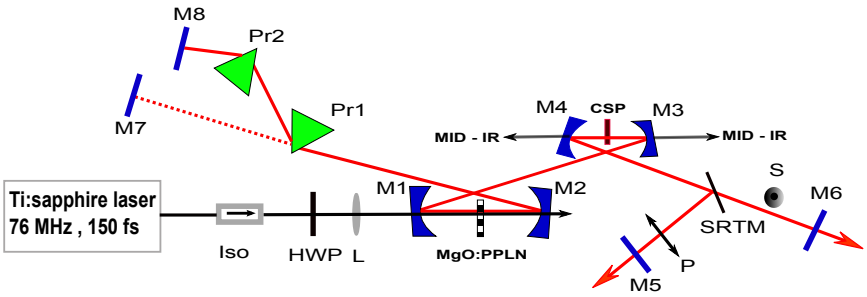

Figure 9.1: Schematic of the experimental setup. ISO: Faraday isolator, HWP: Half-wave plate, L: Focusing lens, M1-8: Mirrors, Pr1-2: Prism pair, SRTM: Selectively reflecting and transmitting mirror, S/P: Polarisation states.

The singly resonant standing wave cavity mainly consists of three parts in the standing-wave X-cavity design. Firstly, the SPOPO cavity is based on PPLN as a nonlinear medium. Secondly, a prism pair with a separation 21.6 cm was deployed in one of the arms of the X-cavity for GVD compensation. Thirdly, the second arm consists of two concave mirrors, M3-4 (r=100 mm) separated by 100 mm, a thin (1 mm) selectively reflecting and transmitting mirror (SRTM) and two highly reflecting mirrors M5, M6. The SRTM is highly reflective (R>99%) for 1000-1100 nm and highly transmitive (T> 98%) for the wavelength region 1150-1350 nm. Initially, with SRTM operated in reflection mode, the mirror M5 mounted on a precision linear translational stage was scanned to match the pump laser repetition rate. Hence the oscillating signal from PPLN follows the optical path M2-Pr1-Pr2-M8-Pr2-Pr1-M2-M1-M3-M4-SRTM-M5. This singly resonant oscillating signal of the PPLN serves as a pump to the second nonlinear crystal CSP. Thus IC-SPOPO consists of two SPOPO cavities. While the primary SPOPO is

formed by concave mirrors, M1-M4 (r=100 mm), SRTM and plane mirrors, M5 and M8, the secondary SPOPO is formed by mirrors, M1-M4 and M8, but with plane mirror, M6, completing the cavity. All mirrors are broadband HR (R>99.8%) over 980-1640 nm and HT (T>90%) over 710-840 nm, ensuring singly-resonant signal oscillation in both SPOPOs. A lens L (f=8 cm) is used to focus the pump beam to a waist radius, ω_o ∼16 μm, inside the MgO:PPLN crystal. A half-wave plate provides required e pump polarization for *type 0* (e→ee) phase-matching in the MgO:PPLN crystal. The generated signal pulses from the MgO:PPLN SPOPO are ∼210 fs with a bandwidth of ∼7.3 nm, and, in turn, provide the e polarization to pump the CSP SPOPO under *type I (e→oo)* NCPM.

9.3 Results and Discussions

We used the signal from the singly resonant SPOPO cavity based on the PPLN to serve as an intracavity pump source for the second nonlinear crystal CSP, deployed in the folded X-cavity between the mirrors M3-4. The CSP crystal has an aperture of 4×5 mm, and is AR coated (T>99%) for 1020-1300 nm and 5900-6700 nm (T > 95%) in the *near* and *MIR* wavelength regions respectively. The CSP is scanned to find the best focus in between the mirrors M3 and M4. After the insertion of the CSP and the cavity length was compensated to match the repetition rate of the pump laser, we find that there is a slight reduction (from 72 mW to 68 mW) in the PPLN signal power extracted through a thin film beam-splitter. This confirms that the CSP crystal coatings are nearly lossless. For a fixed PPLN signal wavelength of 1024 nm, the mirror M6 mounted on precision linear translational stage is scanned through the SRTM (in transmission mode) to find the synchronization position for the CSP SPOPO. When SPOPO cavity of the CSP is matched exactly to the repetition rate of the PPLN SPOPO, we observed the simultaneous oscillation of two signals (signal from PPLN which served as pump to CSP and the generated signal from CSP SPOPO) as shown in *figure* 9.2.

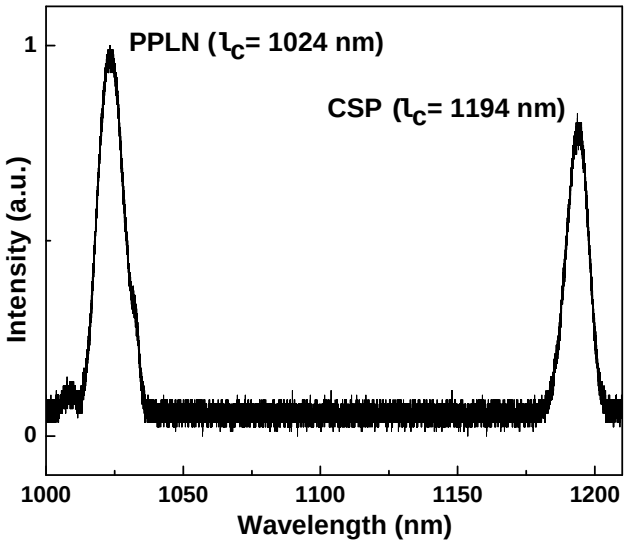

Figure 9.2: Simultaneous oscillation of the both signal wavelengths from PPLN and CSP inside the composite cavity.

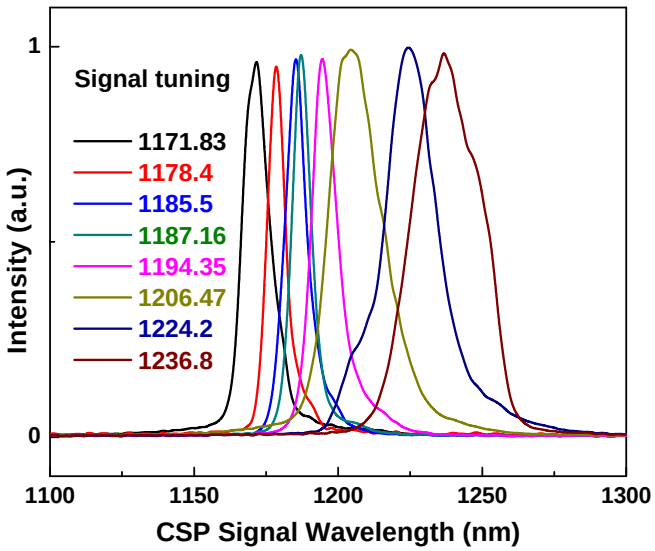

Figure 9.3: Rapid and broad band cavity length tuning of the signal spectra from the CSP SPOPO.

It is worthwhile to note that the path M8-Pr2-Pr1-M2-M1-M3-M4-SRTM is common for both the SPOPO signals oscillating under *type 0* ($e \rightarrow ee$ for PPLN) and *type I* ($e \rightarrow oo$ for CSP) respectively. The SRTM acts as an interlink between the two SPOPOs that can be controlled and tuned independently using the cavity length delay with M5 and M6 respectively. The vertical arrow and dot after the SRTM (shown in the *figure.* 9.1) differentiates the respective polarizations of the oscillating signals from PPLN and CSP SPOPOs. The CSP SPOPO signal can be tuned between 1170-1235 *nm* by rapidly adjusting the cavity length of nearly 100 μm delay as shown in *figure.* 9.3. This corresponds to an idler tuning in the deep-*MIR* region from 8110 nm-5950 *nm*. Using the conservation laws, we reconstructed idler spectra from the depleted pump spectrum and the generated signal spectra which are shown in *figure.* 9.4.

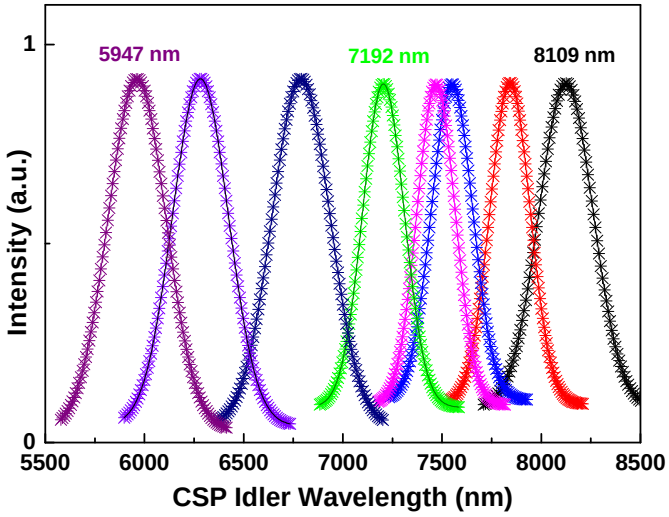

Figure 9.4: Reconstructed idler spectra of the CSP SPOPO corresponding to the various signal spectra.

Thus for a signal tuning range of nearly 65 *nm*, the idler tuning is as broad as 2150 *nm*, which is the record level of tunability achieved so far based on any of CSP based optical parametric sources. More importantly, it is to be noted that the system operates at room temperature.

Also, we measured the average CSP SPOPO signal power with change in the cavity delay length. We defined zero delay as the position where the system has its best performance in terms of average signal power leak through the mirror M6. With all the cavity mirrors highly reflecting for both the oscillating fields, the measured average signal power of CSP SPOPO is shown in *figure.* 9.5. A maximum power of 356 μW was recorded at the best performance (Delay=0) with the signal spectrum centred around 1206 nm. We also observed a strong visible red (SHG of CSP signal) after the curved mirror M4.

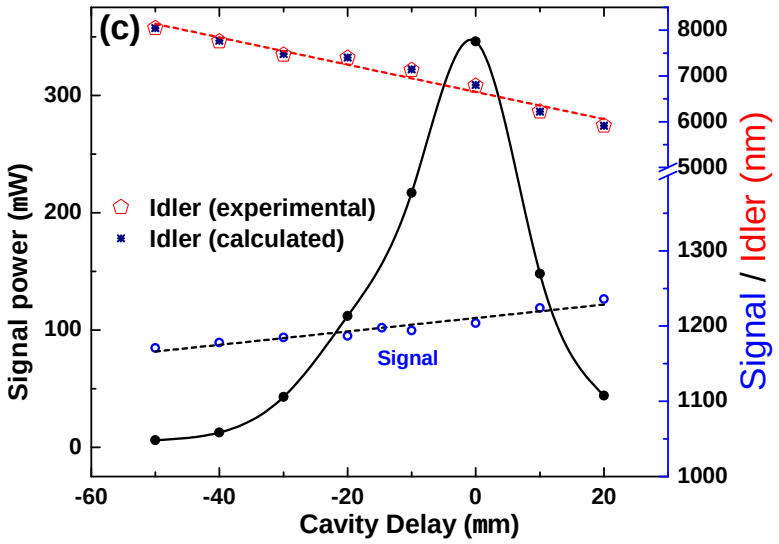

Figure 9.5: Average signal power of the CSP SPOPO across the tuning range.

By replacing the mirror M6 with a 5% output coupler, we were able to extract 9 mW of signal power from the CSP SPOPO. Furthermore, we have recorded an idler power of 64 μW after the mirror M4. This small idler power leak was mainly constrained by the cavity mirrors (M3, M4) made up of fused silica substrates, which absorbs most of the generated idler radiation in a single-pass through the CSP SPOPO. With a 6 mm fused silica substrates used in the cavity, the measured idler transmitivity is only 12%, which indicates that nearly 88% of the generated idler is being absorbed inside the substrate itself. The strength of the idler was detected using a fast

photo voltaic junction detector of HgCdTe that responds within the optical region of 2 to 8 μm. The measured threshold of the IC-SPOPO is 600 mW of average Ti:sapphire input pump power. Additionally, we measured the CSP idler stability using an OPHIR power meter (which could measure as low as 3 nW) of the freely running IC-SPOPO as shown in the *figure.* 9.6.

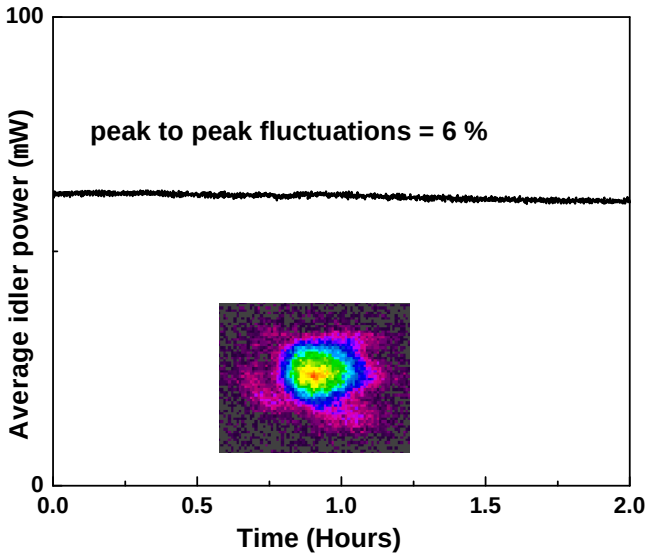

Figure 9.6: Idler stability with peak-peak fluctuations of 6% and the beam profile of the idler measured using a far IR camera.

Without any active stabilization, the IC-SPOPO has a peak-peak fluctuation of 6% and this could be attributed to the fluctuations in the Ti:sapphire pump source that are inherently transferred to the SPOPOs.

9.4 Conclusions

In conclusion, we have demonstrated for the first time, Ti:sapphire pumped *fs* CSP SPOPO, with a novel concept of internal cascaded pumping. The technique is universal and can be deployed in any OPO irrespective of temporal regime and for any wavelength region. Also since the two cavities can be controlled independently, there is no need of any active stabilisation unlike in cascaded SPOPOs [100]. The combination of solid state Ti:sapphire

pump source with technologically matured PPLN crystal, opens new avenues to pump most of the existing and new novel nonlinear media such as AGS, AGSe, ZGP, OP-GaAs etc. that requires pump sources greater than 1 μm. As PPLN has transparency cut-off till 4.5 μm, the entire region from 1 to 4.5 μm can be made accessible by pumping with traditionally well-established solid state KLM Ti:sapphire working around 800 nm. Thus, the concept of IC-SPOPOs can be extended to pump any nonlinear media that requires pump sources from 1 μm in the *NIR* to as far as 4.5 μm in the *MIR* to reach the deep-*MIR* regions by careful selection of the nonlinear media.

Chapter 10

Summary and outlook

In this thesis, we have demonstrated various ultrafast SPOPOs based on different nonlinear media which includes systems, novel techniques and concepts for accessing spectral regions from 1 μm in the *NIR* to 8 μm in the deep-*MIR*.

The main outcomes of this thesis are summarised below:

* First demonstration of *fs* SPOPO based on BIBO directly pumped by a KLM Ti:sapphire laser.
* Developed a technique called synchronous retro-reflection for threshold reduction and signal amplification.
* First demonstration of a self phase-locked *fs* SPOPO based on birefringent nonlinear medium BIBO.
* Developed and demonstrated an universal technique for coupling two *fs* optical oscillators using anti-resonant ring (ARR) interferometer.
* Developed a high-power, high-repetition rate ps SPOPO in the near to mid infrared regions with arbitrary and independent tuning capability.
* Developed the concept of deploying two nonlinear media inside a single SPOPO for intracavity signal amplification and demonstrated how the interaction length can be increased without compromising on gain bandwidth.
* Developed a novel concept of internal cascaded pumping scheme to deploy an OPO within another OPO.

As a direction for the future projects, the above presented work can be extended as follows:

♦ The self phase-locked SPOPO is a viable alternative to mode-locked Er and Yb fiber lasers for frequency comb generation in the *NIR* for a wide range of applications in spectroscopy and frequency metrology.
♦ The ARR coupled *fs* SPOPOs can be used to generate intracavity *fs* coherent THz radiation by deploying a suitable nonlinear crystal inside the ARR. This will greatly enhance the conversion efficiency which exploits the high intracavity intensities of the oscillating fields.
♦ Also the work of dual-wavelength ps SPOPO can be extended for generating THz radiation external to the cavity in ps regime.
♦ Finally the concept of internal cascaded pumping can be extended to develop various SPOPOs based on different nonlinear media for accessing spectral domains beyond 4.5 μm in the *MIR* region to as far as 18 μm in the deep-*MIR* region.